



# **Time-Reversal Based Range Extension Technique for Ultra-wideband (UWB) Sensors and Applications in Tactical Communications and Networking**

Technical Report (Quarterly)

to

US Office of Naval Research

875 North Randolph Street

Arlington, VA 22203-1995

for

Grant # N00014-07-1-0529

Prepared by

Robert C. Qiu

**(Principal Investigator)**

together with

(Contributing Researchers at Wireless Networking Systems Lab)

Nan (Terry) Guo  
Qiang (John) Zhang  
Chenming (Jim) Zhou  
Zhen (Edward) Hu  
Peng (Peter) Zhang  
Dalwinder Singh  
Corey Cooke

**October 16, 2007**

Department of Electrical and Computer Engineering

Center for Manufacturing Research

Tennessee Technological University

Cookeville, TN 38501

# **20071113080**

**REPORT DOCUMENTATION PAGE**

*Form Approved  
OMB No. 0704-0188*

The public reporting burden for this collection of information is estimated to average 1 hour per response, including the time for reviewing instructions, searching existing data sources, gathering and maintaining the data needed, and completing and reviewing the collection of information. Send comments regarding this burden estimate or any other aspect of this collection of information, including suggestions for reducing the burden, to Department of Defense, Washington Headquarters Services, Directorate for Information Operations and Reports (0704-0188), 1215 Jefferson Davis Highway, Suite 1204, Arlington, VA 22202-4302. Respondents should be aware that notwithstanding any other provision of law, no person shall be subject to any penalty for failing to comply with a collection of information if it does not display a currently valid OMB control number.  
**PLEASE DO NOT RETURN YOUR FORM TO THE ABOVE ADDRESS.**

<b>1. REPORT DATE (DD-MM-YYYY)</b> 16-10-2007	<b>2. REPORT TYPE</b> Technical Report (Quarterly)	<b>3. DATES COVERED (From - To)</b> July 16, 2007--October 16, 2007
--	---	--

<b>4. TITLE AND SUBTITLE</b> Time-Reversal Based Range Extension Technique for Ultra-wideband (UWB) Sensors and Applications in Tactical Communications and Networking	<b>5a. CONTRACT NUMBER</b>
	<b>5b. GRANT NUMBER</b> N00014-07-1-0529
	<b>5c. PROGRAM ELEMENT NUMBER</b>

<b>6. AUTHOR(S)</b> Qiu, Robert C.; Guo, Nan; Zhang, Qiang; Zhou, Chenming; Hu, Zhen; Zhang, Peng; Singh, Dalwinder; Corey Cooke.	<b>5d. PROJECT NUMBER</b>
	<b>5e. TASK NUMBER</b>
	<b>5f. WORK UNIT NUMBER</b>

<b>7. PERFORMING ORGANIZATION NAME(S) AND ADDRESS(ES)</b> Tennessee Technological University 115 W. 10th Street Cookeville, TN 38501	<b>8. PERFORMING ORGANIZATION REPORT NUMBER</b>
---	---

<b>9. SPONSORING/MONITORING AGENCY NAME(S) AND ADDRESS(ES)</b> US Office of Naval Research 875 North Randolph Street Arlington, VA 22203-1995	<b>10. SPONSOR/MONITOR'S ACRONYM(S)</b> ONR
	<b>11. SPONSOR/MONITOR'S REPORT NUMBER(S)</b> 07PR05074-00

**12. DISTRIBUTION/AVAILABILITY STATEMENT**  
release for public distribution.

**13. SUPPLEMENTARY NOTES**

**14. ABSTRACT**  
This technical report (quarterly) details the work for Office of Naval Research (ONR) by Tennessee Tech. The goal of this project—jointly funded by ONR, NSF, and ARO—is to build a general purpose testbed with time reversal capability at the transmitter side. The envisioned application is for UWB sensors and tactical communications in RF harsh environments where multipath is rich and can be exploited through the use of time reversal. The report summarizes the results for both theoretical research and experimental testbed.

**15. SUBJECT TERMS**  
UWB, testbed, time reversal, range extension, sensors

<b>16. SECURITY CLASSIFICATION OF:</b>			<b>17. LIMITATION OF ABSTRACT</b> UU	<b>18. NUMBER OF PAGES</b> 24	<b>19a. NAME OF RESPONSIBLE PERSON</b> Francis Otuonye
<b>a. REPORT</b> U	<b>b. ABSTRACT</b> U	<b>c. THIS PAGE</b> U			<b>19b. TELEPHONE NUMBER (Include area code)</b> 931-372-3374

## Acknowledgment

This work has been improved by discussions with S. K. Das (ONR), B. M. Sadler (ARL), R. Ulman (ARO), and L. Lunardi (formerly with NSF). K. Currie (CMR, TTU) has provided a lot of support for this project. S. Parke (ECE, TTU) has supported our research in different ways. We also want to thank P. K. Rajan for helpful discussions.

## Executive Summary

This technical report (quarterly) details the work for Office of Naval Research (ONR) by Tennessee Tech. The goal of this project—jointly funded by ONR, NSF, and ARO—is to build a general purpose testbed with time reversal capability at the transmitter side. The envisioned application is for UWB sensors and tactical communications in RF harsh environments where multipath is rich and can be exploited through the use of time reversal. The report summarizes the results for each of two major tasks. Specifically, the project can be broken into

- Task 1—Theoretical Research
- Task 2—Experimental Testbed

In the part of theoretical research, the central result is to enable non-fading transmission through the use of time reversal. Next, the optimum pulse shaping is also considered, to extend the range. Finally, the chirp pulse waveform—practical and useful—is considered. This chirp UWB system, combined with time reversal, will be promising for long range sensor networking.

In the experimental testbed part, progress in the second generation of the testbed—with time reversal—is described. At this moment of writing, the first generation of the testbed—without time reversal—is working at the PI's Lab, over the air with a bandwidth of more than 500 MHz. The second generation will be built upon the first generation. The primary modification is the arbitrary modulation waveform generation at the transmitter.

# Contents

<b>1 Introduction</b>	<b>1</b>
<b>I Theoretical Research</b>	<b>5</b>
<b>2 Non-Fading Transmission</b>	<b>7</b>
2.1 Significance . . . . .	9
2.2 UWB Short Pulse Propagation . . . . .	9
2.2.1 Related Work . . . . .	9
2.2.2 Research Plan . . . . .	10
2.3 Time Reversal Modal Modulation . . . . .	10
2.3.1 Related Work . . . . .	10
2.3.2 Research Plan . . . . .	11
2.3.3 Preliminary Work . . . . .	14
<b>3 Optimum Transmission Waveform in Canonical Channels</b>	<b>27</b>
3.1 Introduction . . . . .	27
3.2 Pulse Distortion and Its Impact on UWB System Design . . . . .	28
3.2.1 Pulse Distortion Caused by Wide Bandwidth . . . . .	28
3.2.2 The Impact of Pulse Distortion on System Design . . . . .	29
3.3 Time Domain Channel Modeling . . . . .	30

3.3.1	Wedge Channel . . . . .	30
3.3.2	Rectangular Building . . . . .	31
3.3.3	Two Parallel Half Plane Model . . . . .	35
3.4	Time Domain Optimum Transmit Waveform Design . . . . .	36
3.4.1	Optimum Transmit Waveform for Distorted Channel . . . . .	36
3.4.2	Numerically Computing Eigenfunctions . . . . .	40
3.5	Numerical Results . . . . .	41
3.5.1	Calculation of Singularity in the Impulse Response of Wedge Diffraction . . . . .	41
3.5.2	Rectangular Building . . . . .	44
3.5.3	Two Parallel Half Planes Model . . . . .	45
3.5.4	Optimum Transmit Waveform Design . . . . .	46
3.6	Conclusion . . . . .	47
<b>4</b>	<b>Optimum Transmission Waveform in RF Harsh Environments</b>	<b>51</b>
4.1	Introduction . . . . .	51
4.2	Pulse Propagation in Rectangular Metal Cavity . . . . .	52
4.3	Time Reversal Transmission with Chirp Signaling . . . . .	53
4.3.1	Modal Modulation . . . . .	53
4.3.2	Time Reversal Modal Modulation . . . . .	56
4.3.3	Time Reversal Chirp System . . . . .	56
4.3.4	System Performance Comparison . . . . .	58
4.3.5	BER Performance for Time Reversal Chirp System . . . . .	63
4.4	Capacity in Rectangular Metal Cavity . . . . .	64
<b>5</b>	<b>Chirp UWB Systems</b>	<b>71</b>
5.1	Chirp UWB . . . . .	71
5.1.1	Challenges for IR-UWB . . . . .	71

<i>CONTENTS</i>	7
5.1.2 Range Extension . . . . .	71
5.1.3 NBI Suppression . . . . .	72
5.1.4 Other Advantages . . . . .	74
5.2 Advantages of CSS over DSSS . . . . .	77
5.3 Implementation . . . . .	77
5.4 The History of CSS . . . . .	78
5.5 A Time Reversed Chirp UWB—Forward Looking . . . . .	80
<b>6 UWB Channel Sounding</b>	<b>87</b>
6.1 Measurement Setup . . . . .	87
6.1.1 Time Domain Measurement Technique . . . . .	87
6.1.2 Frequency Domain Measurement Technique . . . . .	88
6.2 Measurement Examples . . . . .	90
6.2.1 Measurement for SISO Case . . . . .	90
6.2.2 Measurement for MIMO Case . . . . .	101
6.3 Conclusion . . . . .	105
<b>II Experimental Testbed</b>	<b>109</b>
<b>7 Overview of Testbed</b>	<b>111</b>
<b>8 System Design and Architecture</b>	<b>113</b>
8.1 Bandpass Time Reversal . . . . .	113
8.2 System Architecture . . . . .	114
8.3 Link Budget . . . . .	114
<b>9 RF Front-Ends and Mixed-Signal Stage</b>	<b>117</b>
9.1 Local Oscillator . . . . .	117

- 9.2 Modulator . . . . . 117
- 9.3 Digital to Analogy Converter . . . . . 118
- 9.4 MAX108 A/D . . . . . 120
- 9.5 SPI Control . . . . . 122
  
- 10 Digital Back-Ends . . . . . 129**

  - 10.1 System Control Flow . . . . . 129
  - 10.2 Filter Design . . . . . 129
    - 10.2.1 The Typical Methods for Filter Design . . . . . 129
    - 10.2.2 Quantization Consideration . . . . . 130

  
- 11 Graphic User Interface (GUI) between FPGA and PC . . . . . 137**

  - 11.1 Architecture . . . . . 137
  - 11.2 Communications between FPGA and host PC . . . . . 137
  - 11.3 Implementation . . . . . 138
  - 11.4 Application: BER Measurement . . . . . 139
  - 11.5 Application: FPGA Test . . . . . 141
  - 11.6 Limitations . . . . . 141

# Chapter 1

## Introduction

Civilian and naval vessels have long been potential targets for criminal and terrorism activities. There are concerns that terrorists can ship various types of weapons of mass destruction (WMD) to international ports using commercial ships and their cargoes. One of the major steps in preparedness for such danger is reliable wireless communications both between the boarding party as well as effective ship-to-ship and ship-to-shore communications once the first sign of threat is detected. This need is made possible, only recently [1], with the advent of revolutionary ultra-wideband (UWB) technology [2, 3, 4, 5, 6, 7, 8, 9]. This proposed research is motivated for RF challenged environments such as hospital, coal-mine, intra-ship, intra-vehicle, intra-engine, manufacturing plants, assembly lines, nuclear plants, body area network sensors surrounded by vehicles and tanks, etc.

In the part of theoretical research, the central result of this report is to enable non-fading transmission through the use of time reversal. Next, the optimum pulse shaping is also considered, to extend the range. Finally, the chirp pulse waveform—practical and useful—is considered. This chirp UWB system, combined with time reversal, will be promising for long range sensor networking.

In the experimental testbed part, progress in the second generation of the testbed—with time reversal—is described. At this moment of writing, the first generation of the testbed—without time reversal—is working at the PI's Lab, over the air with a bandwidth of more than 500 MHz. The second generation will be built upon the first generation. The primary modification is the arbitrary modulation waveform generation at the transmitter. It is expected that the receiver part of the second generation mainly reuses that of the first generation.

A key understanding is achieved so far: to further extend the range, the design of modulation waveforms must be carefully selected, according to some criteria. A good criterion is to maximize the signal to noise ratio (SNR) measured at the point after the matched filter. The frequency selectivity caused by the huge bandwidth (or pulse waveform distortion in the absence of multipath) will lead to the unique problem of pulse waveform optimization.

Another key understanding is that the effective channel enabled by time reversal can be treated “Non-Fading”—a dream for wireless engineers from half an century. The system design will greatly simplified under this non-fading framework. Although this theoretical breakthrough is reached, the design principle and system parameters to exploit this new phenomenon are far from clear.

One lesson learned from this research is that time reversal is basic, for a dense multipath environment—a continuous-time impulse response of extremely long delay spread.

The key UWB system design consists of two parts: (1) time reversal to deal with dense multipath; (2) the selection of UWB modulation pulse waveform—software defined or cognitive. From an information-theoretical viewpoint, the two parts as a whole form so-called “pre-coding”.

## Bibliography

- [1] A. Bordetsky, A. Dougan, and F. Nekoogar, "Network-Centric Maritime Radiation Awareness and Interdiction Experiments," *DOE Final Report, Lawrence Livermore National Laboratory*, pp. 1–20, 2006.
- [2] R. Scholtz, "Multiple Access with Time-hopping Impulse Modulator (invited paper)," in *MILCOM'93*, pp. 11–14, October 1993.
- [3] M. Win and R. Scholtz, "Ultra-wide Bandwidth Time-hopping Spread Spectrum Impulse Radio for Wireless Multiple-access Communications," *IEEE Trans. Commun.*, vol. 48, pp. 679–689, April 2000.
- [4] D. Porcino and W. Hirt, "Ultra-wideband Radio Technology: Potential and Challenges Ahead," *IEEE Commun. Mag.*, vol. 41, pp. 66–74, July 2003.
- [5] N. Belfari-Melazzi, M. Di Benedetto, M. Gerla, M. Win, and P. Withington, "Ultra-wideband Radio in Multiaccess Wireless Communications," *IEEE J. Select. Areas Commun., Editorial on Special Issue on UWB*, vol. 20, December 2002.
- [6] S. Roy, J. Foerster, V. Somayazulu, and D. Leeper, "Ultra-wideband Radio Design: The Promise of High-speed, Short Range Wireless Connectivity," in *Proceedings of the IEEE*, vol. 92, pp. 295–311, February 2004.
- [7] R. C. Qiu, R. Scholtz, and X. Shen, "Ultra-Wideband Wireless Communications— A New Horizon," *IEEE Trans. Veh. Technol., Editorial on Special Issue on UWB*, vol. 54, September 2005.
- [8] R. C. Qiu, H. P. Liu, and X. Shen, "Ultra-Wideband for Multiple Access," *IEEE Commun. Mag.*, vol. 43, pp. 80–87, February 2005.
- [9] X. Shen, M. Guizani, H. Chen, R. C. Qiu, and A. Molisch, "Ultra-wideband Wireless Communications," *IEEE J. Select. Areas Commun., Editorial on Special Issue on UWB*, vol. 24, 2nd Quarter 2006.



**Part I**

**Theoretical Research**

## Chapter 2

# Non-Fading Transmission

We propose a time reversal system paradigm for localization, communication, and networking. UWB transmission may lead to (almost deterministic) no-fading communication—a dream for wireless industry over half a century—to enable some applications, for which narrowband techniques may fail.

The transceiver structure has been the central topic in the UWB community. The PI's research roughly follows this trend. First, the RAKE structure [10, 11, 12, 13, 14, 15, 16, 17] is used, and found too costly—after a long painful search, due to the large number of paths (fingers) and timing requirement [6, 7, 8, 9]. In particular, pulse waveform distortion will cause a design problem, first recognized (one decade ago) by the PI based on his channel model [10, 11, 12, 13, 14, 15, 16, 17], which was accepted into IEEE standard [18]. The orthogonal frequency division multiplexing (OFDM) system [19, 20] is slightly more complicated than the RAKE system. Secondly, the transmitted reference (TR) structure [21, 22, 23, 24, 25, 26, 27, 28, 29, 30, 31, 32] is used to reduce the timing requirement, and avoid the need of channel estimation. Thirdly, for sensor networks of low-cost and low power, non-coherent energy detection (analog frontend) [33, 34, 35, 36, 37, 38, 39, 40, 41, 42, 43] is preferred to the TR, although both systems are adopted in IEEE 802.15.4a. Inter-symbol-interference (ISI) limits the achievable data rates of the TR and energy-detection systems.

Fourth, for data rate higher than the TR and energy-detector, time reversal at the transmitter—perhaps viewed as continuous-time, channel-matching filter, or generalized RAKE [17] at the transmitter—is combined with transmitted reference structure [44, 45, 46, 47], and non-coherent energy detection [48, 49, 50]. It is even extended to the UWB multiple input and multiple output (MIMO) system [8, 52, 53, 54, 55, 56, 57, 58]. Time reversal has been used in UWB radio [59, 60, 61, 62, 63, 64, 65, 66, 67, 68, 69, 70, 71, 72, 73]. It is used extensively in acoustics by Fink's team [74, 75, 76, 77, 78, 79, 80, 81, 82, 83, 84, 85, 86], and later to underwater acoustic communications mainly by Kuperman's team [87, 88, 88, 89, 90, 91, 92, 93, 94, 95, 96, 97, 98, 99, 100, 101, 102, 103] to deal with rich multipath phenomenon which is similar to UWB. It has been first used in wire-line communication by Bell Labs [104, 105] and IBM [106]. In spirit, time reversal is similar to the classical phase conjugation concept in optics [107, 108, 109], and retro-directive array in microwaves [110, 111, 112, 113, 62, 114, 115, 116, 117, 118, 119, 120, 121, 122, 123, 124, 125, 126]. The objective of all the above schemes is to exploit the channel itself as part of channel-matched transceiver. This principle has the advantage of real-time, since the operation is finished in a continuous-time, analog form, in contrast to the algorithm convergence of the discrete-time form used by such systems as equalizers [127, 128, 129, 130, 131, 132, 133]. A key observation [53, 52, 134, 135, 136] has been recognized that, if time reversal is always used at the transmitter side, no fading needs be explicitly addressed in a UWB impulse radio. This effect derives from the (multipath and frequency) diversity gain offered by the huge signal

bandwidth. The proposed research is based on this key effect—to exploit multipath and signal bandwidth (or pulse duration).

With time reversal—of the channel impulse response (CIR) illustrated in Fig. 4.3—at the transmitter side, the effective channel between a pair of a modulation waveform and a demodulation waveform is the autocorrelation of the CIR—illustrated in Fig. 2.1(c). This new channel is much more stationary than its old counterpart [134, 135]. An analogy is as follows. If the CIR is a realization of a random process—the first order statistics is changing rapidly from one realization to another realization, the second order statistics is much more reliable and stable. Its time-varying property highly relies on the number of multipath which, in return, is determined by the pulse signal bandwidth, as a function of RF environments. The significance of this proposal is to convert the conventional CIR problem into a new, autocorrelation problem, and systematically establish a theoretical framework based on this principle. This understanding is in parallel with the historical development of the white Gaussian noise theory in early 1950s [137, 138, 139, 140, 141, 142, 143, 144, 145, 146, 147, 148, 149, 150, 151, 152]: what really matters is not the CIR's first order statistics, but its second order statistics!

Once the key conceptual breakthrough is made, the formulation of this idea in a mathematical framework is relatively straightforward: The system model consists of a linear-time-invariant (LTI), dispersive channel with additive (Gaussian or non-Gaussian) noise and interference [20]. We have converted a *time-varying*, dispersive (wireless) channel into a *time-invariant*, dispersive channel—that is much easier to handle. An exhaustive research has been done regarding this classical system model [153, 154, 19, 155, 156, 133, 157, 158, 159, 160], since it is the model used for wire-line [153, 156, 133, 157, 19]—DSL and VDSL [19]—for which the Bell systems have the deep-packet resources [127, 128, 129, 130, 131, 132, 133]. The well-understood model is an excellent tool for the proposed research, and paves the way for our next engineering breakthrough. As one example, the modal modulation used by Holsinger (1964) [153] is a starting point for our new adventure. Time reversal is used at the transmitter. The so-called time reversal modal modulation is proposed here. Our system model consists of an *effective* LTI, dispersive channel<sup>1</sup> with additive (Gaussian or non-Gaussian) noise and interference. The simplified mathematical framework will lead to a better design, since the dimensions of bandwidth and multipath can be focused on, through the effective LTI channel. The unified theory links up all the fundamental system parameters such as bandwidth, multipath, and space, and box them into an effective CIR. In practice, all we only need to do is to replace the LTI model of the classical theory with our effective LTI model: it is that simple! Now, the open question is to spell out all the necessary conditions—such as pulse duration and waveform as a function of RF environments—for this new framework to be valid.

Built upon the above new understanding, theory and prototype testbed are proposed to test and validate this new system design paradigm. A 5 GHz UWB radio testbed has a special meaning in the context of the new paradigm, since, for indoor channels, 2 GHz has been found to be the critical bandwidth, beyond which the effective channel can be considered as “deterministic (non-fading) in practice, provided receivers exploiting the full channel energy are employed” quoted from [161]<sup>2</sup>. Mixed signal processing is the bottleneck. To overcome this problem, a new patented design [162, 163] from radar community can be used.

Similar to short pulse radar [164, 165, 166, 167, 168, 169], waveform optimization for detection is a basic problem. For UWB MIMO, we have derived a formulation based on the eigenfunctions of the integral equation. This problem may be related to the multiuser MIMO problem that can be effectively solved via a convex optimization [170, 171, 172, 173, 174, 175]. Bear in mind the fact that, since a practical UWB system works in a very low SNR range, optimization for detection (maximizing SNR) is the primary problem—not the one to maximize the mutual

<sup>1</sup>If the CIR of the LTI, dispersive channel is  $h(\tau)$ , then the CIR of the effective LTI channel is  $h(-\tau) * h(\tau)$  where “\*” is the linear convolution.

<sup>2</sup>In the long process of studying time reversal, the PI's team recognized this result, independently of [161].

information.

## 2.1 Significance

Time-varying fading is the hallmark of narrowband wireless communications. It seems safe to say that almost all the major progress made in wireless industry, such as MIMO and OFDM, has been motivated to exploit fading through (multipath and spatial) diversity. Fading caused by multipath, however, may be negligible for UWB communication using a sufficiently large signal bandwidth, e.g. 2 GHz for indoor [161]. The proposed research is motivated to explore the dimensions of bandwidth and multipath in real-life environments—an issue unique to UWB impulsive radio. The number of paths is roughly proportional to the bandwidth, when it is below 2 GHz for indoors. In particular, an extremely large number of (time-invariant) resolvable multiple paths—treated as continuous-time, dense waveform over a duration of 800 ns, see Fig. 4.3—will be encountered in real-life applications [1, 176, 177, 178, 179], and will be investigated as an example. When fading can be ignored in practice, the mathematical tools are simplified to a level accessible by engineers with only undergraduate education [20, 180]. The body of knowledge based on fading communication mathematics [181, 182]—generally very difficult for engineers and students, even at a graduate level—can be circumvented, perhaps for the first time, in the wireless communication curriculum. The new mathematical framework will pave the way for a novel system paradigm and a new understanding of the mystic multipath.

## 2.2 UWB Short Pulse Propagation

The non-fading (deterministic) treatment of a wireless channel is based on the experimental study of the UWB propagation channel. There is a class of extremely rich multipath environments. This class of channel has been recently investigated by the PI's team [53, 52, 134, 56, 57, 58, 135]. It is found that the number of paths is much larger than that of the office environment—compare Fig. 4.3 and Fig. 2.1(d). Communications and networking in confined metal environments [134, 135, 57] in this class—Fig.2.1(a)—is motivated for applications such as intra-ship [1], intra-vehicle [176], intra-engine [52], manufacturing plants, assembly lines, nuclear plants, body area network sensors surrounded by vehicles and tanks, etc.

### 2.2.1 Related Work

One difficult problem is communications over such RF challenged environments as a confined metal box. Narrow band wireless technologies have proved ineffective in these environments, due to resonance caused by the metal walls [177, 178, 176, 179]. Chirp-like signals are observed in a jet engine [178]. Only recently [1], this problem has the promise to be solved with the advent of UWB technology. Lawrence Livermore National Laboratory (LLNL) just demonstrated UWB transmission in a ship in 2006 [1]. The PI's team demonstrated this in an engine [52], and an metal cavity [134, 135, 57]. Strict physics for the latter case is given by L. B. Felsen [177] who introduced the UWB problem to the PI in 1993, and W. Geyi [179] who was introduced to this problem by the PI in 2007 IEEE APS conference. In general, this problem is open, especially in the context of non-fading transmission. The mobility of antennas needs to be considered.

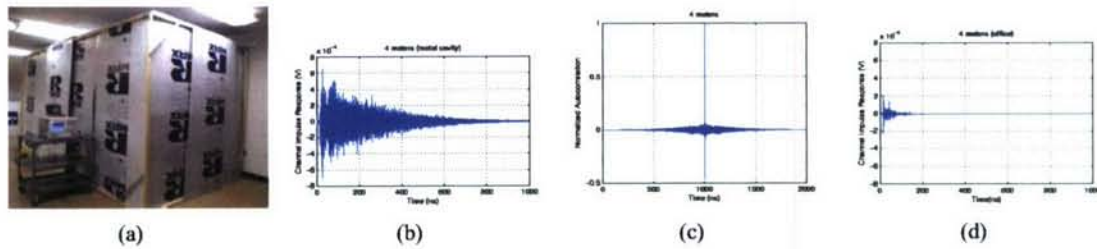


Figure 2.1: UWB short pulse propagates in RF harsh environments. (a) Rectangular metal cavity; (b) CIR in a rectangular metal cavity. The pulse has its spectrum from 3 GHz to 10 GHz. (c) autocorrelation of CIR in (b); (d) CIR in an office environment. The experimental setup is identical to that of (b).

## 2.2.2 Research Plan

The central task of the proposed research in this context is to validate the system design assumption, and parameterize the effective channel  $h(-\tau) * h(\tau)$ . When the testbed is available, the field test will be carried out, to demonstrate the system principle in different RF harsh environments. A lot of new experiments are needed, in the process of the proposed research. Fortunately, the PI, a veteran in channel modeling, has the expertise and the required equipment to perform these tasks.

### Preliminary Work

The PI has accumulated more than one decade's experience in this channel modeling area. His Lab has two the-state-of-the-art channel sounding systems for UWB communication. The time domain system Fig. 2.3(b) is based on digital sampling oscilloscope (DSO), Tektronix TDS 7000E3. The time domain sounder has the capability to handle the MIMO channel sounding—not using virtual array approach. The frequency domain system uses a vector network analyzer (VNA), Agilent N5230A (300kHz-13.5GHz). These sounders helped to produce two PhD degrees, five MS degrees, and five undergraduates used them through NSF's REU (Research for Undergraduates) program.

Fig. 2.1 illustrates a new phenomenon—an extremely long train of multipath echoes. Fig. 4.3 contains much more paths than that of Fig. 2.1(d). The measurement is performed using frequency domain technique to analyze the characteristics of the UWB channel in the confined metal environment. The rectangular confined metal cavity in Fig. 2.1(a) measures 16 feet by 8 feet by 8 feet. The materials of the walls are aluminum. The sounding is carried out by sweeping a set of narrowband sinusoid signals (tones) through a wide frequency band. The data of channel frequency response is collected using the VNA based channel sounder in the PI's lab. The VNA sweeps from 3 GHz to 10 GHz using 7001 points with frequency step of 1 MHz. The power of each tone is 10dBm.

## 2.3 Time Reversal Modal Modulation

### 2.3.1 Related Work

When time reversal is used, the effective channel is regarded as deterministic (no-fading) channel. The proposed time reversal modal modulation is different from OFDM in several ways. First, OFDM is a special limit of this modulation, when the pulse duration becomes infinite. Most UWB pulses are short in duration, similarly to UWB

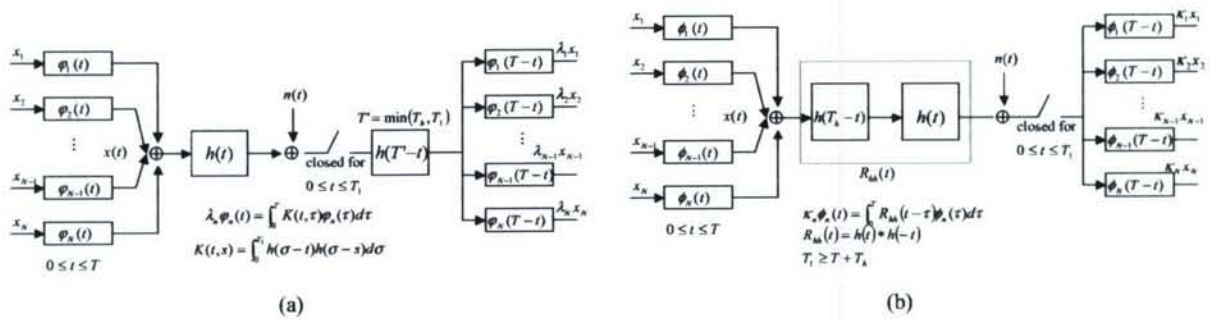


Figure 2.2: Time reversal modal modulation is proposed to simplify the transceiver complexity. The channel matched filter  $h(T-t)$  is moved to the transmitter side. The self-reproducing  $\phi_n(t)$  can be defined.

radar. Secondly, OFDM can be viewed as multiple tones (multiple carriers), implying each tone assumes a single frequency value. This is not true for the proposed modulation. The effective channel can be diagonalized by its eigenfunctions (eigen-waveforms)—changing with RF environments, similar to the radar problem [165, 166, 167, 168, 169]. These eigen-waveforms are used for modulation, and may be wideband (say 100 MHz). Thirdly, the pros and cons of this modulation relative to OFDM are unclear, in the context of system implementation.

2.3.2 Research Plan

The proposed system formulation for optimum modulation waveform is based on two assumptions:

- The channel is linear, time-invariant (LTI) for every symbol transmission.
- The spectra of noise and interference signals are available at both the transmitter and receiver.

The first assumption has been established recently by the PI’s group, through experiments [53, 52, 134, 56, 57, 58, 135], in the framework of time reversal. Knopp’s team reaches the same result [161], from a channel modeling view. The second assumption is the practice in current industry.

The mathematical formulation for the so-called modal modulation traces back to the well known work of Holsinger (1964) at MIT [153, 19], originally motivated for telephone line—widely regarded as the first work for OFDM—regarding optimum modulation for a deterministic, dispersive, LTI channel with memory. It is found that OFDM is an asymptotic case of Holsinger’s modal modulation, when the duration of the modulation pulse goes infinite. For a narrowband technique, the modulation pulse is a sinusoidal pulse of *infinite* duration. Since modal modulation is optimum—to be made more clear later, OFDM is accepted widely without question. With the advent of UWB devices, we must reexamine the practice for narrowband techniques. With the aid of the effective channel introduced in Section 2, the mathematical framework of Holsinger’s is sufficient: Our task is to replace his LTI channel model with the effective channel model—comparing Figs. 4.6 and 4.7.

It is found recently by the PI’s team that *modal modulation is not equivalent to OFDM for UWB modulation pulses of short finite duration*. It appears that this finding requires a paradigm shift in that UWB transmission does not have to use a sinusoidal pulse!

**Single Input and Single Output (SISO)** Let us fix some notations for more precise discussions about Holsinger’s modal modulation, illustrated in Fig. 4.6, for colored noise and an arbitrary, finite observation interval. If  $x(t)$  is

the input to the LTI channel—based on assumption 1—with channel pulse response  $h(t)$ . The symbol duration of  $x(t)$  is  $[0, T_S]$ , and the arbitrary, finite waveform duration of  $x(t)$  is  $[0, T]$ —which implies that  $x(t)$  is equal to zero if  $t$  is between  $T$  and  $T_S$ . The output waveform  $r(t) = \int_0^T x(\tau)h(t-\tau) d\tau$ ,  $0 \leq t \leq T_1$ , for an arbitrary, finite observation interval  $[0, T_1]$ . A colored noise with a spectral density  $N(f)$ —based on assumption 2—defines a kernel function  $K_1(t, s)$  by

$$\int_0^{T_1} R_n(t-\sigma)K_1(\sigma, s)d\sigma = \delta(t-s), \quad 0 \leq t, s \leq T_1 \quad (2.1)$$

where  $R_n(\tau) = \int_{-\infty}^{\infty} N(f)e^{j\omega\tau} df$  defines a function  $K(t, s)$  by

$$K(t, s) = \int_0^{T_1} \int_0^{T_1} h(\sigma-t)K_1(\sigma, s)h(\rho-t)d\sigma d\rho \quad 0 \leq t, s \leq T \quad (2.2)$$

and define a possibly infinite-size set of eigenfunctions,  $\varphi_n(t)$ , through a integral equation [183, 184]

$$\lambda_n \cdot \varphi_n(t) = \int_0^T K(t, \tau)\varphi_n(\tau)d\tau, \quad 0 \leq t \leq T \quad (2.3)$$

That is a function  $\varphi_n(t)$  that when convolved with  $K(t, s)$  over the interval  $[0, T]$  reproduces itself, scaled by a constant  $\lambda_n$ , called eigenvalue. The  $\varphi_n(t)$   $n = 1, 2, \dots, \infty$  form a set of complete, orthonormal basis functions, so  $x(t)$ —an arbitrary modulation waveform of finite duration  $T$ —can be expanded in terms of  $x(t) = \sum_{n=0}^{\infty} x_n \varphi_n(t)$ ,  $0 \leq t \leq T$  and  $x_n = \int_0^T x(t) \varphi_n(t) dt$ ,  $n = 1, 2, \dots, \infty$ , so the energy of the transmitted signal waveform,  $E_t = \int_0^T |x(t)|^2 dt$ , can be expressed as  $E_t = \sum_{n=1}^{\infty} x_n^2$ . When white Gaussian noise is assumed, a simple matched filter can be used: The output signal to noise ratio (SNR) is  $2E/N_0$ , where  $E = \sum_{n=1}^{\infty} \lambda_n x_n^2$  and  $N_0/2$  is the double sided noise spectral density. So the probability of error for the detector is given by

$$P_e = \frac{1}{\sqrt{2\pi}} \int_{\sqrt{2E/N_0}}^{\infty} \exp(-\frac{1}{2}x^2) dx \quad (2.4)$$

In order to minimize  $P_e$ , SNR should be maximized. Since, by convention,  $\lambda_1 \geq \lambda_2 \geq \lambda_3 \geq \dots$ , if the energy of  $x(t)$  is fixed, maximizing  $E$  means  $x(t) = x_1 \varphi_1(t)$ —the optimal modulation waveform. So, the maximum SNR can be expressed as  $\text{SNR}_{\max} = \frac{2\lambda_{\max} x_1^2}{N_0}$  with the maximum eigenvalue  $\lambda_{\max} = \lambda_1$  for our above notation. This is ideal for range extended UWB sensors—the primary goal of this project.

From another (capacity) point of view, the modal modulation system have many parallel orthogonal channels, and each channel corresponds to one eigenfunction  $\varphi_n(t)$ . We can use the classical water filling scheme to calculation coefficients  $x_n$   $n = 1, 2, \dots, \infty$ , based on the energy constraint of transmitted signal  $x(t)$ .

A new time reversal modal modulation, illustrated in Fig. 4.7, is proposed to simplify the transceiver complexity. The  $h(T_h - t)$ , time reversal filter, is moved to the transmitter side. Without loss of generality, we use white Gaussian noise as an example to illustrate the concept. Similarly to the modal modulation, the self-reproducing eigenfunctions  $\phi_n(t)$  with eigenvalues  $\kappa_n$  illustrated in Fig. 4.7 can be defined as

$$\kappa_n \cdot \phi_n(t) = \int_0^T R_{hh}(t-\tau)\phi_n(\tau)d\tau, \quad 0 \leq t \leq T \quad (2.5)$$

where  $R_{hh}(t) = h(t) * h(-t)$ . There are four proposed tasks in the SISO system:

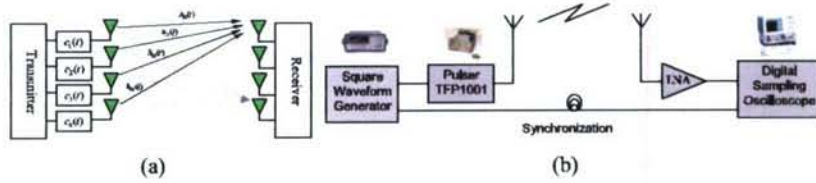


Figure 2.3: UWB MIMO System. (a) MIMO System; (b) Channel Sounding.

- **Concept proof** The no-fading mathematic framework needs to be proved, and made more precise, by spelling out system parameters such as bandwidth and waveform. Real-world experimental data will be used for this purpose.
- **Optimization of modulation waveforms over different RF environments** This requires modulation waveform optimization, as a function of waveform duration  $T$ , defined in Eq. (4.5).
- **Interference spectrum estimation and its impact** Cognitive radio must have the function of “detect and avoid” other narrowband radios such as Wi-Fi and WiMax. This is a challenging problem, even for a narrowband radio. One simple method is to estimate the background interference over the ultra-wide bandwidth—say 5 GHz—and optimize the waveform, based on the key equation (4.5).

**Multiple Input and Multiple Output (MIMO)** Let us consider the system block diagram of the time-reversed impulse MIMO in Fig. 2.3. Let us denote  $h_{nm}(t)$  the channel impulse response (CIR) relating the  $m$ -th element at the transmitter to the  $n$ -th element at the receiver. The set of impulse responses is called the **propagation operator**. If pulse waveform vector  $\mathbf{a}(t) = [a_1(t), a_2(t), \dots, a_M(t)]^\dagger$  of finite duration  $T_1$  is sent from the transmitter, then the vector  $\mathbf{b}(t) = [b_1(t), b_2(t), \dots, b_N(t)]^\dagger$  is received at the receiver, for an arbitrary, finite observation interval  $[0, T_2]$ . The superscript “ $\dagger$ ” represents the conjugate transpose (Hermitian) of a vector or matrix. It follows that

$$\mathbf{b}(t) = \mathbf{H}(t) * \mathbf{a}(t), \quad 0 \leq t \leq T_2 \quad (2.6)$$

where  $\mathbf{H}(t)$  is the matrix of  $N \times M$  with elements of  $h_{nm}(t)$ . The notation of “ $*$ ” represents element-by-element convolution. On the other hand, due to the spatial reciprocity, if one sends a signal  $e_n, n = 1, \dots, N$  from the receive array, the signal  $f_m(t), m = 1, \dots, M$  is obtained in the transmit array. Defining column vectors  $\mathbf{e}$  and  $\mathbf{f}$  as  $\mathbf{a}$  and  $\mathbf{b}$ , respectively, it follows that

$$\mathbf{f}(t) = \mathbf{H}^\dagger(t) * \mathbf{e}(t), \quad 0 \leq t \leq T_2 \quad (2.7)$$

As a consequence,  $\mathbf{H}(t)$  permits one to calculate the forward propagation of impulses from the transmit array to the receive array, while  $\mathbf{H}^\dagger(t)$  the backward propagation from the receive array to the transmit array. If the time reversed matrix  $\mathbf{H}^\dagger(-t)$  is used as part of the precoding matrix—in analogy with Fig. 4.7, the equivalent matrix channel is

$$\mathbf{R}_{\text{HH}}(t) = \mathbf{H}(t) * \mathbf{H}^\dagger(-t) \quad (2.8)$$

Eq. (2.8) will contain the temporal-spatial focusing—unique to UWB pulse signals. One objective of UWB MIMO is to enable non-fading transmission. Cooperative distributed antennas can be used. MIMO multiuser networking is our future research focus, in the framework of time reversal.

In analogy with (4.14), the self-reproducing eigenfunction vector  $\boldsymbol{\theta}_n(t)$  can be defined as

$$\kappa_n \cdot \boldsymbol{\theta}_n(t) = \int_0^T \mathbf{R}_{\text{HH}}(t - \tau) \boldsymbol{\theta}_n(\tau) d\tau, \quad 0 \leq t \leq T \quad (2.9)$$

Once Eq. (2.9) is solved, the rest of signal processing is similar to the SISO system above. An alternative approach to solve for optimum MIMO waveform may use the recent result of information theory, based on convex optimization [170, 171, 172, 173, 174, 175]. There are three proposed tasks in the MIMO system:

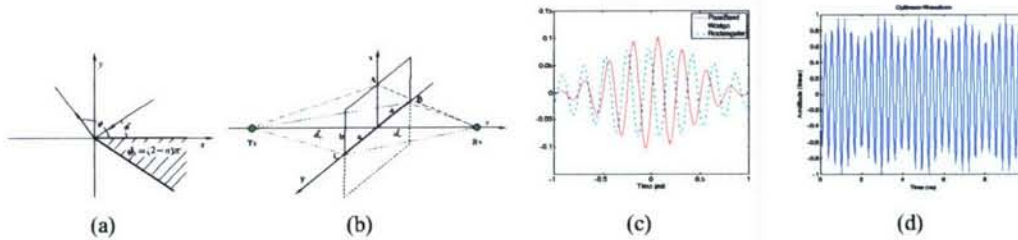


Figure 2.4: Comparison of modulation waveforms for optimum modal modulation for different environments. (a) wedge (street corner); (b) rectangular plate (building); (c) waveform comparisons: A passband channel has an ideal passband filter as its frequency response; (d) optimum modal modulation waveform calculated using CIR of Fig. 4.3

- **Concept proof** Similar to the SISO system, experimental and theoretical work is required to extend the framework to the MIMO system. The focus is on the validity of the framework, by considering multiple antennas. The PI's lab has two channel sounding systems (in both time—in Fig. 2.3(b)—and frequency domain) for this purpose.
- **Spatio-temporal optimization** Optimization of waveform is required, by taking into account the space dimension, through Eq. (2.9).
- **Spectrum estimation** Sensing the spectrum is a critical part of cognitive radio. Algorithms for spectrum estimation need be investigated.

### 2.3.3 Preliminary Work

Compared with the benchmark of the time reversal chirp system, there is a big room for optimization (Table ??)—as a function of waveform duration—by using time reversal modal modulation system. This has been justified from two different metrics. Different propagation environments define different optimum modulation waveforms, as illustrated in Fig. 2.4.

*From Detection Point of View* The SNR after matched filter in the receiver side is the metric to determine the system performance.

*From Data Rate Point of View* In the time reversal modal modulation system, there are many parallel orthogonal channels, and each channel corresponds to the orthonormal eigenfunction  $\phi_n(t)$  and eigenvalue  $\kappa_n$  from Eq. 4.14. One waveform design example of the  $\phi_n(t)$  is given in Fig. 2.4. We assume  $\kappa_1 \geq \kappa_2 \geq \kappa_3 \geq \dots$ . Meanwhile, the bits transmitted in these different channels are assumed to be totally independent. If L-level pulse amplitude modulation (PAM) is considered, there are L equally likely amplitude values. In time reversal system, the transmitter waveform filter is  $G_T(t)$ , while the time reversal filter is  $h(-t)$ . In the time reversal chirp system,  $G_T(t)$  is chirp waveform. When BER  $P_b$  is set to  $10^{-4}$  and the same PAM constellation is considered, e.g., for  $L = 8$ , the data rate gap (in dB) between time reversal modal modulation system and time reversal chirp system is shown to 7.5, 11.1, 13.9, for the waveform duration of T (in ns) equal to 1, 10, 100.

## Bibliography

- [1] A. Bordetsky, A. Dougan, and F. Nekoogar, "Network-Centric Maritime Radiation Awareness and Interdiction Experiments," *DOE Final Report, Lawrence Livermore National Laboratory*, pp. 1–20, 2006.
- [2] R. Scholtz, "Multiple Access with Time-hopping Impulse Modulator (invited paper)," in *MILCOM'93*, pp. 11–14, October 1993.
- [3] M. Win and R. Scholtz, "Ultra-wide Bandwidth Time-hopping Spread Spectrum Impulse Radio for Wireless Multiple-access Communications," *IEEE Trans. Commun.*, vol. 48, pp. 679–689, April 2000.
- [4] D. Porcino and W. Hirt, "Ultra-wideband Radio Technology: Potential and Challenges Ahead," *IEEE Commun. Mag.*, vol. 41, pp. 66–74, July 2003.
- [5] N. Blefari-Melazzi, M. Di Benedetto, M. Gerla, M. Win, and P. Withington, "Ultra-wideband Radio in Multiaccess Wireless Communications," *IEEE J. Select. Areas Commun., Editorial on Special Issue on UWB*, vol. 20, December 2002.
- [6] S. Roy, J. Foerster, V. Somayazulu, and D. Leeper, "Ultra-wideband Radio Design: The Promise of High-speed, Short Range Wireless Connectivity," in *Proceedings of the IEEE*, vol. 92, pp. 295–311, February 2004.
- [7] R. C. Qiu, R. Scholtz, and X. Shen, "Ultra-Wideband Wireless Communications— A New Horizon," *IEEE Trans. Veh. Technol., Editorial on Special Issue on UWB*, vol. 54, September 2005.
- [8] R. C. Qiu, H. P. Liu, and X. Shen, "Ultra-Wideband for Multiple Access," *IEEE Commun. Mag.*, vol. 43, pp. 80–87, February 2005.
- [9] X. Shen, M. Guizani, H. Chen, R. C. Qiu, and A. Molisch, "Ultra-wideband Wireless Communications," *IEEE J. Select. Areas Commun., Editorial on Special Issue on UWB*, vol. 24, 2nd Quarter 2006.
- [10] R. C. Qiu, *Digital Transmission Media: UWB Wireless Channel, MMIC, and Chiral Fiber*. PhD thesis, Polytechnic University, Brooklyn, NY, January 1996.
- [11] R. C. Qiu and I. T. Lu, "Multipath Resolving with Frequency Dependence for Broadband Wireless Channel Modeling," *IEEE Trans. Veh. Tech.*, vol. 48, pp. 273–285, January 1999.
- [12] R. C. Qiu, "A Study of the Ultra-wideband Wireless Propagation Channel and Optimum UWB Receiver Design (Part 1)," *IEEE J. Selected Areas in Commun. (JSAC), the First JASC special issue on UWB Radio*, vol. 20, pp. 1628–1637, December 2002.

- [13] R. C. Qiu, "A generalized time domain multipath channel and its application in ultra-wideband (uwb) wireless optimal receiver design: Part 2 wave-based system analysis," *IEEE Trans. Wireless Communications*, vol. 3, pp. 2312–2324, November 2004.
- [14] R. C. Qiu, "A Generalized Time Domain Multipath Channel and Its Application in Ultra-Wideband (UWB) Wireless Optimal Receiver Design: Part 3 System Performance Analysis," *IEEE Trans. Wireless Communications*, vol. 5, no. 10, 2006. to appear.
- [15] R. C. Qiu, "Optimum and Sub-Optimum Detection of Physics-based UWB Signals," *Dynamics of Continuous, Discrete and Impulsive Systems—An International Journal for Theory and Applications (Series B)*, vol. 12, no. 3, pp. 321–334, 2005.
- [16] R. C. Qiu, C. Zhou, and Q. Liu, "Physics-Based Pulse Distortion for Ultra-Wideband Signals," *IEEE Trans. Veh. Tech.*, vol. 54, September 2005.
- [17] R. C. Qiu, J. Q. Zhang, and N. Guo, "Detection of Physics-Based Ultra-Wideband Signals Using Generalized RAKE and Multi-User Detection (MUD)," *IEEE J. Selected Areas in Commun. (JSAC), the Second JSAC special issue on UWB Radio*, vol. 24, May 2006.
- [18] A. Molisch, "Status of models for UWB propagation channel," *IEEE 802.15.4a Channel Model (Final Report)*, August 2004.
- [19] J. M. Cioffi, *Digital Communications*, ch. 4. <http://www.stanford.edu/group/cioffi/>, 2007. Course Reader.
- [20] S. Haykin, *Communication Systems, 4th Edition*. New York: John Wiley, 2001.
- [21] R. Hoctor and H. Tomlinson, "An Overview of Delay-hopped, Transmitted-reference RF Communications," *GE Research and Development Center, Technical Information Series*, pp. 1–29, 2002.
- [22] R. Hoctor and H. Tomlinson, "Delayed-hopped Transmitted-reference RF Communications," in *IEEE Conf. Ultra Wideband Systems and Technologies (UWBST)*, pp. 265–269, 2002.
- [23] E. Hoctor, "Multiple Access Capacity in Multipath Channels of Delayed-Hopped Transmitted-Reference UWB," in *2003 IEEE Conference on UWBST*, pp. 16–19, November 2003.
- [24] J. Pierce and A. Hopper, "Nonsynchronous Time Division Withholding and With Random Sampling," in *Proc. IRE*, pp. 1079–1088, September 1952.
- [25] C. Rushforth, "Transmitted-reference Techniques for Random or Unknown Channel," *IEEE Trans. on Information Theory*, vol. 10, pp. 39–42, January 1964.
- [26] R. Gagliardi, "A Geometric Study of Transmitted Reference Communication Systems," *IEEE Trans. Comm. Tech.*, vol. 12, pp. 118–123, December 1964.
- [27] G. Hingorani and J. Hancock, "A Transmitted Reference System for Communication in Random or Unknown Channels," *IEEE Trans. Comm. Tech.*, vol. 13, pp. 293–301, September 1965.
- [28] J. Choi and W. Stark, "Performance of Ultra-Wideband Communications with Suboptimal Receivers in Multipath Channels," *IEEE J. Select. Areas Commun.*, vol. 20, pp. 1754–1766, December 2002.
- [29] Q. Trindade, A.-J. Dang, and van der Veen, "Signal Processing Model for a Transmit-reference UWB Wireless Communication System," in *2003 IEEE Conference on UWBST*, November 2003.

- [30] H. Zhang and D. Goechel, "Generalized Transmitted-reference UWB Systems," in *2003 IEEE Conference on UWBST*, pp. 147–151, November 2003.
- [31] Y. Chao and R. Scholtz, "Optimal and Suboptimum Receivers for Ultra-wideband Transmitted Reference Systems," in *Proc. IEEE GLOBECOM'03*, pp. 759–763, December 2003.
- [32] D. Goeckel and Q. Zhang, "Slightly Frequency-shifted Transmitted-reference Ultrawideband Radio: TR-UWB without the Delay Element," in *IEEE MILCOM*, October 2005.
- [33] Y. Souilmi and R. Knopp, "On the Achievable Rate of Ultra-Wideband Systems in Multipath Fading Environments," in *IEEE ISIT 2003*, p. 387, June 2003.
- [34] Y. Souilmi and R. Knopp, "On the Achievable Rate of Ultra-Wideband Systems in Multipath Fading Environments," in *Proc. IEEE ICC'03*, vol. 5, pp. 3530–3534, May 2003.
- [35] M. Weisenhorn and W. Hirt, "Robust Noncoherent Receiver Exploiting UWB Channel Properties," in *Proc. IEEE Joint UWBST & IWUWBS*, pp. 156–160, 2004.
- [36] M. Oh, B. Jung, H. R., and D. Park, "A New Noncoherent UWB Impulse Radio Receiver," *IEEE Commun. Letters*, vol. 9, no. 2.
- [37] Oppermann, "UWB Wireless Sensor Networks: UWEN—A Practical Example," *IEEE Commun. Mag.*, vol. 42, pp. S27–S32, December 2004.
- [38] L. Stoica, A. Rabbachin, and L. Opperman, "An Ultra Wideband System Architecture for Wireless Sensor Networks," *IEEE Trans. Veh. Technol.*, vol. 54, September 2005.
- [39] S. Dubouloz, B. Denis, S. Rivaz, and L. Ouvry, "Performance Analysis of LDR UWB Non-coherent Receivers in Multipath Environments," in *IEEE International Conference on Ultra-Wideband*, pp. 491–496, September 2005.
- [40] M. Sahin and H. Arslan, "Inter-symbol Interference in High Data Rate UWB Communications Using Energy Detector Receivers," in *IEEE International Conference on Ultra-Wideband*, pp. 176–179, September 2005.
- [41] M. Weisenhorn and W. Hirt, "ML Receiver for Pulsed UWB Signals and Partial Channel State Information," in *IEEE International Conference on Ultra-Wideband*, pp. 180–184, September 2005.
- [42] F. Troesch, F. Althaus, and A. Witteneben, "Modified Pulse Repetition Coding Boosting Energy Detector Performance in Low Data Rate Systems," in *IEEE International Conference on Ultra-Wideband*, pp. 508–513, September 2005.
- [43] S. Jung and D. Park, "Design of Preamble Signal for Synchronization with UWB Non-Coherent Energy Detection Receiver," in *IEEE International Conference on Ultra-Wideband*, pp. 464–468, September 2005.
- [44] S. Kaza, *Performance Analysis of Ultra-wideband Transmitted Reference System and Enhancement Techniques: A Thesis Presented to the Faculty of the Graduate School, Tennessee Technological University*. PhD thesis, Tennessee Technological University, 2004.
- [45] N. Guo, R. C. Qiu, and B. M. Sadler, "An Ultra-Wideband Autocorrelation Demodulation Scheme with Low-Complexity Time Reversal Enhancement," in *IEEE Military Communications Conference*, vol. 5, pp. 3066–3072, October 2005.
- [46] N. Guo and R. C. Qiu, "Improved Autocorrelation Demodulation Receivers Based on Multiple-symbol Detection for UWB Communications," *IEEE Trans. Wireless Communications*, to appear.

- [47] N. Guo, R. C. Qiu, and B. M. Sadler, "A Transmitted Reference UWB System with Time Reversal Based on Experimental UWB Channel Measurements," *IEEE Trans. Wireless Comm.*, to appear.
- [48] R. C. Qiu, C. Zhou, N. Guo, and J. Q. Zhang, "Time Reversal with MISO for Ultra-Wideband Communications: Experimental Results (invited paper)," in *IEEE Radio and Wireless Symposium*, (San Diego, CA), 2006.
- [49] C. Zhou and R. C. Qiu, "Spatial Focusing of Time-Reversed UWB Electromagnetic Waves in a Hallway Environment," in *System Theory, 2006 Proceeding of the Thrity-Eighth Southeastern Symposium on*, pp. 318–322, 2006.
- [50] R. C. Qiu, C. Zhou, N. Guo, and J. Q. Zhang, "Time Reversal with MISO for Ultra-Wideband Communications: Experimental Results," *IEEE Antenna and Wireless Propagation Letters*, to appear.
- [51] R. C. Qiu, "A Theory of Time-Reversed Impulse Multiple-Input Multiple-Output (MIMO) for Ultra-Wideband (UWB) Communications (invited paper)," in *2006 Int'l Conf. UWB*, October 2006.
- [52] R. C. Qiu, C. Zhou, J. Q. Zhang, and N. Guo, "Channel Reciprocity and Time-Reversed Propagation for Ultra-Wideband Communications," in *IEEE AP-S International Symposium on Antennas and Propagation, Honolulu, Hawaii*, vol. 1, June 2007.
- [53] R. C. Qiu, C. Zhou, J. Q. Zhang, and N. Guo, "Channel Reciprocity and Time-Reversed Propagation for Ultra-Wideband Communications," *IEEE Antenna and Wireless Propagation Letters*, vol. 5, no. 1, pp. 269–273, 2006.
- [54] C. M. Zhou, B. M. Sadler, and R. C. Qiu, "Performance Study on Time Reversed Impulse MIMO for UWB Communications Based on Realistic Channels," in *IEEE Conf. Military Comm., MILCOM'07*, (Orlando, FL), October 2007.
- [55] N. Guo, Q. Zhang, R. C. Qiu, and S. Mo, "UWB MISO Time Reversal With Energy Detector Receiver over ISI Channels," in *4th Annual IEEE Consumer Communications and Networking Conference, CCNC'07*, (Las Vegas, Nevada), January 2007.
- [56] M. Calderon and R. C. Qiu, "Time Reversal for Ultra-wideband (UWB) Sensor Networking," tech. rep., Final Report to Army Research Office, Grant no. W911NF-06-1-0349, 151 pages, TTU, Cookeville, TN, July 2007.
- [57] R. C. Qiu and et al, "Ultra-wideband Communications Systems and Testbed," tech. rep., Final Report to Army Research Office, Grant no. W911NF-05-01-0111, 240 pages, TTU, Cookeville, TN, July 2007.
- [58] C. M. Zhou, N. Guo, and R. C. Qiu, "A Study on Time Reversed Impulse UWB with Multiple Antennas Based on Measured Spatial UWB Channels," *IEEE Trans. Vehicular Tech.*, submitted for publication, 2007.
- [59] P. Kyritis and F. Lee, "Notes from AIM Workshop on Time Reversal Communications in Richly Scattering Environments," October 2004. available at <http://www.aimath.org/WWN/timerev/timerev.pdf>.
- [60] T. Strohmer, M. Emami, J. Hansen, G. Papanicolaou, and A. Paulraj, "Application of Time-Reversal with MMSE Equalizer to UWB Communications," in *Global Telecommunications Conference*, vol. 5, IEEE, 2004.
- [61] P. Kyritsi, G. Papanicolaou, P. Eggers, and A. Oprea, "MISO Time Reversal and Delay-Spread Compression for FWA Channels at 5 GHz," *Antennas and Wireless Propagation Letters*, vol. 3, 2004.
- [62] Y. Chang, H. Fetterman, I. Newberg, and S. Panaretos, "Microwave Phase Conjugation using Antenna Arrays," *Microwave Theory and Techniques, IEEE Transactions on*, vol. 46, no. 11 Part 2, pp. 1910–1919, 1998.

- [63] J. Tuovinen, G. Shiroma, W. Forsyth, W. Shiroma, V. Technol, and F. Espoo, "Multipath Communications using a Phase-Conjugate Array," *Microwave Symposium Digest, 2003 IEEE MTT-S International*, vol. 3, 2003.
- [64] C. Oestges, A. Kim, G. Papanicolaou, and A. Paulraj, "Characterization of Space-Time Focusing in Time-Reversed Random Fields," *IEEE Transactions on Antennas and Propagation*, vol. 53, no. 1, pp. 283–293, 2005.
- [65] S. Emami, J. Hansen, A. Kim, G. Papanicolaou, A. Paulraj, D. Cheung, and C. Prettie, "Predicted Time Reversal Performance in Wireless Communications using Channel Measurements," *IEEE Communications Letters*, 2005.
- [66] M. Emami, M. Vu, J. Hansen, A. Paulraj, and G. Papanicolaou, "Matched Filtering with Rate Back-off for Low Complexity Communications in very Large Delay Spread Channels," in *Conference Record of the Thirty-Eighth Asilomar Conference on Signals, Systems and Computers*, vol. 1, 2004.
- [67] J. Hansen, D. Baum, and A. Paulraj, "Design Approach for a Time Reversal Test Bed for Radio Channels," in *Proceedings of the Eusipco*, 2004.
- [68] H. Nguyen, J. Andersen, and G. Pedersen, "The Potential Use of Time Reversal Techniques in Multiple Element Antenna Systems," *IEEE Communications Letters*, vol. 9, no. 1, pp. 40–42, 2005.
- [69] H. Nguyen, I. Kovacs, and P. Eggers, "Time Reversal Transmission Approach for Multi-user UWB Communications," *IEEE Trans. Ant. Prop.*, vol. 54, pp. 3216–3224, Nov. 2006.
- [70] A. Cepni, D. Stancil, Y. Jiang, and J. Zhu, "Microwave Nulling Using Multiple Antennas and Time-Reversal Method," in *IEEE Vehicular Technol. Conf. (VTC'05)*, 2005.
- [71] A. Cepni and D. Stancil, "Single Antenna Microwave Nulling Using Time-Reversal Technique," *Microwave Symposium Digest, 2005 IEEE MTT-S International*, pp. 1723–1726, 2005.
- [72] J. Moura, Y. Jin, D. Stancil, J. Zhu, A. Cepni, Y. Jiang, and B. Henty, "Single Antenna Time Reversal Adaptive Interference Cancellation," in *IEEE International Conference on Acoustics, Speech, and Signal Processing (ICASSP'05)*, vol. 4, 2005.
- [73] D. Liu, S. Vasudevan, J. Krolik, G. Bal, and L. Carin, "Electromagnetic Time Source Localization in Changing Media: Experiment and Analysis," *IEEE Trans. Ant. Prop.*, vol. 55, pp. 344–354, Feb. 2007.
- [74] M. Fink and J. Cardoso, "Diffraction Effects in Pulse-echo Measurements," *IEEE Trans. Ultrason. Ferroelec. Freq. Control*, vol. 31, no. 4, pp. 313–329, 1984.
- [75] M. Fink, C. Prada, F. Wu, and D. Casserea, "Self-focusing Inhomogeneous Media with Time-reversal Acoustic Mirrors," in *Proc. IEEE Ultrason. Symp.*, pp. 681–686, 1989.
- [76] D. Casserea, F. Wu, and M. Fink, "Limits of Self-focusing Using Time-reversal Cavities and Mirrors—Theory and Experiment," in *Proc. IEEE Ultrason. Symp.*, pp. 1613–1618, 1990.
- [77] M. Fink, "Time-reversal of Ultrasonic Fields—Part I: Basic Principles," *IEEE Trans. Ultrason. Ferroelec. Freq. Control*, vol. 39, no. 5, pp. 555–566, 1992.
- [78] F. Wu, J. Thomas, and M. Fink, "Time-reversal of Ultrasonic Fields—Part II: Experimental results," *IEEE Trans. Ultrason. Ferroelec. Freq. Control*, vol. 39, no. 5, pp. 567–578, 1992.

- [79] D. Cassereau and M. Fink, "Time-reversal of Ultrasonic fields—Part III: Theory of the Closed Time-reversal Cavity," *IEEE Trans. Ultrason. Ferroelec. Freq. Control*, vol. 39, no. 5, pp. 579–592, 1992.
- [80] A. Derode, P. Roux, and M. Fink, "Robust Acoustic Time Reversal with High-Order Multiple Scattering," *Physical Review Letters*, vol. 75, no. 23, pp. 4206–4209, 1995.
- [81] P. Roux, B. Roman, and M. Fink, "Time-reversal in an Ultrasonic Waveguide," *Appl. Phys. Lett.*, vol. 40, pp. 1811–1813, 1997.
- [82] M. Fink, "Time Reversed Acoustics," *Scientific American*, pp. 91–97, 1999.
- [83] H. Song, P. Roux, and W. Kuperman, "Focal Translation by Frequency Shift in Free Space," *IEEE Tran. Ultrasonics Ferro. Freq. Control*, vol. 47, no. 3.
- [84] P. Roux and M. Fink, "Time Reversal in a Waveguide: Study of the Temporal and Spatial Focusing," *J. Acoust. Soc. Am.*, vol. 107, pp. 2418–2429, 2000.
- [85] M. Tanter, J. Aubry, J. Gerber, J. Thomas, and M. Fink, "Optimal focusing by spatio-temporal inverse filter. I. Basic principles," *The Journal of the Acoustical Society of America*, vol. 110, p. 37, 2001.
- [86] M. Fink, "Acoustic Time-Reversal Mirrors," *Imaging*, vol. 84, pp. 17–43, 2002.
- [87] A. Parvulescu and C. Clay, "Reproducibility of Signal Transmission in the Ocean," *Radio Elec. Eng.*, vol. 29, pp. 223–228, April 1965.
- [88] D. Dowling and D. Jackson, "Phase Conjugation in Underwater Acoustics," *J. Acoust. Soc. Am.*, vol. 89, pp. 171–181, 1990.
- [89] D. Dowling, "Acoustic Pulse Compression Using Passive Phase Conjugate Processing," *J. Acoust. Soc. Am.*, vol. 95, pp. 1450–1458, 1994.
- [90] W. Kuperman, W. Hodgkiss, H. Song, T. Akal, C. Ferla, and D. Jackson, "Phase Conjugation in The Ocean: Experimental Demonstration of An Acoustic Time-reversal Mirror," *J. Acoust. Soc. Am.*, vol. 103, no. 1, pp. 25–40, 1998.
- [91] H. Song, W. Kuperman, and W. Holdgkiss, "A Time Reversal Mirror with Variable Range Focusing," *J. Acoust. Soc. Am.*, vol. 103, no. 6, pp. 3234–3240, 1998.
- [92] W. Hodgkiss, H. Song, W. Kuperman, T. Akal, C. Ferla, and D. Jackson, "A Long-Range and Variable Focus Phase-Conjugation Experiment In Shallow Water," *J. Acoust. Soc. Am.*, vol. 105, pp. 1597–1604, 1999.
- [93] H. Song, "Iterative Time Reversal in the Ocean," *J. Acoust. Soc. Am.*, vol. 105, no. 6.
- [94] S. Kim, G. Edelmann, W. Kuperman, W. Hodgkiss, and H. Song, "Spatial Resolution of Time-reversal Arrays in Shallow Water," *J. Acoust. Soc. Am.*, vol. 110, pp. 820–829, 2001.
- [95] D. Rouseff, D. Jackson, W. Fox, C. Jones, R. J.A., and D. Dowling, "Underwater Acoustic Communication by Passive-Phase Conjugation: Theory and Experimental Results," *IEEE J. Ocean. Eng.*, vol. 26, pp. 821–831, 2001.
- [96] M. Heinemann, A. Larazza, and K. Smith, "Acoustic Communications in an Enclosure Using Single-Channel Time-Reversal Acoustics," *Appl. Phys. Lett.*, vol. 80, pp. 694–696, 2002.
- [97] G. Edelmann, T. Akal, W. Hodgkiss, S. Kim, K. W.A., and H. Song, "An Initial Demonstration Of Underwater Acoustic Communications Using Time Reversal," *IEEE J. Ocean. Eng.*, vol. 27, pp. 602–609, 2002.

- [98] T. Yang, "Temporal Resolution of Time-Reversal and Passive-Phase Conjugation For Underwater Acoustic Communications," *IEEE J. Ocean. Eng.*, vol. 28, pp. 229–245, 2003.
- [99] A. Derode, A. Tourin, J. de Rosny, M. Tanter, S. Yon, and M. Fink, "Taking Advantage of Multiple Scattering to Communicate with Time-Reversal Antennas," *Physical Review Letters*, vol. 90, no. 1, p. 14301, 2003.
- [100] L. Borcea, G. Papanicolaou, and C. Tsogka, "Theory and Applications of Time Reversal and Interferometric Imaging," *Inverse Problems*, vol. 19, no. 6, pp. S139–S164, 2003.
- [101] K. Smith, A. A.M., and A. Larraza, "Examination of Time Reversal Acoustics in Shallow Water and Applications to Noncoherent Underwater Communications," *J. Acoust. Soc. Am.*, vol. 113, no. 6, pp. 3095–3110, 2003.
- [102] M. Heinemann, A. Larraza, and K. Smith, "Experimental Studies of Applications of Time Reversal Acoustics to Noncoherent Underwater Communications," *J. Acoust. Soc. Am.*, vol. 113, no. 6, pp. 3111–3116, 2003.
- [103] D. Rouseff, "Intersymbol Interference in Underwater Acoustic Communications using Time-Reversal Signal Processing," *J. Acoust. Soc. Am.*, vol. 117, no. 2, pp. 780–788, 2005.
- [104] B. P. Bogert, "Demonstration of Delay Distortion Correction by Time-Reversal Techniques," *IRE Comm. Tech. Trans.*, pp. 2–7, 1957.
- [105] F. K. Becker, L. N. Holzman, R. W. Lucky, and E. Port, "Automatic Equalization for Digital Communication," *Proc. IRE*, pp. 96–97, 1965.
- [106] K. E. Schreiner, H. L. Funk, and E. Hopner, "Automatic Distortion Correction for Efficient Pulse Transmission," *IBM*, pp. 20–30, 1965.
- [107] D. Pepper, "Nonlinear Optical Phase Conjugation," *Optical Engineering*, vol. 21, pp. 156–183, 1982.
- [108] R. Fisher *et al.*, *Optical phase conjugation*. Academic Press New York, NY, 1983.
- [109] A. Yariv, *Optical electronics*. Holt, Rinehart and Winston, 1985.
- [110] A. VAN, "Electromagnetic reflector," October 1959. US Patent 2 908 002.
- [111] C. Pon, "Retrodirective Array Using the Heterodyne Technique," in *IEEE Trans. Antennas Propagat.*, vol. AP-12, pp. 176–180, March 1964.
- [112] M. Skolnik and D. King, "Self-phasing Array Antennas," *IEEE Trans. Antennas Propagat.*, vol. AP-12, pp. 142–149, February 1964.
- [113] C. Pobanz and T. Itoh, "A Conformal Retrodirective Array for Radar Applications Using a Heterodyne Phased Scattering Element," *IEEE MTT-S Int. Microwave Symp. Dig.*, pp. 905–908, June 1995.
- [114] S. Karode and V. Fusco, "Self-tracking Duplex Communication Link Using Planar Retrodirective Antennas," *IEEE Trans. Antennas Propagat.*, vol. 47, pp. 993–1000, June 1999.
- [115] D. Ah Yo, W. Forsyth, and W. Shiroma, "A 360 Degrees Retrodirective Self-oscillating Mixer Array [using HEMTs]," *IEEE MTT-S Int. Microwave Symp. Dig.*, pp. 813–816, June 2000.
- [116] R. Miyamoto, Y. Qian, and T. Itoh, "Active Retrodirective Array for Remote Tagging and Wireless Sensor Applications," in *IEEE MTT-S Int. Microwave Symp. Dig.*, pp. 1431–1434, June 2000.

- [117] T. Brabetz, V. Fusco, and S. Karode, "Balanced Subharmonic Mixers for Retrodirective-array Applications," *IEEE Trans. Microwave Theory Tech.*, vol. 49, pp. 465–469, March 2001.
- [118] L. DiDomenico and R. Rebeiz, "Digital Communications Using Self-phased Arrays," *IEEE Trans. Microwave Theory Tech.*, vol. 49, pp. 677–684, April 2001.
- [119] R. Miyamoto, Y. Qian, and T. Itoh, "An Active Integrated Retrodirective Transponder for Remote Information Retrieval-on-demand," *IEEE Trans. Microwave Theory Tech.*, vol. 49, pp. 1658–1662, September 2001.
- [120] K. Leong, R. Miyamoto, S.-S. Jeon, Y. Wang, and T. Itoh, "A Frequency Autonomous Retrodirective Array Transponder," in *IEEE MTT-S Int. Microwave Symp. Dig.*, vol. 2, pp. 1349–1352, May 2001.
- [121] P. Blomgren, G. Papanicolaou, and H. Zhao, "Super-Resolution in Time-Reversal Acoustics," *The Journal of the Acoustical Society of America*, vol. 111, p. 230, 2002.
- [122] K. Leong, R. Miyamoto, S.-S. Jeon, C.-C. Chang, and T. Itoh, "A Frequency Agile Retrodirective Array Using a Phase-locked Loop Local Oscillator," in *Asia-Pacific Microwave Conf.*, pp. 1427–1430, 2002.
- [123] K. Leong, Y. Wang, and T. Itoh, "A Full Duplex Capable Retrodirective Array System for High-Speed Beam Tracking and Pointing Applications," *Microwave Theory and Techniques, IEEE Transactions on*, vol. 52, no. 5, pp. 1479–1489, 2004.
- [124] K. Leong, Y. Wang, and T. Itoh, "A Radar Target Transceiver using a Full Duplex Capable Retrodirective Array System," *Microwave Symposium Digest, 2003 IEEE MTT-S International*, vol. 2, 2003.
- [125] G. Lerosey, J. de Rosny, A. Tourin, A. Derode, G. Montaldo, and M. Fink, "Time Reversal of Electromagnetic Waves," *Physical Review Letters*, vol. 92, no. 19, p. 193904, 2004.
- [126] B. Henty and D. Stancil, "Multipath-Enabled Super-Resolution for RF and Microwave Communication using Phase-Conjugate Arrays," *Physical Review Letters*, vol. 93, no. 24, p. 243904, 2004.
- [127] R. W. Lucky, "Automatic Equalization for Digital Communication," *Bell System Tech. J.*, vol. XLIV, no. 4, pp. 547–588, 1965.
- [128] R. W. Lucky, "Techniques for Adaptive Equalization of Digital Communication Systems," *Bell System Tech. J.*, pp. 256–286, 1966.
- [129] R. A. Gibby and J. W. Smith, "Some Extensions of Nyquist's Telegraph Transmission Theory," *Bell System Tech. J.*, pp. 1487–1510, September 1965.
- [130] J. W. Smith, "The Joint Optimization of Transmitted Signal and Receiving Filter for Data Transmission Systems," *Bell System Tech. J.*, pp. 2363–2392, September 1965.
- [131] D. A. George, "Matched Filters for Interfering Signals," *IEEE Trans. Inform. Theory*, pp. 153–154, Jan. 1965.
- [132] D. W. Tufts, "Nyquist's Problem—The Joint Optimization of Transmitter and Receiver in Pulse Amplitude Modulation," in *Proc. IEEE*, pp. 248–259, March 1965.
- [133] J. Salz, "Digital Transmission over Cross-coupled Linear Channels," *AT & T Tech. Journal*, vol. 64, no. 6, pp. 1147–1159, 1985.
- [134] R. C. Qiu, B. M. Sadler, and Z. Hu, "Time Reversed Transmission with Chirp Signaling for UWB Communications and Its Application in Confined Metal Environments," in *International Conference on Ultra-wideband, ICUWB'07*, (Singapore), September 2007.

- [135] R. C. Qiu, Z. Hu, and B. M. Sadler, "UWB Cognitive Radio and Its Application in Confined Metal Environments," *IEEE Trans. Wireless Commun.*, submitted for publication, 2007.
- [136] C. M. Zhou and R. C. Qiu, "Pulse Distortion and Optimum Transmit Waveform for UWB Cognitive Radio," *IEEE Trans. Vehicular Tech.*, submitted for publication, 2007.
- [137] S. O. Rice, "Mathematical Analysis of Random Noise," *Bell System Tech. J.*, vol. 23, no. 2, pp. 282–332, 1944.
- [138] D. O. North, "Analysis of the Factors Which Determine Signal/Noise Discrimination," *RCA Tech. Report PTR-6-C, June 1943; reprinted in Proc. IRE*, vol. 51, pp. 1016–1028, 1963.
- [139] A. Van der Ziel, *Noise*. Englewood Cliffs, New Jersey: Prentice-Hall, 1954.
- [140] D. Slepian, "Estimation of Signal Parameters in the Presence of Noise," *Trans. IRE*, vol. 3, no. 1, pp. 68–89, 1954.
- [141] J. H. Laning and R. H. Battin, *Random Processes in Automatic Control*. New York: McGraw-Hill, 1956.
- [142] S. Darlington, "Linear Least-Square Smoothing and Prediction with Applications," *Bell System Tech. J.*, vol. 37, no. 6, pp. 1221–1294, Sept. 1958.
- [143] D. Middleton, *Introduction to Statistical Communication Theory*. New York: McGraw-Hill, 1960.
- [144] E. J. Kelly, I. S. Reed, and W. L. Root, "Detection of Radar Echoes in Noise, I," *J. Soc. Indust. Appl. Math.*, vol. 8, no. 2, pp. 309–341, 1960.
- [145] E. J. Kelly, I. S. Reed, and W. L. Root, "Detection of Radar Echoes in Noise, II," *J. Soc. Indust. Appl. Math.*, vol. 8, no. 3, pp. 481–507, 1960.
- [146] G. L. Turn, "An Introduction to Matched Filter," *IRE Trans. Inform. Theory*, pp. 311–329, June 1961.
- [147] C. W. Helstrom, *Statistical Theory of Signal Detection*. London: Pergamon, 1960.
- [148] S. D. and H. O. Pollak, "Prolate Spheroidal Wave Functions, Fourier Analysis and Uncertainty, I," *Bell System Tech. J.*, vol. 40, no. 1, pp. 43–64, 1961.
- [149] H. J. Landau and H. O. Pollak, "Prolate Spheroidal Wave Functions, Fourier Analysis and Uncertainty, II," *Bell System Tech. J.*, vol. 40, no. 1, pp. 65–84, 1961.
- [150] H. J. Landau and H. O. Pollak, "Prolate Spheroidal Wave Functions, Fourier Analysis and Uncertainty, III," *Bell System Tech. J.*, vol. 41, p. 1295, 1962.
- [151] C. W. Helstrom, "Solution of the Detection Integral Equation for Stationary Filtered White Noise," *IEEE Trans. Inform. Theory*, vol. 11, no. 6, pp. 335–339, July 1965.
- [152] H. L. Van Trees, *Detection, Estimation, and Modulation Theory*. New York: John Wiley, 1968.
- [153] J. L. Holsinger, "Digital Communication over Fixed Time-Continuous Channels with Memory—With Special Applications to Telephone Channels," tech. rep., MIT Research Lab of Electronics, 1964.
- [154] R. A. Gallager, *Information Theory and Reliable Communication*. NY: John Wiley, 1966.
- [155] E. J. Baghdady, *Lectures on Communication System Theory*. New York: McGraw-Hill, 1961.

- [156] R. W. Lucky, J. Salz, and E. J. Weldon, *Principles of Data Communication*. New York: McGraw-Hill, 1968.
- [157] N. Al-Dhahir and J. M. Cioffi, "Block Transmission over Dispersive Channels: Transmit Filter Optimization and Realization, and MMSE-DFE Receiver Performance," *IEEE Trans. Inform. Theory*, vol. 42, no. 1, pp. 137–160, 1996.
- [158] M. K. Simon and W. C. Lindsey, *Digital Communication Techniques: Signal Design and Detection*. Englewood Cliffs, NJ: Prentice-Hall, 1st ed., 1995.
- [159] J. G. Proakis, *Digital Communications*. McGraw Hill, 4th ed., 2001.
- [160] N. Al-Dhahir and A. H. Sayed, "The Finite-length Multi-input Multi-output MMSE-DFE," *IEEE Trans. Sig. Proc.*, vol. 48, pp. 2921–2936, Oct. 1996.
- [161] R. Saadane, A. Menouni, R. Knopp, and D. Aboutajdine, "Empirical Eigenanalysis of Indoor UWB Propagation Channels," in *IEEE GLOBECOM*, pp. 76–81, 2004.
- [162] E. K. Walton, "Radar System Using Random RF Noise," 2004. US Patent 6 864 834.
- [163] E. K. Walton, "Radar System Using RF Noise," 2006. US Patent 7 196 657.
- [164] J. Chalk, "The Optimum Pulse-Shape for Pulse Communication," in *Proc. IEE*, p. 8892, 1950.
- [165] P. G. Grieve and J. R. Guerci, "Optimum Matched Illumination-reception Radar," December 1992. U.S. Patent 5 175 552.
- [166] P. Grieve and J. Guerci, "Optimum Matched Illumination-reception Radar for Target Classification," January 1995. U.S. Patent 5 381 154.
- [167] S. Pillai, H. Oh, D. Youla, and J. Guerci, "Optimum Transmit-receiver Design in The Presence of Signal-dependent Interference and Channel Noise," *IEEE Transactions on Information Theory*, vol. 46, pp. 577–584, March 2000.
- [168] D. Garren, A. Osborn, M. and Odom, S. Goldstein, J. and Pillai, and J. Guerci, "Enhanced Target Detection and Identification via Optimized Radar Transmission Pulse Shape," in *IEE Proceedings-Radar, Sonar, and Navigation (special issue on modelling and simulation of radar systems)*, vol. 148, pp. 130–138, June 2001.
- [169] D. Garren, A. Odom, M. Osborn, J. Goldstein, S. Pillai, and J. Guerci, "Full-Polarization Matched-illumination for Target Detection and Identification," *IEEE Transactions Aerospace and Electronic Systems*, vol. 38, pp. 824–836, July 2002.
- [170] M. R. Bell, "Information Theory and Radar Waveform Design," *IEEE Trans. Inform. Theory*, vol. 39, pp. 1578–1597, September 1997.
- [171] Y. Yang and R. S. Blum, "MIMO Radar Waveform Design Based on Mutual Information and Minimum Mean-Square Error Estimation," *IEEE Trans. on Aerospace Electron. Sys.*, vol. 43, no. 1, pp. 1–12, Jan. 2007.
- [172] Y. Yang and R. S. Blum, "Minimax Robust MIMO Radar Waveform Design," *IEEE J. Select. Topics in Sig. Proc. (JSTSP)*, vol. 1, no. 1, pp. 1–9, Jan. 2007.
- [173] A. Leshem, O. Naparsitek, and A. Nehorai, "Information Theoretical Adaptive Radar Waveform Design for Multiple Extended Targets," *IEEE J. Select. Topics in Sig. Proc. (JSTSP)*, vol. 1, no. 1, pp. 42–55, Jan. 2007.
- [174] W. Yu, R. Lui, and R. Centrillon, "Dual Optimization Methods for Multiuser OFDM Systems," in *Proc. GLOBECOM 2004*, pp. 225–229, 2004.

- [175] S. Boyd and L. Vandenberghe, *Convex Optimization*. UK: Cambridge Press, 2004.
- [176] A. Heddebaut, A. Deniau, and K. Adouane, "In-Vehicle WLAN Radio-Frequency Communication Characterization," *IEEE Transactions on Intelligent Transportation Systems*, vol. 5, pp. 114–121, June 2004.
- [177] E. Heyman, G. Friedlander, and L. B. Felsen, "Ray-Mode Analysis of Complex Resonances of an Open Cavity," *Progress In Electromagnetics Research*, vol. 77, no. 5, pp. 780–787, May 1989.
- [178] M. R. Bell and R. Grubbs, "JEM Modeling and Measurement for Radar Target Identification," *IEEE Tran. Aerospace Electronic Systems*, vol. 29, no. 1, pp. 73–87, Jan. 1993.
- [179] W. Geyi, "Time Domain Theory of Cavity Resonator," *Progress In Electromagnetics Research*, vol. 78, no. 2, pp. 219–253, June 2008.
- [180] J. G. Proakis and M. Salehi, *Communication Systems Engineering*. Englewood Cliffs, NJ: Prentice-Hall, 2002.
- [181] M. K. Simon and M. S. Alouini, *Digital Communication over Fading Channels*. New York: John Wiley, 2000.
- [182] A. Goldsmith, *Wireless Communications*. Cambridge University Press, 2005.
- [183] W. V. Lovitt, *Linear Integral Equations*. NY: Dover, 1950.
- [184] E. G. Tricomi, *Integral Equations*. NY: Dover, 1985.



## Chapter 3

# Optimum Transmission Waveform in Canonical Channels

The purpose of this chapter is to introduce readers the time domain modeling for the UWB signals. For wide-band signals such as UWB, by principle, time domain frame work appears to be a better frame work to study its propagation. The time domain impulse responses for a series of scattering environments have been derived for the first time. Specifically, several electromagnetic communication fundamental channels, including perfect conduct electromagnetic wedge, large rectangular plates, and parallel planes waveguide, are studied. The receiving signal, calculated through convolution in the time domain impulse response, can provide waveform information, as well as the amplitude information (Path loss). The pulse waveforms passing through these channels are compared with their original waveforms. The comparison show that for wideband signal, pulse could be extremely distorted by diffraction mechanism. The results converted from frequency domain by applying a inverse fast Fourier Transform (IFFT) serves as sanity checks for our time domain derivation. Given the time domain channel impulse response, we also study the optimum transmit waveform such as the signal to noise ratio (SNR) at the receiver side is maximized, under the constraint of fixed transmitted power.

### 3.1 Introduction

The purpose of this chapter is to derive the channel impulse responses for a series of environments and analyze the corresponding optimum transmit pulse waveforms. The UWB system are generally based on the transmission of many consecutive pulses. Therefore, by principle, time domain framework appears to be a better framework to study the radiation, propagation and reception of UWB signals. Moreover, comparing with traditional frequency domain framework, time domain framework provides more physical insight. For example, except predicting path loss, time domain convolution with TD-UTD can also predict the receiving pulse waveform and show the possible pulse distortion caused by diffraction, which has been proved to be a significant issue for wideband signals such as UWB [1]-[3].

The essential benefits of the time domain framework motivate this work. However, the traditional time domain methods such as Finite Difference Time Domain (FDTD) and time domain integral equation become intractable when the width of the incident pulse is very narrow compared with the geometric dimensions of the scattering objects, which is the case when we study the propagation of UWB signals. In this chapter, we will try to attack the

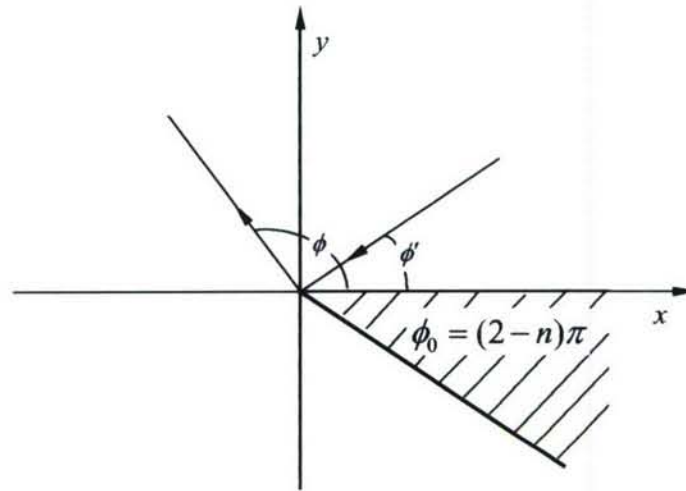


Figure 3.1: Plane wave normally incident on a perfectly conducting wedge

propagation problems for wideband signals directly in the time domain, with a closed form solution. We derived the time domain impulse response for a series of scattering environments. The pulse waveform after diffraction is compared with the incident waveform. The results converted from frequency domain by applying an inverse fast Fourier Transform (IFFT) will serve as sanity checks.

Since waveform is distorted by the channel, we need to design transmit waveform in accordance with the different channels. Another contribution of the chapter is that we analyze the optimum transmit waveform based on derived time domain impulse response.

## 3.2 Pulse Distortion and Its Impact on UWB System Design

### 3.2.1 Pulse Distortion Caused by Wide Bandwidth

Traditional communication theory are based on the assumption of distortionless propagation, which suggests that the receiving signal consist of a series of the replica of the transmitting signals. This assumption is valid when the signal bandwidth is not wide. However, for wideband signals, especially pulse based signals like UWB, this assumption might not hold anymore. As a simple example, Fig. 3.2 shows the waveform distortions for pulses with different bandwidths after they pass through a 90-degree wedge (diffraction) channel. The incident pulse in Fig. 3.2(a) is a second order derivative of Gaussian waveform with a pulse width of  $0.2ns$ , corresponding a 5.86 GHz 10-dB bandwidth in the frequency domain, and the pulse in Fig. 3.2(a) is about  $10ns$  wide, corresponding a 128 MHz 10-dB bandwidth. For the convenience of waveform comparison, the amplitude of both incident waveform and the diffracted waveform have been normalized. It is evident that the shorter pulse (wider bandwidth) experienced more distortion after they passing through the same diffraction channel. When the signal bandwidth is not very wide (e.g., the 128 MHz waveform in Fig. 3.2(a)), the distortion caused by channel is negligible. However, when the signal width is increasing, the distortion becomes noticeable. The details of the calculation of the diffraction waveform for a wedge diffraction will be given in the Section 3.5.1.

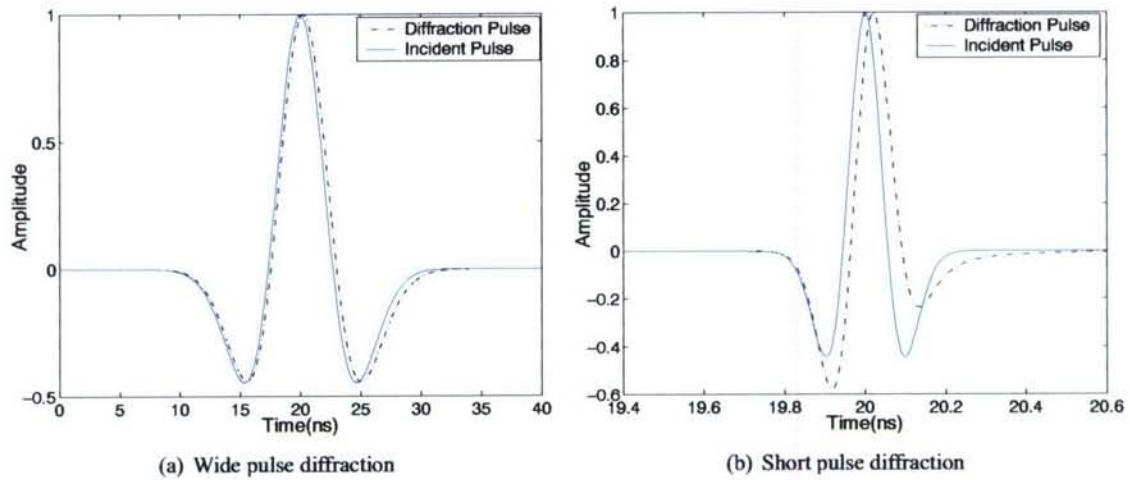


Figure 3.2: Pulse distortion for pulses with different bandwidths. The incident pulse for (a) is about 10.2 ns wide, corresponding to a 10 dB bandwidth of 128 MHz, and for (b) is about 0.2 ns wide, corresponding to a 10 dB bandwidth of 5.86 GHz. Amplitudes were scaled to the same level to better compare the waveforms

### 3.2.2 The Impact of Pulse Distortion on System Design

Consider a communication system illustrated in Fig. 3.3. Here,  $p(t)$  is the transmitted pulse waveform, and  $h(t)$  denotes the CIR. The received signal before  $c_1(t)$  can be written as

$$r(t) = p(t) * h(t) + n(t), \quad (3.1)$$

where  $n(t)$  is Additive White Gaussian Noise (AWGN) with a two-sided power spectral density of  $N_0/2$ . Given  $s(t)$ , a matched filter matched to  $s(-t)$  provides the maximum signal-to-noise power (SNR) ratio at its output. The matched filter here can be virtually decomposed into two filters, with the first filter matched to the CIR  $h(t)$  and the second matched to the pulse waveform  $p(t)$ . As shown in Fig. 3.3, this decomposition can be done by setting  $c_1(t) = h(-t)$  and  $c_2(t) = p(-t)$ . conventionally channel is modeled as a tapped delay line.

$$h(t) = \sum_{l=1}^L \alpha_l \delta(t - \tau_l) \quad (3.2)$$

where  $L$  is the number of multipath components and  $\alpha_l$  and  $\tau_l$  are its individual amplitudes and delays. The received signals are just a series of replicas of the transmitted signals, with different attenuations and time delays.

In practice, the estimation of  $h(t)$  is generally a very difficult task, especially when there is per-pulse distortion for the wide band signals. The receiver suffers significant performance loss (as big as 4 dB), if the system is designed without the necessary compensation for pulse distortion [10]. Along with system performance loss, pulse distortion can cause timing and synchronization error as well. It has been shown in [10] that the timing error caused by distortion due to cylinder diffraction can be much larger than the Cramer-Rao lower bound, thus is another fundamental issue that should be considered in system design.

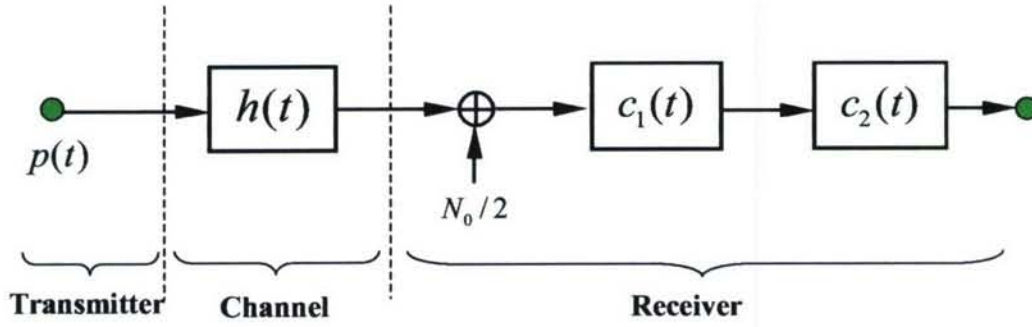


Figure 3.3: General model for data transmission

A new channel model that takes into account per-path distortion is then proposed in [15]

$$h(t) = \sum_{l=1}^L h_l(t) * \delta(t - \tau_l) \quad (3.3)$$

where distortion factor  $h_l(t)$  includes both attenuation and distortion of the signal when pass through the channel.

Note that waveform information can only be provided by time domain framework, which justifies our effort for the time domain analysis.

### 3.3 Time Domain Channel Modeling

In this section we study several simple models that is mathematically tractable. For these models, the analytical results can often be obtained through exploring the physical mechanism behind it. These analytical results provide us unique insight into the signal propagation in different practical environments. In this section, we are aimed to derive the time domain channel impulse response for these models. We will firstly start with its frequency domain model and then transform it to time domain via Laplace transform.

#### 3.3.1 Wedge Channel

Rather than seeking the exact solution for Maxwell's equations, Geometric Theory of Diffraction (GTD) uses generalization of Fermat's principle to find high-frequency harmonic Maxwell equation solutions for many complicated objects. The Uniform Theory of Diffraction (UTD) was proposed to complement GTD in the situations where GTD was invalid [4]. The original GTD/UTD was proposed in frequency domain and then was widely used in narrow-band radio propagation, e.g., for path loss prediction. In 1990, time domain UTD was firstly derived by Veruttipong and Kouyoumjian in [5] by applying an inverse Laplace transform to the corresponding frequency domain results. TD-UTD diffraction coefficient for a straight Perfect Electric Conduct (PEC) wedge can be expressed as [5]

$$D^{s,h}(t) = \frac{-1}{2n\sqrt{2\pi}\sin\beta_0} \sum_{m=1}^4 K_m^{s,h} F(X_m, t) \quad (3.4)$$

where

$$\begin{aligned} K_1^{s,h} &= \cot\left(\frac{\pi+\phi-\phi'}{2n}\right) \\ K_2^{s,h} &= \cot\left(\frac{\pi-\phi-\phi'}{2n}\right) \\ K_3^{s,h} &= \pm \cot\left(\frac{\pi+\phi+\phi'}{2n}\right) \\ K_4^{s,h} &= \pm \cot\left(\frac{\pi-\phi+\phi'}{2n}\right) \end{aligned} \quad (3.5)$$

and

$$F'(X_m, t) = \frac{X_m}{\sqrt{\pi ct} (t + \frac{X_m}{c})} \quad (3.6)$$

The value of  $X_m$  in (3.6) is given by

$$\begin{aligned} X_1 &= 2L \cos^2\left(\frac{2n\pi N^+ - (\phi - \phi')}{2}\right) \\ X_2 &= 2L \cos^2\left(\frac{2n\pi N^- - (\phi - \phi')}{2}\right) \\ X_3 &= 2L \cos^2\left(\frac{2n\pi N^+ - (\phi + \phi')}{2}\right) \\ X_4 &= 2L \cos^2\left(\frac{2n\pi N^- - (\phi + \phi')}{2}\right) \end{aligned} \quad (3.7)$$

where  $N^\pm$  is the nearest integer solution of equation  $2\pi n N^\pm - \theta^\pm = \pm\pi$ , and  $L$  is the distance parameter determined by the incident wavefront. For plane wave incidence, we have  $L = r \sin^2 \beta_0$ , where  $r$  is the distance along the diffraction ray from the edge to the observation point. The rest of parameters used in (3.4)-(3.7) are described as follows:

- “ $s, h$ ” soft and hard boundary conditions
- $n$  the parameter describing wedge angle; wedge angle  $\phi_0 = (2 - n)\pi$
- $\beta_0$  the angle between the edge and the incident ray
- $\phi$  the angle between the wedge surface and the diffraction ray
- $\phi'$  the angle between the wedge surface and the incident ray

These parameters are also illustrated in Fig. 3.1, which shows a special case when  $\beta_0 = \pi/2$ .

If the observation angle is not in the transition zone, we have the time domain diffraction coefficient for GTD (Keller) solution [5]

$$D^{s,h}(t) = \sqrt{\frac{c}{2t}} \frac{\sin \frac{\pi}{n}}{n \pi \sin \beta_0} \cdot \left[ \frac{1}{\cos \frac{\pi}{n} - \cos\left(\frac{\phi - \phi'}{n}\right)} \mp \frac{1}{\cos \frac{\pi}{n} - \cos\left(\frac{\phi + \phi'}{n}\right)} \right] \quad (3.8)$$

It should be noted that Veruttipong's TD wedge diffraction coefficient given in (3.4) is a special case of the diffraction coefficient for curved wedge in [6], where an analytical signal representation for the transient fields has been used. The details for analytical TD-UTD will be given in the Section 3.5.1.

### 3.3.2 Rectangular Building

The first propagation model of interest is rectangular model. Rectangular is one of the typical shapes often encountered in a practical propagation environment. Moreover, a lot of obstacles in the propagation environment can be approximated by a rectangular, with a limited degree of accuracy [7]. This model has been widely studied in the past

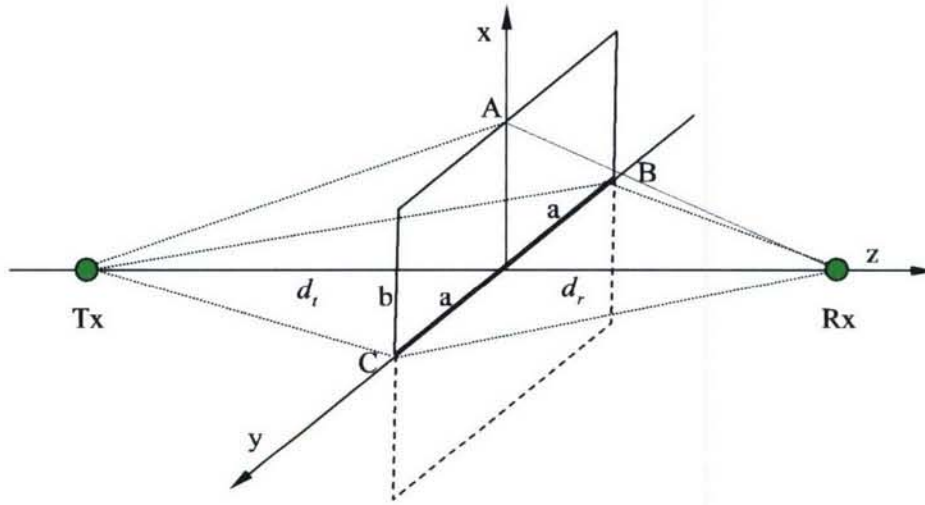


Figure 3.4: UWB pulse diffracted by a rectangular building. Tx: Transmitter antenna, Rx: Receiver antenna.  $d_t/d_r$  denotes the distance between Tx/Rx and the building. The size of the building is  $2a \times b$ . The lower half plane plotted by dash line denotes the image of the building relative to the ground.

decades. However, most of research is focused on frequency domain such as path loss prediction under different frequency band. In this chapter, we investigate its time domain characteristics such as pulse distortion introduced by diffraction in the edge of the building. We also analyze the optimum transmit waveform based on this time domain channel model.

As illustrated in Fig. 3.4, we consider a simple UWB channel consists of a transmitter, a receiver, and a rectangular building that blocks the LOS transmission. In Fig. 3.4,  $d_t$ ,  $d_r$  denote the distance from the building to Tx, Rx, respectively. The size of the building is  $2a \times b$ . The lower half plane plotted by dash line denotes the image of the building relative to the ground and is considered as perfectly absorbing.

A good analysis of the path loss prediction in frequency domain can be found in [7] and the references therein. Generally, two approaches, Fresnel-Kirchhoff scalar approach and GTD approach considering a four-ray propagation system, are applied to study the effects of rectangular building diffraction.

## Propagation Model Based on Fresnel-Kirchhof Integral

### A1.1 Frequency Domain Model

Fresnel-Kirchhoff is one of the traditional approaches used to calculate the propagation loss due to the blocking of a rectangular building. We Define the channel transfer function as the ratio of the strength of the received signal to the transmitted signal. Mathematically transfer function can be expressed as  $H(j\omega) = \frac{E(j\omega)}{E_0(j\omega)}$ . Then the transfer function describes the rectangular diffraction can be expressed as [7]:

$$H(j\omega) = \frac{1}{2} \left[ 1 - 2j \int_0^A \exp(-j\frac{\pi}{2}y^2)dy \int_0^B \exp(-j\frac{\pi}{2}x^2)dx \right] e^{-jkd} \quad (3.9)$$

where  $k$  is the wavenumber and  $d$  is the propagation distance. In our case we have  $d = d_t + d_r$ . In (3.9), variable  $A$

and  $B$  are the normalized half width and normalized height of the building, given by

$$A = a\sqrt{\frac{2(d_t + d_r)}{\lambda d_t d_r}} \quad B = b\sqrt{\frac{2(d_t + d_r)}{\lambda d_t d_r}} \quad (3.10)$$

where  $\lambda$  is the wavelength. It should be noted that the validity of (3.9) is based on the condition that the distances to and from the obstacle must be greater than its dimensions and the wavelength, i.e.,  $d_t, d_r \gg a, b, \lambda$ .

#### A1.2 Time Domain Model

In this section, we will derive the time domain channel impulse response based on (3.9). We firstly work on one of the integrals and formulate them to a form ready for Laplace transform.

$$\begin{aligned} \int_0^A \exp(-j\frac{\pi}{2}y^2)dy &= \int_0^A \exp\left\{-\left(\sqrt{\frac{\pi j}{2}}y\right)^2\right\}dy \\ &= \sqrt{\frac{2}{\pi j}} \int_0^{A'} \exp(-z^2)dz \\ &= \frac{1}{2}(1-j)(1 - \text{erfc}(A')) \end{aligned} \quad (3.11)$$

where the complementary error function is defined as

$$\text{erfc}(x) = \frac{2}{\sqrt{\pi}} \int_x^\infty \exp(-t^2)dt,$$

and

$$A' = A \cdot \sqrt{\frac{\pi j}{2}} = \sqrt{s\tau_a},$$

Here  $s = j\omega$ , the propagation delay  $\tau_a = a^2(d_t + d_r)/(2d_t d_r c)$ , and  $c$  is the speed of light.

Similarly we have

$$\int_0^B \exp(-j\frac{\pi}{2}y^2)dy = \frac{1}{2}(1-j)(1 - \text{erfc}(\sqrt{s\tau_b})). \quad (3.12)$$

where  $\tau_b = b^2(d_t + d_r)/(2d_t d_r c)$ .

Substitute (3.12) into (3.9) and after some manipulations we can reformulate (3.9) as

$$H(s) = \frac{1}{2} [1 - (1 - \text{erfc}(\sqrt{s\tau_a})) (1 - \text{erfc}(\sqrt{s\tau_b}))] e^{-s\tau_0}. \quad (3.13)$$

where  $\tau_0 = d/c$  is the common time delay.

Recall the Laplace transform pair

$$\text{erfc}(\sqrt{s\tau_a}) \xleftrightarrow{\text{Laplace}} \frac{\sqrt{\tau_a}}{\pi} \frac{1}{t\sqrt{t-\tau_a}} u(t-\tau_a). \quad (3.14)$$

where the unit step function  $u(t)$  is defined as

$$u(t) = \begin{cases} 1, & t \geq 0 \\ 0, & t < 0 \end{cases}$$

By applying inverse Laplace transform to (3.13), time domain impulse response can be obtained

$$h(t) = \delta(t - \tau_0) * \left[ \frac{1}{2\pi t} \left( \sqrt{\frac{\tau_a}{t - \tau_a}} u(t - \tau_a) + \sqrt{\frac{\tau_b}{t - \tau_b}} u(t - \tau_b) \right) - \frac{\sqrt{\tau_a \tau_b}}{2\pi^2} \left( \frac{u(t - \tau_a)}{t\sqrt{t - \tau_a}} * \frac{u(t - \tau_b)}{t\sqrt{t - \tau_b}} \right) \right]. \quad (3.15)$$

When  $a \rightarrow \infty$ ,  $\tau_a \rightarrow \infty$ , thus (3.15) reduces to

$$h(t) = \frac{1}{2} \delta(t - \tau_0) * \frac{1}{\pi t} \sqrt{\frac{\tau_b}{t - \tau_b}} u(t - \tau_b), \quad (3.16)$$

which is exactly the time domain formula for the well-known expression for knife edge diffraction [P.503, [17]]. This serves as our sanity check.

Eq. (3.15) consists of three parts. The physical explanations for the three parts are straightforward. They represent the response from horizontal edge, vertical edge, and the mutual interaction between these two edges, respectively.

### Propagation Model Based on GTD

Ray concept is involved when we attack the diffraction problem with GTD/UTD. The total received field strength is calculated by adding contributions from the various rays, which is also referred to as multipath components in the wireless communication. [7] provided a good GTD-based model in the frequency domain

$$H(j\omega) = \check{D}^{s,h}(j\omega, \psi', \psi) \sqrt{\frac{d_1 + d'_1}{d_1 d'_1}} e^{-jk(d_1 + d'_1)} + \check{D}^{s,h}(j\omega, \phi', \phi) \sqrt{\frac{d_2 + d'_2}{d_2 d'_2}} e^{-jk(d_2 + d'_2)}, \quad (3.17)$$

where the frequency domain GTD diffraction coefficient for half plane (zero-angle wedge)  $\check{D}^{s,h}(j\omega, \psi', \psi)$  can be expressed as

$$\check{D}^{s,h}(j\omega, \Omega', \Omega) = -\frac{e^{-j\pi/4} \sqrt{\lambda}}{4\pi} \cdot \left[ \frac{1}{\cos(\frac{\Omega' - \Omega}{2})} \mp \frac{1}{\cos(\frac{\Omega' + \Omega}{2})} \right], \quad (3.18)$$

The corresponding angle and the distance parameters in (3.17) and (3.18) are given by

$$\begin{aligned} \psi' &= \tan^{-1}\left(\frac{d_t}{b}\right) & \psi &= \psi' + \pi + \tan^{-1}\left(\frac{b}{d_t}\right) + \tan^{-1}\left(\frac{b}{d_r}\right) \\ \phi' &= \tan^{-1}\left(\frac{d_t}{a}\right) & \phi &= \psi' + \pi + \tan^{-1}\left(\frac{a}{d_t}\right) + \tan^{-1}\left(\frac{a}{d_r}\right) \\ d_1 &= \sqrt{d_t^2 + a^2} & d'_1 &= \sqrt{d_r^2 + a^2} \\ d_2 &= \sqrt{d_t^2 + b^2} & d'_2 &= \sqrt{d_r^2 + b^2} \end{aligned} \quad (3.19)$$

The key term to transform (3.12) to time domain is the GTD diffraction coefficient, which here can be obtained by setting  $n = 2$  and  $\beta_0 = \pi/2$ , from the GTD solution (3.8) for wedge diffraction in Section 3.3.1

$$D^{s,h}(t, \Omega', \Omega) = \frac{-1}{2\pi} \sqrt{\frac{c}{2t}} \cdot \left[ \frac{1}{\cos(\frac{\Omega - \Omega'}{2})} \mp \frac{1}{\cos(\frac{\Omega + \Omega'}{2})} \right]. \quad (3.20)$$

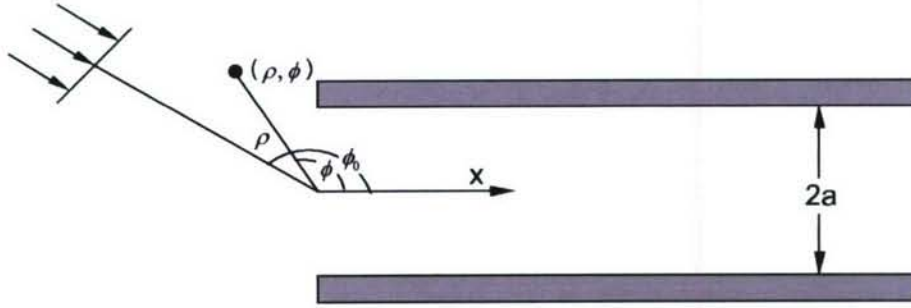


Figure 3.5: UWB pulse diffracted by parallel plates.

### 3.3.3 Two Parallel Half Plane Model

Diffraction of a pulse or a transient wave (acoustic or electromagnetic) by a half plane is one of the early diffraction problems. Exact time domain solution of the CIR for such a channel has been obtained. In this paper, another case for the pulse diffracted by two parallel half planes will be studied. Again, we firstly borrow the existing exact frequency domain solution and then transform it to time domain by Laplace transform. It will be interesting to compare the field diffracted by two parallel half planes with that diffracted by a single half plane.

In reality, a lot of environments can be approximately modeled as the problem of diffraction by two parallel planes. Fig. 3.5 illustrates an example. We assume the transmitting antenna is located far away from the planes and thus the incident wave could be viewed as a plane wave. Moreover, we assume the observation point is far from the planes so that the distance parameter  $\rho \rightarrow \infty$ . We restrict that the incident angle  $\phi_0$  is in the range of  $0 < \phi_0 < \pi$  and the observation angle  $\phi \neq \pi \pm \phi_0$ , which means  $\phi$  is not in the vicinity of the geometrical optics shadow boundary and the reflection boundary. The transfer function for such an channel would be [16]

$$H(j\omega) = \sqrt{\frac{2}{\pi k \rho}} e^{j(k\rho + \frac{1}{4}\pi)} \frac{2 \sin \frac{1}{2} \phi \sin \frac{1}{2} \phi_0}{\cos \phi + \cos \phi_0} \left[ \begin{aligned} & \cos [ka(\sin \phi + \sin \phi_0)] + \\ & + \frac{e^{\frac{1}{4}j\pi}}{\sqrt{4\pi ka}} \left( \frac{1}{\cos \phi} + \frac{1}{\cos \phi_0} \right) \sum_{m=0}^{\infty} \frac{e^{j(2m+1)2ka}}{(2m+1)^{3/2}} \cos [ka(\sin \phi - \sin \phi_0)] - \\ & - \frac{e^{\frac{1}{4}j\pi}}{\sqrt{4\pi ka}} \left( \frac{1}{\cos \phi} + \frac{1}{\cos \phi_0} \right) \sum_{m=1}^{\infty} \frac{e^{j(2m)2ka}}{(2m)^{3/2}} \cos [ka(\sin \phi + \sin \phi_0)] + O\left(\frac{1}{ka}\right) \end{aligned} \right] \quad (3.21)$$

where  $a$  is the distance between two planes. Note that another assumption made here is  $ka \gg 1$ , which can be satisfied either if the distance  $a$  is large or the frequency is high.

Taking a Laplace inversion (by setting  $s = -j\omega$ ), the time domain impulse response can be obtained as

$$h(t) = \left\{ \begin{aligned} & A_0 \frac{u(t)}{\sqrt{t}} * \left[ \begin{aligned} & \delta(t - a/c(\sin \phi + \sin \phi_0) - \rho/c) + \\ & \delta(t + a/c(\sin \phi + \sin \phi_0) - \rho/c) \end{aligned} \right] + \\ & A_1 \sum_{m=0}^{\infty} \frac{1}{(2m+1)^{3/2}} u(t) * \left[ \begin{aligned} & \delta(t - a/c(\sin \phi - \sin \phi_0) - 2(2m+1)a/c - \rho/c) + \\ & \delta(t + a/c(\sin \phi - \sin \phi_0) - 2(2m+1)a/c - \rho/c) \end{aligned} \right] \\ & - A_1 \sum_{m=1}^{\infty} \frac{1}{(2m)^{3/2}} u(t) * \left[ \begin{aligned} & \delta(t - a/c(\sin \phi + \sin \phi_0) - 2(2m)a/c - \rho/c) + \\ & \delta(t + a/c(\sin \phi + \sin \phi_0) - 2(2m)a/c - \rho/c) \end{aligned} \right] \end{aligned} \right\} \quad (3.22)$$

where

$$A_0 = \frac{\sqrt{2}}{\pi} \frac{1}{\sqrt{\rho/c}} \frac{\sin \frac{1}{2}\phi \sin \frac{1}{2}\phi_0}{\cos \phi + \cos \phi_0} \quad A_1 = \frac{1}{\sqrt{2\pi}} \frac{\sin \frac{1}{2}\phi \sin \frac{1}{2}\phi_0}{\cos \phi + \cos \phi_0} \left( \frac{1}{\cos \phi} + \frac{1}{\cos \phi_0} \right) \frac{c}{\sqrt{\rho a}} \quad (3.23)$$

Physical meaning for (3.22) is as follows. The first term in (3.22) consists of a superposition of edge waves from the two half planes, with the condition that each is excited by the incident pulse alone. The edge wave is characterized by a kernel of  $u(t)/\sqrt{t}$  and can be explained with fraction calculus as “semi-integral”.

$$f(t) * \frac{u(t)}{\sqrt{t}} = \Gamma(1/2) \cdot D^{-1/2} \{f(t)\}$$

where  $\Gamma(x)$  is the Gamma function and the fractional integral of order  $\gamma$  is defined by

$$D^{-\gamma} \{f(t)\} = \frac{1}{\Gamma(\gamma)} \int_{-\infty}^t (t - \xi)^{\gamma-1} f(\xi) d\xi$$

The second and the third terms are infinite sums, which represent the successive mutual interactions between the two half planes. These two terms are characterized by a kernel of  $u(t)$  and we have

$$f(t) * u(t) = \int_{-\infty}^t f(\xi) d\xi$$

The coefficient  $\frac{1}{(2m+1)^{3/2}}$  or  $\frac{1}{(2m)^{3/2}}$  decreases rapidly as the value of  $m$  is increased. Practically, computation of infinite sums in (3.22) requires but few terms to obtain reasonable accuracy. This will be verified in our numerical results in the Section 3.5.

It should be noted that if both the transmitter antenna and the receiver antenna are located in the canyon between two half planes, then there is no diffraction phenomena and multiple reflections dominate the received signal. Time domain CIR for such a channel has been studied in [18].

### 3.4 Time Domain Optimum Transmit Waveform Design

Section 3.2.2 shows the optimum receiver should be a matched filter matched to the waveform distorted by the channel, not the transmitted waveform itself. However, from system point of view, such a matched filter alone is not enough. We can further maximize SNR at the receiver side by carefully designing the transmitted waveform [6]. The primary difference between the problem in this paper with the standard matched filter problem is the pulse distortion caused by channel. We will show later that if channel is distortionless, then the SNR at the receiver side is independent of transmitted waveform and then there is no optimum transmitted waveform.

#### 3.4.1 Optimum Transmit Waveform for Distorted Channel

The transmitted waveform optimization problem can be stated as follows. Given the channel impulse response  $h(t)$  and fixed transmitted power  $P_t$  (average power), we wish to achieve the maximum SNR at the receiver side by joint design the transmitted waveform and a good receiver. This problem has been discussed in [6] for radar detection.

Assuming the transmitted pulse  $p(t)$  (to be optimized) is confined to the symmetric time interval  $[-T/2, T/2]$ . The energy of transmitted pulse is then

$$E_p = \int_{-T/2}^{T/2} |p(t)|^2 dt . \quad (3.24)$$

It follows from detection theory that the best receiver is still a matched filter matched to the signal component in  $r(t)$ , the SNR after such a matched filter is given as.

$$SNR = 2E_y/N_0. \quad (3.25)$$

where  $E_y = \int_{-T/2}^{T/2} |p(t) * h(t)|^2 dt$  is the received signal energy. The problem is then reduced to find the optimum  $p(t)$  such that  $E_y$  is maximized, under the constraint of fixed  $E_p$ .

It has been shown in [13] (p. 125) and [6] that the optimum  $p(t)$  can be obtained by solving the following homogeneous Fredholm integral equation

$$\mu_n \phi_n(t) = \int_{-T/2}^{T/2} \kappa(t - \tau) \phi_n(\tau) d\tau , \quad (3.26)$$

and let  $p(t) = \phi_0(t)$ , where  $\phi_0(t)$  is the eigenfunctions corresponding to the maximum eigenvalue  $\mu_0$  and the time reversal operator  $\kappa(t)$  is defined as  $\kappa(t) = h(t) * h(-t)$ . Without loss of generality, it has been assumed that  $\mu_0 > \mu_1 > \mu_2, \dots$ . Pulse waveform  $\phi_0(t)$  reproduces itself, scaled by a constant  $\mu_0$ , when convolved with the time reversal operator over the interval  $[-T/2, T/2]$ .

With optimum  $p(t)$  and  $c(t)$ , we achieve maximum SNR

$$SNR = 2\mu_0 E_p / N_0. \quad (3.27)$$

It is worth noting that to meet the requirement of optimum information transmission might result in another transmit waveform. Maximization SNR requires the transmitter to put as much as possible energy to the frequency with high transmission capability through the channel, under the fixed transmitted energy constraints, while ignore the other frequency modes with small transmission capability. It is possible that these smaller modes contain a significant quantity of information useful for the system. We consider an extreme case here. When  $T \rightarrow \infty$ , it has been shown in [15] (p. 360) that all the energy should be placed into one single frequency  $f_{max}$  in the operation band for which  $H(f)$  is the greatest. This leads to a transmitted waveform of a sine wave at  $f_{max}$ . However, it should be noted that a signal of arbitrarily narrow bandwidth conveys information at a zero rate. Therefore, trade-off should be made between SNR and information transmission.

To illustrate the principle, we study the optimum transmit waveform for the following channels. Consider practically all the communication systems are band limited, we artificially impose a band pass filter in the system. The transfer function of this filter  $H_F(f)$  is defined as

$$H_F(f) = \begin{cases} 1, & f_1 < |f| < f_2 \\ 0, & \text{otherwise} \end{cases}$$

where  $f_1$  and  $f_2$  are the low and high frequency of the filter, respectively. Its time domain impulse response can be expressed as

$$h_F(t) = 2f_2 \text{sinc}(2f_2 t) - 2f_1 \text{sinc}(2f_1 t)$$

The autocorrelation of the impulse response of this filter can be written as

$$\begin{aligned}
 h_F(t) * h_F(-t) &= [2f_2 \text{sinc}(2f_2 t) - 2f_1 \text{sinc}(2f_1 t)] * [2f_2 \text{sinc}(-2f_2 t) - 2f_1 \text{sinc}(-2f_1 t)] \\
 &= 2f_2 \text{sinc}(2f_2 t) + 2f_1 \text{sinc}(2f_1 t) - 4f_1 \text{sinc}(2f_1 t) \\
 &= h_F(t)
 \end{aligned} \tag{3.28}$$

Apparently autocorrelation of the function  $h_F(t)$  reproduces itself.

It should be noted that for cognitive radio purpose, the frequency response of this filter could be in an arbitrary passband (e.g.,  $k$ th element subband) located under the FCC spectral mask (3.1 GHz -10.6 GHz) [19].

Assuming the CIR of a specific channel  $h_c(t)$ , then the overall of the CIR will be  $h(t) = h_F(t) * h_c(t)$ .

### Wedge Channel

Consider a case that light of sight (LOS) is blocked by a PEC wedge, as illustrated in Fig. 3.1, the CIR of such a channel without consideration of bandwidth can be expressed as

$$\begin{aligned}
 h_c(t) &= \sqrt{\frac{c}{2t}} \cdot \frac{\sin \frac{\pi}{n}}{n\pi \sin \beta_0} \cdot \left[ \frac{1}{\cos \frac{\pi}{n} - \cos(\frac{\phi - \phi'}{n})} \mp \frac{1}{\cos \frac{\pi}{n} - \cos(\frac{\phi + \phi'}{n})} \right] \cdot u(t) \\
 &= C(n, \beta_0, \phi, \phi') \cdot \frac{u(t)}{\sqrt{t}}
 \end{aligned} \tag{3.29}$$

where

$$C(n, \beta_0, \phi, \phi') = \sqrt{\frac{c}{2}} \frac{\sin \frac{\pi}{n}}{n\pi \sin \beta_0} \cdot \left[ \frac{1}{\cos \frac{\pi}{n} - \cos(\frac{\phi - \phi'}{n})} \mp \frac{1}{\cos \frac{\pi}{n} - \cos(\frac{\phi + \phi'}{n})} \right]$$

is a constant whose value is depending on the environment.

Note that  $u(t)/\sqrt{t}$  is an even function. The autocorrelation of the above CIR is

$$h_c(t) * h_c(-t) = C^2 \cdot \frac{u(t)}{\sqrt{t}} * \frac{u(t)}{\sqrt{t}}$$

Then the autocorrelation of the overall CIR for a wedge channel is written as

$$\begin{aligned}
 \kappa(t) &= h_c(t) * h_c(-t) * h_F(t) * h_F(-t) \\
 &= C^2 \cdot \Gamma^2(1/2) \cdot D^{-1} \{h_F(t) * h_F(-t)\} \\
 &= C^2 \pi \cdot \int_{-\infty}^t [2f_2 \text{sinc}(2f_2 t) - 2f_1 \text{sinc}(2f_1 t)] dt \\
 &= C^2 \cdot [Si(2\pi f_1 t) - Si(2\pi f_2 t)] + C^2 \pi^2 / 2
 \end{aligned} \tag{3.30}$$

where sine integral function  $Si(x)$  is defined as

$$Si(x) = \int_0^x \frac{\sin t}{t} dt$$

Note that  $Si(x)$  can be implemented with a Matlab built-in function. substitute (3.30) into (3.26) and solve (3.26) for  $\phi(t)$  numerically we can obtain the optimum waveform for wedge channels.

### Rectangular Channel

The time domain CIR for such a channel has been derived in Section 3.3.2. It follows from Eq. (3.15) that the CIR consists of three parts. Practically, the contribution from the third part (mutual interaction between two edge waves) in (3.15) is very weak and could be ignored. We will also verify the validation of this assumption through our numerical results subsequently. Then the CIR can be approximated by the first two parts

$$h(t) \approx \frac{\sqrt{\tau_a}}{2\pi} \cdot \frac{1}{(t + \tau_a)\sqrt{t}} u(t) * \delta(t - \tau_a) + \frac{\sqrt{\tau_b}}{2\pi} \cdot \frac{1}{(t + \tau_b)\sqrt{t}} u(t) * \delta(t - \tau_b) \quad (3.31)$$

Note in (3.31) we have ignored the common time delay  $\tau_0$ , for simplicity.

For the term  $\frac{1}{(t + \tau_{a,b})\sqrt{t}}$ , most of the energy is focused at the singularity where  $t = 0$ , thus we have  $\frac{1}{(t + \tau_{a,b})\sqrt{t}} = \frac{1}{\tau_{a,b}\sqrt{t}}$ . Then (3.31) can be further approximated as

$$h(t) \approx C_a \frac{u(t)}{\sqrt{t}} * \delta(t - \tau_a) + C_b \frac{u(t)}{\sqrt{t}} * \delta(t - \tau_b) \quad (3.32)$$

where  $C_a = \frac{1}{2\pi\sqrt{\tau_a}}$  and  $C_b = \frac{1}{2\pi\sqrt{\tau_b}}$ .

The time reversal operator  $\kappa(t)$  for such a rectangular channel can be expressed as

$$\begin{aligned} \kappa(t) \approx & (C_a^2 + C_b^2) \cdot [Si(2\pi f_1 t) - Si(2\pi f_2 t)] \\ & + C_a C_b \cdot [Si(2\pi f_1 t) - Si(2\pi f_2 t)] * [\delta(t - \tau_a + \tau_b) + \delta(t + \tau_a - \tau_b)] + (C_a + C_b)^2 \pi^2 / 2 \end{aligned} \quad (3.33)$$

### Two Half Planes Waveguide Channel

As stated in Section 3.3.3, the half planes waveguide model is a little more complicated than the other two models studied above, due to the exist of multiple replicas (caused by waveguide phenomena). However, we can simplify the problem by focus on the main lobe of the  $\kappa(t)$  instead of the whole  $\kappa(t)$ . The main lobe of  $\kappa(t)$  for two half planes channel can be approximated as

$$\begin{aligned} \kappa(t) \approx & 2A_0^2 \cdot [Si(2\pi f_1 t) - Si(2\pi f_2 t)] \\ & + 2A_1^2 \left( \sum_{m=1}^{\infty} m^{-3} \right) \cdot \left[ \frac{1}{\pi} (Si(2\pi f_1 t) - Si(2\pi f_2 t)) + \frac{1}{2\pi^2} \left( \frac{\cos(2\pi f_1 t)}{f_1} - \frac{\cos(2\pi f_2 t)}{f_2} \right) \right] \end{aligned} \quad (3.34)$$

For the case of high frequency where  $f_1 \rightarrow \infty$  and  $f_2 \rightarrow \infty$ , interestingly,  $\kappa(t)$  is reduced to a form of

$$\kappa(t) \approx C' \cdot [(Si(2\pi f_1 t) - Si(2\pi f_2 t))]$$

where  $C' = 2A_0^2 + \frac{2A_1^2}{\pi} \left( \sum_{m=1}^{\infty} m^{-3} \right)$  is a constant depending on the environment parameters such as the location of the receive and transmit antennas ( $\rho, \phi, \phi'$ ), and the distance between the two half planes ( $a$ ). Therefore, under these assumptions, the optimum transmit waveform for the two half planes waveguide channel will be the same as a wedge channel, which has been solved above.

### 3.4.2 Numerically Computing Eigenfunctions

Except for some classical case such as band limited signals [13, 6], the eigenfunctions and eigenvalues are generally difficult to be solved in a closed form. In this section we are interested in computing the eigenfunctions and eigenvalues numerically. The idea is to discretize the function and borrow the powerful matrix theory to solve the problem. We firstly discretize the autocorrelation function  $\kappa(t)$  with sufficient low sampling rate such as to include all the significant channel frequencies.

As stated in the previous section, the optimal pulse waveform (maximizing SNR) is a solution to the integral function

$$\mu_n \phi_n(t) = \int_{-T/2}^{T/2} \kappa(t - \tau) \phi_n(\tau) d\tau \quad (3.35)$$

Note that the TR operator  $\kappa(t)$  is an even function, i.e.,  $\kappa(t - \tau) = \kappa(\tau - t)$ , the above equation can be reformulated as

$$\mu_n \phi_n(t) = \int_{-T/2}^{T/2} \kappa(\tau - t) \phi_n(\tau) d\tau \quad (3.36)$$

$$\mu_n \cdot \phi_n(t) = \int_{T/2}^{-T/2} \kappa(t - \tau) \phi_n(t) d\tau \quad n = 1, \dots, \infty, \quad (3.37)$$

$$\mu_n \cdot \begin{bmatrix} \phi_n(-N) \\ \phi_n(-N+1) \\ \vdots \\ \phi_n(N) \end{bmatrix} = \begin{bmatrix} \kappa(-2N) & \dots & \kappa(0) \\ \kappa(-2N+1) & \dots & \kappa(1) \\ \vdots & \ddots & \vdots \\ \kappa(0) & \dots & \kappa(2N) \end{bmatrix} \cdot \begin{bmatrix} \phi_n(-N) \\ \phi_n(-N+1) \\ \vdots \\ \phi_n(N) \end{bmatrix} \cdot \Delta t \quad (3.38)$$

We then transform the integral function to a matrix problem. To find the solution of the integral function (3.35) is then equivalent to finding the eigen function of matrix  $\kappa(t)(2N + 1 \times 2N + 1)$  in (3.38). Several remark notes can be drawn from (3.38)

- The optimum waveform obtained via the numerical solution introduced above is not necessarily the unique one; though the maximum eigenvalue is unique, the corresponding eigenfunction might not.
- If there is no pulse distortion (e.g., free space transmission), the time reversal operator  $\kappa(t) = \alpha_0 \delta(t - \tau_0)$ , where  $\alpha_0$  and  $\tau_0$  are the constants depending on the distance between the transmitter and the receiver. For this special case, there is no optimum transmitted waveform since any waveform will reproduce itself after being convoluted with the time reversal operator.
- We can improve computation accuracy by decreasing sampling interval  $\Delta\tau$ . However, the computation complexity is increased correspondingly.

It is also evident that the availability of time domain CIR  $h(t)$  (and thus its time reversal operator  $\kappa(t)$ ) is critical to computing the optimum waveform  $\phi_0(t)$ . The following will show how to get the time domain CIR for several canonical environments.

## 3.5 Numerical Results

### 3.5.1 Calculation of Singularity in the Impulse Response of Wedge Diffraction

A singularity appears in the impulse response for most of channels where diffraction phenomena is involved, e.g., in Eq. (3.6) (wedge diffraction), when  $t \rightarrow 0$ , then  $D^{s,h}(t) \rightarrow \infty$ , thus in Eq. (3.4), there is a singularity at  $t = 0$ . How to numerically calculate this singularity is not a trivial issue. Since the singularity is exactly where the energy concentrates and also defines the type of the pulse distortion, it can not be directly removed using the time windowing. From an Electromagnetic point of view, this singularity at the diffracted wavefront is essential. An integral-differential (*Int-Diff*) approach has been proposed and proved to be an efficient way to remove this discontinuity at  $t = 0$  during the calculation [3, 10]. In this section, we will further verify this approach by comparing it with the well known ATT approach [8].

#### Int-Diff Approach

Mathematically, the principle of this *Int-Diff* approach can be described as follows,

$$\int_0^t [p(t) * g(t)] dt = p(t) * \int_0^t g(t) dt \quad (3.39)$$

hence, we have

$$p(t) * g(t) = \frac{d}{dt} \left[ p(t) * \int_0^t g(t) dt \right] \quad (3.40)$$

where  $g(t)$  has a singularity in the time domain. The integration  $\int_0^t g(t) dt$  removes the singularity and can often be obtained in a closed form. The reason why we call this approach *Int-Diff* approach is because additional integration and differentiation operation are involved to get the convolution result.

*Int-Diff* approach provides a very efficient way to do the numerical convolution for the case when there is a singularity in the functions to be convolved. This approach is specially important when we deal with the diffraction problem in the time domain because there is always a singularity in the diffraction coefficient due to the nature of diffraction.

Again, we consider wedge diffraction case as an example. Notice that the singularity in (3.4) is solely caused by term  $F(X_m, t)$ . We will focus on this term first. The rest of work is just linear summation. According to *int-diff* approach, firstly we will need to integrate  $F(X_m, t)$ . Happily, we have a closed form for the integration of  $F(X_m, t)$ , which can be expressed as

$$\begin{aligned} \bar{F}(X_m, t) &= \int_0^t F(X_m, t) dt \\ &= 2\sqrt{\frac{X_m}{\pi}} \operatorname{atan} \left( \sqrt{\frac{ct}{X_m}} \right) \end{aligned} \quad (3.41)$$

Let  $\bar{D}^{s,h}(t)$  denotes the integration of the wedge diffraction coefficient  $D^{s,h}(t)$ , then we have

$$\bar{D}^{s,h}(t) = \frac{-1}{2n\sqrt{2\pi}\sin\beta_0} \sum_{m=1}^4 K_m^{s,h} \bar{F}(X_m, t) \quad (3.42)$$

Note that singularity in  $D^{s,h}(t)$  has been removed in the new integration expression  $\bar{D}^{s,h}(t)$ . The latter can be used to do the convolution, followed by a differentiation operation as a compensation.

### Analytic Time Transform (ATT)

ATT is another classic technique used to perform an efficient convolution with a broad class of excitation pulse functions *int-diff*. In this paper, this classic approach will be briefly introduced and serve as a sanity check for the *int-diff* approach.

The second version ATT in [8] is defined as

$$f^+(t) = \frac{j}{\pi} \int_{-\infty}^{\infty} \frac{f(\tau)}{t-\tau} d\tau, \quad \text{for } \text{Im}(t) > 0 \quad (3.43)$$

The “+” sign over  $f$  means an analytical signal in a complex-time domain. Let  $p(t)$ , and  $h(t)$  denote the incident pulse and the impulse response of the system, respectively, then we have,

$$p(t) * h(t) = \frac{1}{2} \text{Re} \left[ p^+(t) * h^+(t) \right] \quad (3.44)$$

Notice that the singularity on real time axis ( $\text{Im}(t) = 0$ ) in  $h^+(t)$  is only a branch point singularity and not a pole. Therefore, the difficulty in calculation the singularity in  $h(t)$  has been removed by ATT in  $h^+(t)$ . Moreover, if we choose the incident pulse such that in the frequency domain  $p(\omega)$  can be modeled using exponential function as

$$p(\omega) = \sum_{n=1}^N A_n e^{-\alpha_n \omega} \quad \text{for } \omega > 0 \quad (3.45)$$

or equivalently, in time domain

$$p^+(t) = \sum_{n=1}^N A_n \delta^+(t + j\alpha_n) \quad (3.46)$$

then the convolution can be evaluated in closed form as

$$p(t) * h(t) = \text{Re} \left[ \sum_{n=1}^N A_n h^+(t + j\alpha_n) \right] \quad (3.47)$$

where the shifting property of the analytic delta function

$$\frac{1}{2} \delta^+(t + j\alpha_n) * h^+(t) = h^+(t + j\alpha_n) \quad (3.48)$$

has been used.

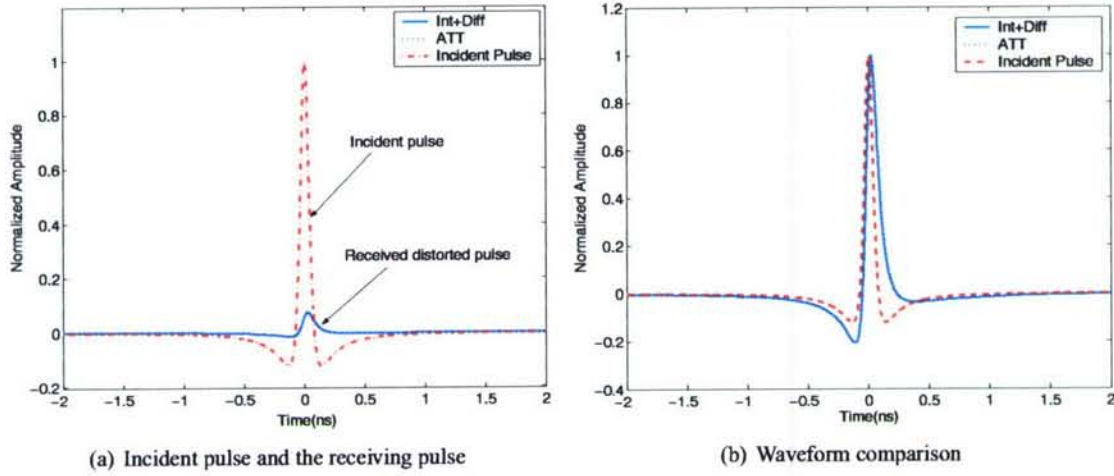


Figure 3.6: Comparison between the approaches of Int-Diff and ATT. In (a) amplitudes have been normalized to the incident pulse to compare the power of the incident pulse and the received pulse. In (b), the incident pulse has been scaled to the same amplitude of the received pulse to compare their waveforms

To verify our result with *int-diff* approach, we use the same incident pulse as used in [8]. Mathematically, the frequency domain of the incident pulse  $p(\omega)$  is defined by

$$p(\omega) = C_0(1 - e^{-\omega T})^{P_1} e^{-\omega P_2 T} \quad (3.49)$$

where  $T' = \frac{1}{2\pi f_c} \ln\left(\frac{P_1 + P_2}{P_1}\right)$ ,  $f_c$  represents the center frequency, which can be adjusted easily according to different requirements. The peak of the  $p(\omega)$  is normalized by choosing  $C_0 = \left(\frac{P_1 + P_2}{P_1}\right)^{P_1} \left(\frac{P_1 + P_2}{P_1}\right)^{P_2}$ . Time domain waveform of the incident pulse can be conveniently obtained by

$$p(t) = Re \left[ \overset{\dagger}{p}(t) \right] = Re \left[ \frac{j}{\pi} \sum_{n=0}^{P_1} \frac{C_0 \binom{P_1}{n}}{t + j(n + P_2)T'} \right] \quad (3.50)$$

where  $\binom{P_1}{n} = \frac{P_1!}{n!(P_1 - n)!}$ .

Let  $\overset{\dagger}{D}(t)$  denote the analytic impulse response of wedge diffraction, then using the convolution property in Table 2.1 in [8], the receiving pulse will be

$$\begin{aligned} r(t) &= Re \left[ \frac{1}{2} \overset{\dagger}{p}(t) * \overset{\dagger}{D}(t) \right] \\ &= Re \left[ \sum_{n=0}^{P_1} C_0 \binom{P_1}{n} \overset{\dagger}{D}(t + j(n + P_2)T') \right] \end{aligned} \quad (3.51)$$

Instead of integration, ATT approach remove the singularity by performing an analytic transform. The analytic transform of an time domain function is not so straightforward, especially when the function itself is complicated.

According to [8], the analytic wedge diffraction coefficient  $D^+(t)$  can be expressed as

$$D^{s,h+}(t) = \frac{-1}{2n\sqrt{2\pi}\sin\beta_0} \sum_{m=1}^4 K_m^{s,h+} F^+(x_m, t) \quad (3.52)$$

where

$$F^+(x_m, t) = \frac{\sqrt{x_m/\pi}}{\sqrt{-jt}(\sqrt{-jt} + \sqrt{jx_m/c})} \quad (3.53)$$

and the rest of the parameters are the same with that of TD-UTD, presented in section II.

Fig. 3.6 shows the received waveforms, calculated with ATT and *Int-Diff* approach, respectively. The incident waveform, marked as red slash curve, is also plotted, as a reference. Firstly, it can be easily observed that the received waveforms, calculated with different approaches, are in excellent agreement. Secondly, it can also be observed from Fig. 3.6(a) that the diffracted pulse is much weaker than the incident pulse, due to the huge energy loss caused by diffraction. To better compare the waveform between incident pulse and the diffracted pulse, we manually scaled their amplitudes to the same value and their waveforms are shown in Fig. 3.6(b). It is evident that the diffracted pulse waveform is much different from the incident one, indicating a pulse distortion caused by diffraction. Finally, the amplitude information (signal strength) can be predicted by traditional frequency domain UTD, the pulse waveform information that presented in this paper, however, can only be provided by time domain formulations.

The parameters used in our simulation are as follows: For the incident pulse,  $R_1 = 2$ ,  $P_2 = 1$ , and  $f_c = 2$  GHz. The parameters for the wedge are:  $\beta_0 = \pi/2$ ,  $n = 3/2$ ,  $\phi = 5\pi/6$ ,  $\phi' = \pi/3$ , and the soft boundary condition has been considered.

### 3.5.2 Rectangular Building

For all the figures (unless otherwise specified) in this paper, the waveform labeled "TD" is obtained by convolution of the incident pulse  $p(t)$  with the time domain CIRs derived in this paper, and the waveform labeled "FD+IFFT" is obtained by applying inverse Fast Fourier Transform (IFFT) to the product of  $P(f)H(f)$ , where  $P(f)$  and  $H(f)$  are Fourier Transform of  $p(t)$  and channel transfer function, respectively. We have verified our time domain derivation by comparing the "TD" result and "FD+IFFT" result.

In the following numerical results, we choose the second order derivative of Gaussian pulse as the incident pulse, which mathematically is defined as

$$p(t) = \left[ 1 - 4\pi \left( \frac{t - t_c}{w} \right)^2 \right] e^{-2\pi \left( \frac{t - t_c}{w} \right)^2} \quad (3.54)$$

where  $w$  is the parameter controlling the width of the pulse (and therefore the frequency bandwidth of the transmit signal) and  $t_c$  is time shift to put the pulse in the middle of the window.

Fig. 3.7 shows a comparison between GTD and Fresnel-Kirchhof models. Here, we set  $w = 0.1$  ns and  $t_c = 0.3$  ns. The environment parameters used in the simulation are as follows:  $d_t = 1000m$ ,  $d_r = 900m$ ,  $a = 15m$ , and  $b = 10m$ .

Several observations can be made from Fig. 3.7.

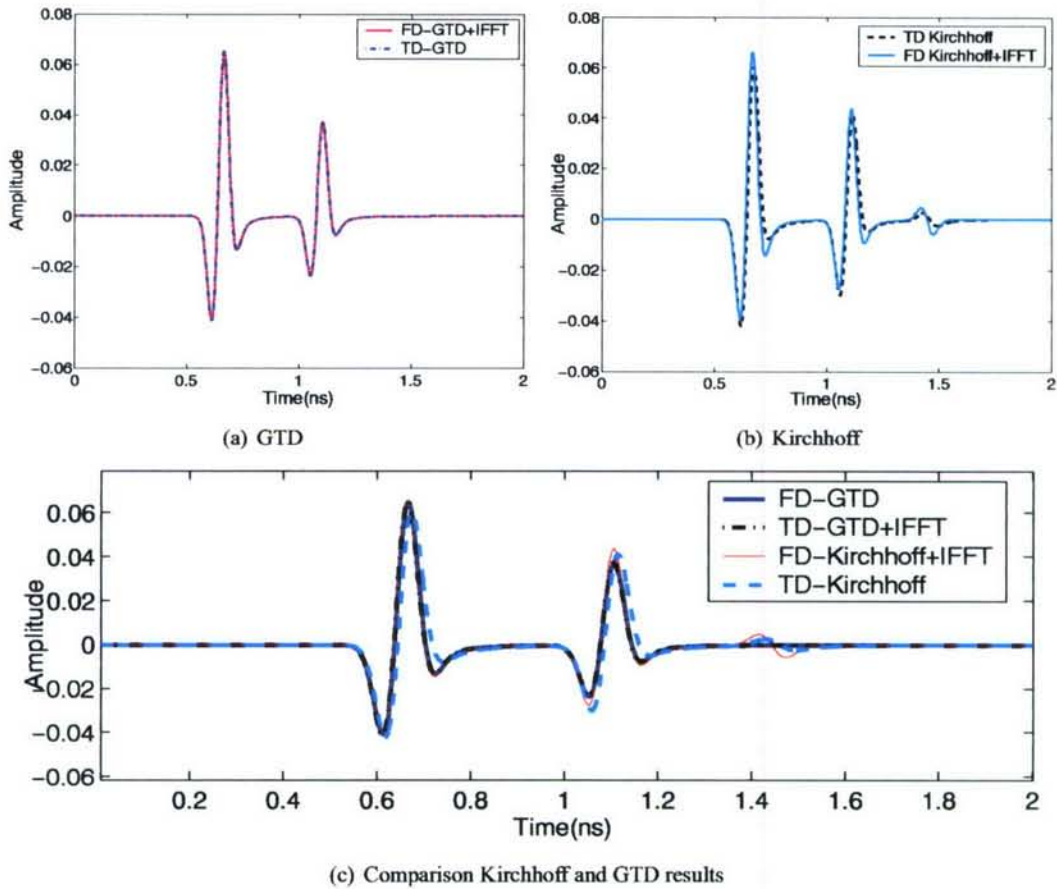


Figure 3.7: Simulated pulse waveforms after a second order derivative of Gaussian pulse pass through a rectangular channel described in Fig. 3.4

- For both GTD model and Fresnel-Kirchhof Model, time domain results show very good agreement with the results transformed from the frequency domain via IFFT (labeled “FD+IFFT”). This verifies our time domain derivation.
- The diffracted waveforms based on GTD and Fresnel-Kirchhof agree very well to each other, except that the Fresnel-Kirchhof result has an additional small waveform response. This extra “baby response” can be identified from its time domain formula to be the mutual interaction (coupling) term between two edges, which has not been taken into account by the GTD-based model.

Again, for the convenience of comparison, common propagation delays has been neglected.

### 3.5.3 Two Parallel Half Planes Model

As mentioned in Section 3.3.3, when a UWB pulse is incident on the parallel half plane channel, the received signal consist of three parts, with each part including two same (but separated in the time) signal components. The relative signal strengths of these three parts depend on the value of the coefficient  $A_0$  and  $A_1$ , which in turn depend on the

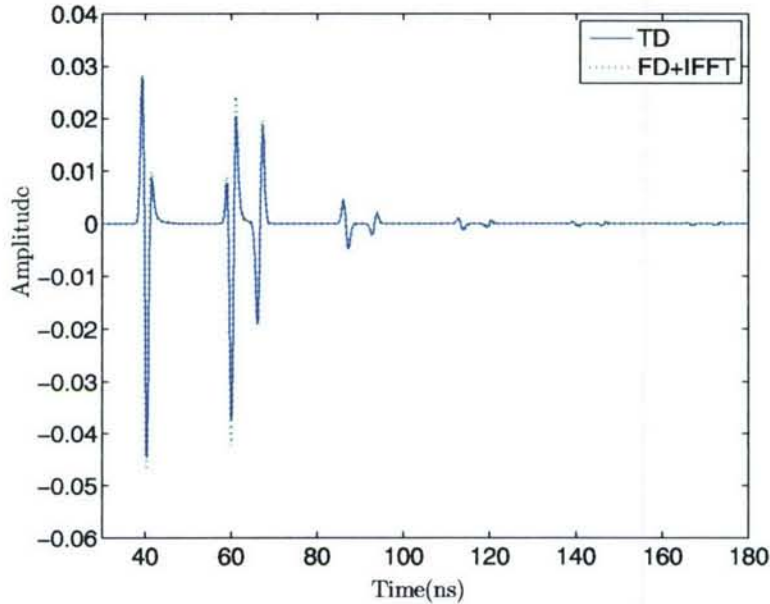


Figure 3.8: UWB pulse diffracted by a parallel plane waveguide

environment and the location of the antenna. Fig. 3.8 shows the received signal when a second order derivative of Gaussian pulse is incident on the parallel half plane channel. The incident pulse width parameter  $w = 2 \text{ ns}$ . The geometrical parameters for parallel planes are as follows:  $\rho = 20m$ ,  $\phi = 8/15\pi$ ,  $\phi_0 = 5/6\pi$ ,  $a = 2m$ .

It can be seen from Fig. 3.8 that the waveforms of the received pulses are not second order derivative Gaussian anymore. It follows from Section 3.3.3 that they are actually “semi-integral” forms of the second order derivative Gaussian pulse. Again, the agreement between the waveform obtained by time domain convolution (labeled “TD”) and frequency domain result (labeled “FD+IFFT”) shows our time domain derivation is correct.

Although Eq. (3.22) shows infinite terms, we can see from Fig. 3.8 that these sums converge very fast.

### 3.5.4 Optimum Transmit Waveform Design

Fig. 3.9 shows the optimum transmit waveforms for different channels. These waveforms have been obtained by substituting  $\kappa(t)$  of corresponding channels into (3.38) and numerically computing  $\phi(t)$  associated with the maximum eigenvalue. For the convenience of waveform comparison, the energy of the computed optimum transmit waveforms ( $\phi(t)$ ) for different channels have been normalized. The parameters used in the simulation are as follows:  $T = 2ns$ ,  $f_1 = 3GHz$ ,  $f_2 = 5GHz$ . Moreover, in each model, the environmental parameters we have used here are the same as those we have used for the computation of distortion waveforms in this section. It has been shown in Section 3.4.1 that the optimum transmit waveform for the two parallel half planes channel is approximately the same as wedge channel, under some circumstances.

For the purpose of maximizing the SNR at the receiver side, all the energy should be sent through the optimum transmit waveform, which is the eigenfunction associated with the maximum eigenvalue of  $\kappa(t)$ . For the purpose

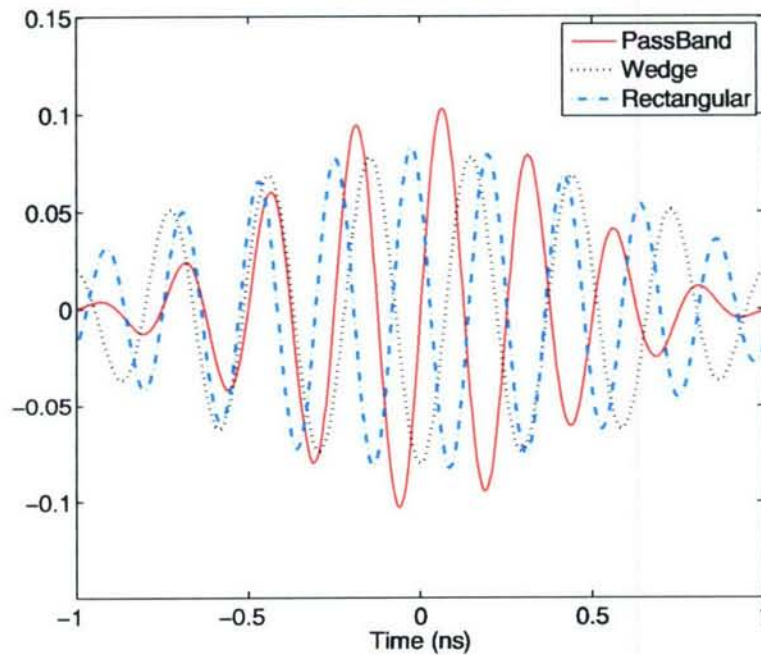


Figure 3.9: Optimum transmit waveform design for bandlimited UWB signal passing through different channels

of flexibility, we are interested in transmission of a linear combination of the eigenfunctions whose eigenvalues are close to the maximum one. Fig. 3.10 shows the first six eigen waveforms for the passband channel. Their corresponding eigenvalues are 1.0000, 0.9999, 0.9979, 0.9976, 0.9621, and 0.9599. We can also transmit these waveforms parallel to increase the data rate. Note that the eigenfunctions for the low pass channel ( $[0, f]$ ) is known as prolate spheroidal wave functions [20], and has been proposed as a novel UWB pulse shaping technique in [21].

### 3.6 Conclusion

For wideband signals such as UWB, by principle, time domain frame work appears to be a better frame work to study its propagation. The time domain impulse responses for a series of scattering environments have been derived for the first time. Specifically, several electromagnetic communication fundamental channels, including perfect conduct electromagnetic wedge, large rectangular plates, and parallel planes waveguide, are studied. The receiving signal, calculated through convolution in the time domain impulse response, can provide waveform information, as well as the amplitude information (Path loss). The pulse waveforms passing through these channels are compared with their original waveforms. The comparison show that for wideband signals, a transmit pulse could be extremely distorted by diffraction mechanism. The results converted from frequency domain by applying a inverse fast Fourier Transform (IFFT) serves as sanity checks for our time domain derivation. Given the time domain channel impulse response, we also study the optimum transmit waveform such that the signal to noise ratio (SNR) at the receiver side is maximized, under the constraint of fixed transmitted power.

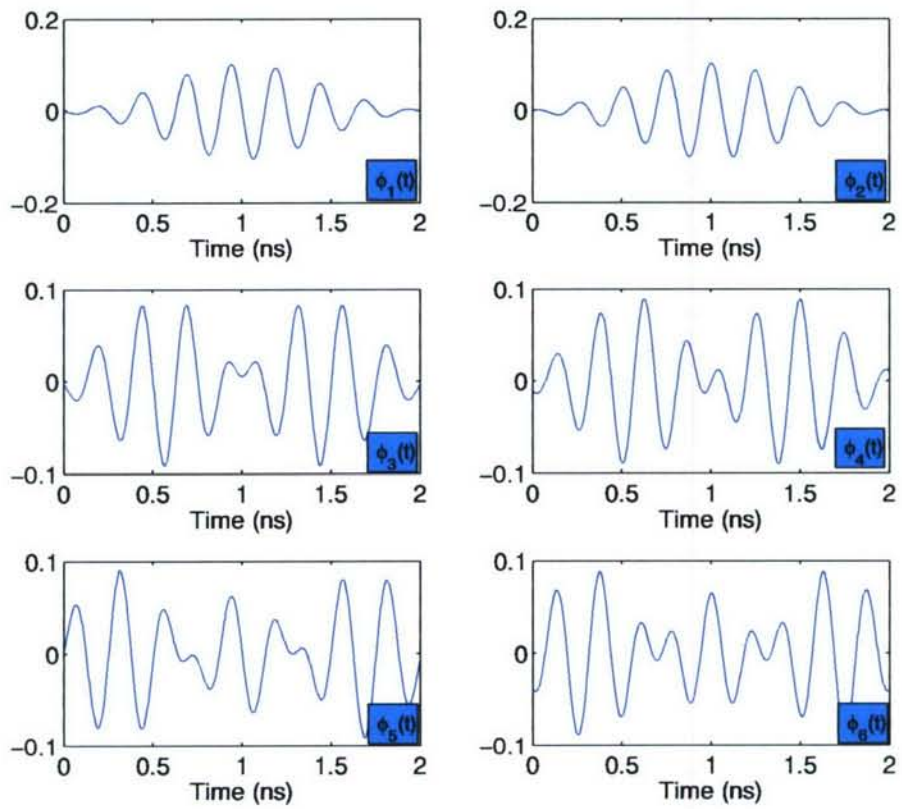


Figure 3.10: The first six eigen waveforms for a passband channel

## Bibliography

- [1] R. C. Qiu, "A theoretical study of the Ultra-Wideband wireless propagation channel and optimum UWB receiver design," *IEEE Journal on Selected Areas in Communications (JSAC)*, special issue on UWB multiple access communications, Vol. 20, No. 12, pp. 1628-1637, Dec. 2002.
- [2] R. C. Qiu, "A generalized time domain multipath channel and its applications in Ultra-wideband (UWB) wireless optimal receiver design," *IEEE Trans. Wireless Communications*, Vol. 3, No. 11, pp. 2312-2324, Nov. 2004.
- [3] R. C. Qiu, C. Zhou and Q. Liu, "Physics-based pulse distortion for Ultra-Wideband signals", *IEEE Trans. Veh. Tech.*, Vol. 54, No. 5, pp. 1546-1554, Sept. 2005.
- [4] R. G. Kouyoumjian and P. H. Pathak, "A uniform geometric theory of diffraction for an edge in a perfectly conducting surfaces," *Proc. IEEE*, Vol. 62, pp. 1448-1461, Nov. 1974.
- [5] T. W. Veruttipong, "Time domain version of the uniform GTD," *IEEE Trans. Antenna Prop.*, Vol. 38, No. 11, pp. 1757-1764, Nov. 1990.
- [6] P. R. Rousseau and P. H. Pathak, "Time domain uniform geometrical theory of diffraction for a curved wedge," *IEEE Trans. Antenna Prop.*, Vol. 43, No. 12, pp. 1375-1382, Dec. 1995.
- [7] H. Mokhtaris, P. Lazaridis, "Comparative study of lateral profile knife-edge diffraction and ray tracing technique using GTD in urban environment," *IEEE Tran. Veh. Tech.*, Vol, 48, No. 1, pp. 255-261. Jan. 1999.
- [8] P. R. Rousseau and P. H. Pathak, "Time domain version of the uniform geometrical theory of diffraction," The Ohio State University, Technical Report 721564-3, Tech. Rep., Feb. 1996.
- [9] J. W. Schuster and R. J. Luebbers, "Using FDTD to evaluate ray-tracing models for propagation prediction in urban microcells," *Proc. 1998 IEEE AP-S Int. Symp.*, vol. 3, pp. 1676-1679, Jun. 1998.
- [10] C. Zhou and R. C. Qiu, "Pulse distortion caused by cylinder diffraction and its impact on UWB communications," *IEEE Trans. Veh. Techn.*, Vol. 56, No. 4, pp. 2385-2391, July 2007.
- [11] M. R. Bell, "Information theory and radar waveform design," *IEEE Trans. on Inf. Theory*, Vol., 39, No. 5, pp. 1578-1597, Sept. 1993.
- [12] J. L. Holsinger, "Digital communication over fixed time-continuous channels with memory – with special applications to telephone channels," *Tech. Report* No. 430, Research Lab of Electronics, MIT, Oct. 1964.
- [13] H. L. Van Trees, *Detection, Estimation, and Modulation Theory, Part I*. New York: Wiley, 1968.
- [14] E. J. Badhdady, *Lectures on communications system theory*, Ch. 14, 1961, New York: McGraw-Hill.

- [15] R. C. Qiu, "A Generalized Time Domain Multipath Channel and its Application in Ultra-Wideband (UWB) Wireless Optimal Receiver Design: Part II Wave-Based System Analysis," *IEEE Trans. Wireless Communications*, Vol. 3, No. 11, pp. 2312-2324, Nov. 2004.
- [16] J. J. Bowman, T. B. A. Senior, P. L. E. Uslenghi, *Electromagnetic and Acoustic Scattering by Simple Shapes*, New York: Hemisphere, 1987.
- [17] E.C. Jordan and K.G. Balmain, *Electromagnetic Waves and Radiating Systems*, Second Edition. Prentice-Hall, 1968.
- [18] C. Zhou and R. C. Qiu, "Spatial focusing of time-reversed UWB electromagnetic waves in a hallway environment," Submitted to *IEEE 38th Southeastern Symposium on System Theory*, Cookeville, TN, USA. March 5-7, 2006.
- [19] H. Zhang, X. Zhou, K. Y. Yazdandoost, I. Chalamtac, "Multiple signal waveforms adaptation in cognitive Ultra-Wideband radio evolution," *IEEE Journal on Selected Areas in Communications (JSAC)*, Vol. 24, No. 4, April, 2006.
- [20] D. Slepian and H.O. Pollak, "Prolate spheroidal wave functions, Fourier analysis, and uncertainty-1," *Bell Syst. Tech. J.*, vol.40, no.1, pp.4346, Jan. 1961.
- [21] R.S. Dilmaghani, M. Ghavami, B. Allen, and H. Aghvami, "Novel UWB pulse shaping using prolate spheroidal wave functions," *Proc. 14th IEEE International Symposium on Personal, Indoor and Mobile Radio Communications (PIMRC 2003)*, pp. 602606, Beijing, Sept. 2003

## Chapter 4

# Optimum Transmission Waveform in RF Harsh Environments

### 4.1 Introduction

Communications and networking in confined metal environments are critical to applications such as intra-ship, intra-vehicle, intra-engine, manufacturing plants, assembly lines, nuclear plants, body area network sensors surrounded by vehicles and tanks, etc. Narrow band wireless technologies have proved ineffective in these environments, due to resonance caused by the metal walls. The physical mechanisms of short pulse propagation in a confined metal environment are studied by Felsen[1], from a transient radar cross section. An Ultra-wideband (UWB) system [2]-[5] is proposed here to resolve the resonance into many time-resolvable pulses—corresponding to extremely rich multipath. The energy of these pulses is difficult to collect using traditional RAKE or multicarrier technologies. As an alternative, a powerful time reversal channel-matching technique is suggested for this purpose.

Periodically modulated radar returns from jet engines can be modeled as a chirp [6]. This view provides some insight into our problem, with measured channel pulse response from a pulse train as long as 800ns.

Chirp UWB systems [7]—accepted into IEEE 802.15.4a in Dec. 2006—have some favorable advantages such as low cost, low transmission power (long range), low battery power, anti-jamming, easy synchronization, robustness to Doppler frequency shift (mobility), etc. Analog SAW filters can be employed to perform receiver matched filter.

This paper is motivated by the UWB applications in the harsh environment, by adapting the existing standards. Time reversal[9][10]—see [8] for a review—has been used to compress the channel response into a sharp main lobe. Similarly, chirp matched filter results in pulse compression. We design the time reversal chirp system from the classical modal modulation and give some relative performances in different situations. Finally, the spectral efficiencies of different transmission schemes are compared to benchmark the time reversal chirp scheme.



Figure 4.1: Rectangular metal cavity used for propagation experiments.

## 4.2 Pulse Propagation in Rectangular Metal Cavity

The measurement is performed using frequency domain technique to analyze the characteristics of the UWB channel in the confined metal environment. The rectangular confined metal cavity in Fig. 4.1 measures 16 feet by 8 feet by 8 feet. The materials of the walls are aluminum.

The sounding is carried out by sweeping a set of narrowband sinusoid signals (tones) through a wide frequency band. The data of channel frequency response is collected using a Vector Network Analyzer (VNA)—Agilent N5230A (300kHz – 13.5GHz). The VNA sweeps from 3GHz to 10GHz using 7001 points with frequency step of 1MHz. The power of each tone is 10dBm, and the same for all the measurements reported in this paper. The number of averaging is 128, which is used to enhance the accuracy of the measurement. Meanwhile, the cables and the connectors are calibrated before measurement to compensate for the frequency dependent losses.

The measurement is done for line of sight (LOS) situation. The distance between transmitter antenna and receiver antenna varies from 0.5m to 4m with distance step of 0.5m and both antennas are placed at 1.35m above the ground. The transmitter antenna is fixed, and the receiver antenna is moved to different locations along the middle line of one side of the rectangular metal cavity.

After the channel response is measured in the frequency domain (Fig. 4.2), zero padding is done between 0Hz and 3GHz, conjugate reflection between  $-10\text{GHz}$  and 0Hz and inverse fast Fourier transform (IFFT) are used to obtain the channel pulse response  $h(t)$  in Fig. 4.3 and Fig. 2.1(d). Channel pulse response in the office environment (Fig. 2.1(d)) is very different from that in the rectangular metal cavity (Fig. 4.3), for the transceiver distance of 4m. Channel pulse response in the metal cavity is long and strong for the transceiver distance of 4m (Fig. 4.3).

The energy of the channel is

$$E_h = \int_0^{T_h} h^2(t) dt \quad (4.1)$$

where  $T_h$  is the time duration of the channel. The autocorrelation of the channel is shown in Fig. 4.4, defined as

$$R_{hh}(t) = h(t) * h(T_h - t). \quad (4.2)$$

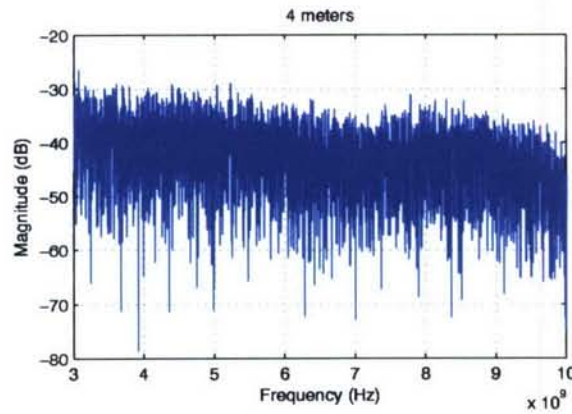


Figure 4.2: Measuring frequency response  $H(f)$  in a rectangular metal cavity. A total of 7001 equal frequency tones are sent from 3GHz to 10GHz (with a step of 1MHz).

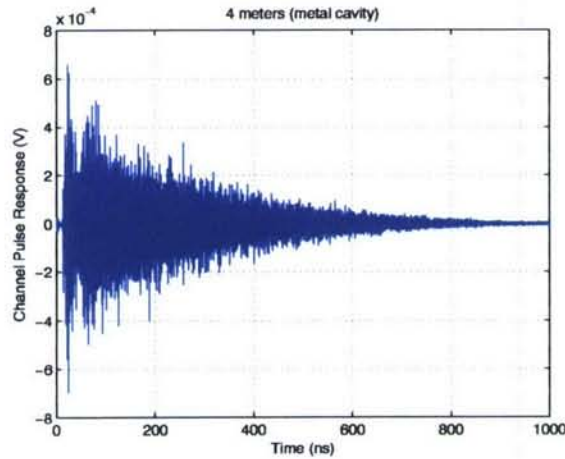


Figure 4.3: Channel pulse propagation  $h(t)$  in a rectangular metal cavity. The pulse has 7001 equal frequency components (with a step of 1MHz) from 3GHz to 10GHz.

It is interesting to notice that the total energy of the channel pulse response in a confined metal cavity drops very slowly as compared to office and hallway environments, as shown in Fig. 4.5.

### 4.3 Time Reversal Transmission with Chirp Signaling

#### 4.3.1 Modal Modulation

The starting point of our system formulation is from the well known result of Holsinger (1964) [13], regarding optimum detectors for a linear time-invariant (LTI) channel with memory, as shown in Fig. 4.6. If  $x(t)$  is the input to the LTI channel with channel pulse response  $h(t)$  mentioned before. The symbol duration is  $T_s$ , and the waveform

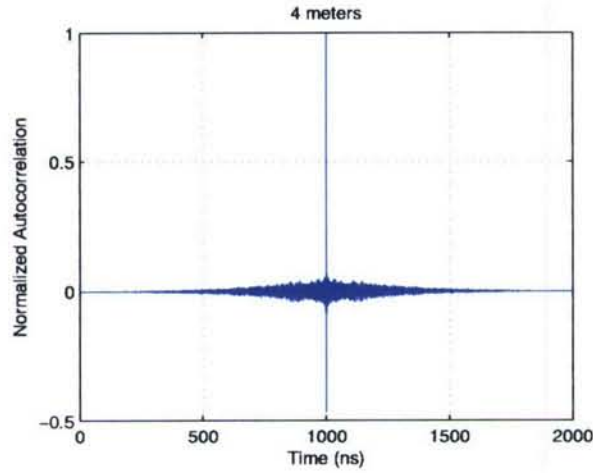


Figure 4.4: Autocorrelation of channel pulse response  $R_{hh}(t) = h(t) * h(l_h - t) / E_h$  in a rectangular metal cavity.

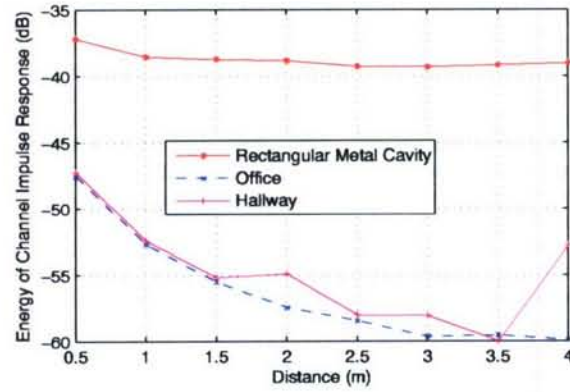


Figure 4.5: The total energy of the channel pulse response in a confined metal cavity decays very slowly, as compared with office and hallway.

duration of  $x(t)$  is  $T$ . The output waveform is

$$r(t) = \int_0^T x(\tau)h(t - \tau) d\tau, \quad 0 \leq t \leq T_1 \quad (4.3)$$

for the observation time  $[0, T_1]$ . White Gaussian noise is assumed. According to the channel pulse response, the observation time and waveform duration, a symmetric function  $K(t, s)$  can be defined as

$$K(t, s) = \int_0^{T_1} h(\sigma - t)h(\sigma - s) d\sigma, \quad 0 \leq t, s \leq T' \quad (4.4)$$

Furthermore, we can define a possibly infinite-size set of orthonormal eigenfunctions,  $\varphi_n(t)$ , that satisfy the relation [13]

$$\lambda_n \cdot \varphi_n(t) = \int_0^T K(t, \tau)\varphi_n(\tau) d\tau, \quad 0 \leq t \leq T \quad (4.5)$$

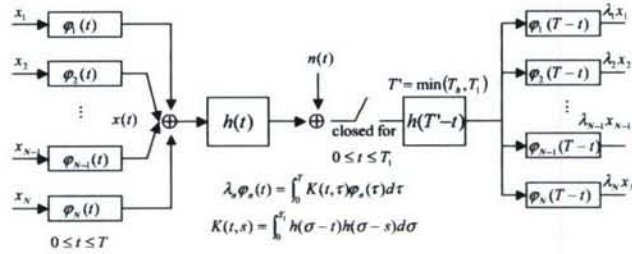


Figure 4.6: Modal modulation is optimum for the LTI channel with memory. When a self-reproducing eigenfunction  $\varphi_n(t)$  is transmitted, after the channel matched filter  $h(\min(T_h, T_1) - t)$ , the same waveform  $\varphi_n(t)$  (within a gain factor  $\lambda_n$ ) is obtained. The optimal detection waveform is matched to the  $\varphi_n(t)$ .

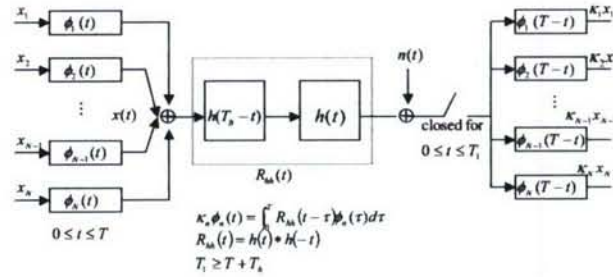


Figure 4.7: Time reversal modal modulation is proposed to simplify the transceiver complexity. The channel matched filter  $h(T_h - t)$  is moved to the transmitter side. The self-reproducing  $\phi_n(t)$  can be defined, similarly to the modal modulation illustrated in Fig. 4.6.

A special form of (4.5) is given by [14]. That is a function  $\varphi_n(t)$  that when convolved with  $K(t, s)$  over the interval  $[0, T]$  reproduces itself, scaled by a constant  $\lambda_n$ , called eigenvalue.

$\varphi_n(t)$   $n = 1, 2, \dots, \infty$  can be seen as a set of basis functions, so  $x(t)$  can be written as

$$x(t) = \sum_{n=0}^{\infty} x_n \varphi_n(t), \quad 0 \leq t \leq T \tag{4.6}$$

and

$$x_n = \int_0^T x(t) \varphi_n(t) dt, \quad n = 1, 2, \dots, \infty \tag{4.7}$$

so the energy of the transmitted signal is

$$E_t = \int_0^T |x(t)|^2 dt \tag{4.8}$$

$$= \sum_{n=1}^{\infty} x_n^2 \tag{4.9}$$

From detection point of view, after matched filter, the output signal to noise ratio (SNR) is  $2E/N_0$ , where

$$E = \sum_{n=1}^{\infty} \lambda_n x_n^2 \tag{4.10}$$

and  $N_0/2$  is the double sided noise spectral density. So the probability of error for the detector is given by

$$P_e = \frac{1}{\sqrt{2\pi}} \int_{\sqrt{2E/N_0}}^{\infty} \exp(-\frac{1}{2}x^2) dx \quad (4.11)$$

In order to minimize  $P_e$ , SNR should be maximized. Since by conversion  $\lambda_1 \geq \lambda_2 \geq \lambda_3 \geq \dots$ , if the energy of  $x(t)$  is fixed, maximizing  $E$  means  $x(t) = x_1\varphi_1(t)$  which is the optimal waveform for detection. So, the maximum SNR can be expressed as,

$$\text{SNR}_{\max} = \frac{2\lambda_1 x_1^2}{N_0} \quad (4.12)$$

$$= \frac{2\lambda_{\max} E_t}{N_0} \quad (4.13)$$

From capacity point of view, the modal modulation system have many parallel orthogonal channels and each channel corresponds to one eigenfunction  $\varphi_n(t)$ . We can use the classical water filling scheme to calculation coefficients  $x_n$   $n = 1, 2, \dots, \infty$  based on the energy constraint of transmitted signal  $x(t)$ .

The observation time  $T_1$  and the symbol duration  $T_S$  are very important for the system design. If  $T_1 < T + T_h$ , then  $T_S$  should be equal to or greater than  $\max(T_1 + \min(T_1, T_h), T + T_h)$ . And if  $T_1 \geq T + T_h$ , then  $K(t, s)$  reduces to  $K(t - s)$  and  $T_S$  should be equal to or greater than  $T + 2T_h$ . In these situations, the generalized Nyquist criterion can be satisfied, so we do not need to consider ISI when using modal modulation.

### 4.3.2 Time Reversal Modal Modulation

Time reversal modal modulation is proposed to simplify the transceiver complexity. The  $h(T_h - t)$ , time reversal filter is moved to the transmitter side. Similarly to the modal modulation illustrated in Fig. 4.6, the self-reproducing eigenfunctions  $\phi_n(t)$  with eigenvalues  $\kappa_n$  illustrated in Fig. 4.7 can be defined as

$$\kappa_n \cdot \phi_n(t) = \int_0^T R_{hh}(t - \tau) \phi_n(\tau) d\tau, \quad 0 \leq t \leq T' \quad (4.14)$$

where

$$R_{hh}(t) = h(t) * h(-t) \quad (4.15)$$

Notice that when  $T_1 \geq T + T_h$  and  $T_S \geq T + 2T_h$ , moving the channel matched filter  $h(T_h - t)$  in Fig. 4.6 to the transmitter side will not affect the optimality of the system. In other words, the systems in Fig. 4.6 and Fig. 4.7 are equivalent in the above situation. In Appendix B, we give the proof that when the optimal waveform is used for detection, the maximum SNR after matched filter is equal to  $2\kappa_{\max} E_t / N_0$  similarly as shown in Eq. 4.13.

### 4.3.3 Time Reversal Chirp System

Time reversal modal modulation gives us a lot of insights to design UWB system. The main work shifts from how to handle ISI to how to design the transmitted waveform. We can calculate the orthonormal eigenfunctions  $\phi_n(t)$   $n = 1, 2, \dots, \infty$  according to the autocorrelation of the memory channel. Each eigenfunction can be seen as

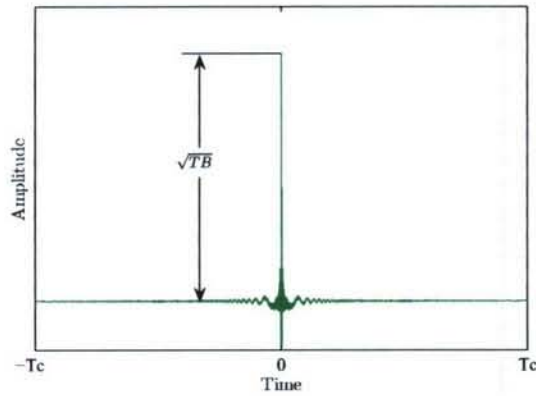


Figure 4.8: Output waveform of the chirp matched filter without time reversal, defined as  $R_{cc}(t)$  in (4.17).

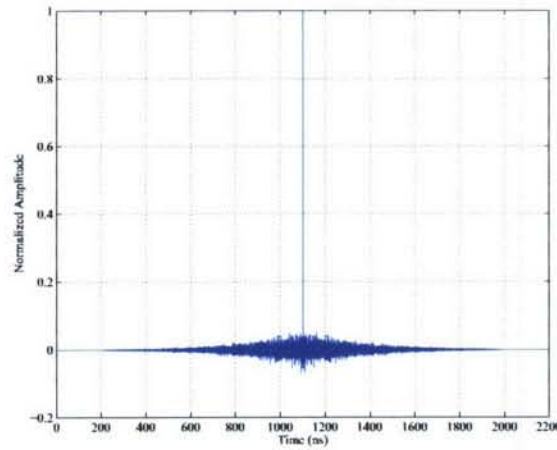


Figure 4.9: Output waveform of the chirp matched filter with time reversal.

a waveform and any linear combinations of these waveforms can be used in different situations and requirements as well.

It is well known that chirp signal has the sharp autocorrelation characteristic and it is widely used in the radar field. We can easily use chirp signal as the waveform instead of the eigenfunction to get the time reversal chirp system.

Chirp signal is defined as

$$c_h(t) = \cos\left(2\pi\left(f_0t \pm \mu\frac{t^2}{2}\right)\right), 0 \leq t \leq T \tag{4.16}$$

where  $f_0, T, \mu$  are center frequency, signal duration and sweep rate, respectively. The amplitude spectrum of a chirp signal approaches to a band pass filter as the time bandwidth product of it becomes large.

The frequency of a chirp sweeps continuously, and its duration can be changed independently. The bandwidth  $B$  of a chirp signal is  $B = \mu * T$ . Signal with  $+\mu$  is an up chirp while  $-\mu$  is a down chirp. The pair is matched to each

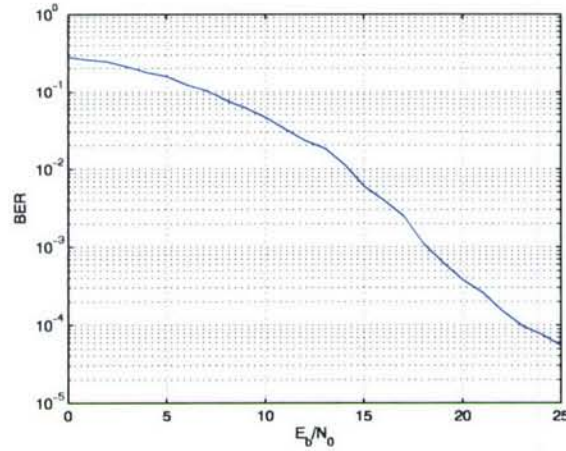


Figure 4.10: Simulation result for time reversal chirp system in the rectangular metal cavity.

other. The output of the matched filtering is  $R_{cc}(t) = c_h(t) * c_h(T' - t)$ —implemented using surface acoustic wave (SAW) devices—expressed by [19]

$$R_{cc}(t) = \sqrt{4\mu} \cos(2\pi f_0(t - T')) \frac{\sin(\pi\mu t(T' - |t - T'|))}{2\pi\mu t}, \quad 0 \leq t \leq 2T' \quad (4.17)$$

which is illustrated by Fig. 5.3.

If time reversal is not considered, after the chirp matched filter, a compressed pulse that has a short duration of  $2/B$  is generated. The peak in Fig. 5.3 is  $\sqrt{TB}$ . As a result of matched filter, a flat envelope pulse with duration  $T$  is compressed into a much shorter waveform of duration  $2/B$ . If time reversal is used, the output waveform of the chirp matched filter is shown in Fig. 4.9.

#### 4.3.4 System Performance Comparison

The system performance comparison between time reversal modal modulation system and time reversal chirp system will be considered here when  $T_S \geq T + 2T_h$ .

##### From Detection Point of View

From detection point of view, SNR after matched filter in the receiver side is the metric to determine the system performance.

The maximum SNR for time reversal modal modulation system can be shown in Eq. 4.108.

For time reversal chirp system, if chirp signal  $c_h(t)$  is used, then,

$$c_h(t) = \sum_{n=1}^{\infty} c_n \phi_n(t), \quad 0 \leq t \leq T \quad (4.18)$$

where

$$c_n = \int_0^T c_h(t) \phi_n(t) dt, \quad n = 1, 2, \dots, \infty \quad (4.19)$$

and  $\phi_n(t)$  is from Eq. 4.14.

The energy of the transmitted signal is

$$E_t = \int \left[ \left( \sum_{n=1}^{\infty} c_n \phi_n(t) \right) * h(-t) \right]^2 dt \quad (4.20)$$

$$= \int \int_0^T \left( \sum_{n=1}^{\infty} c_n \phi_n(\tau) \right) h(\tau - t) d\tau \int_0^T \left( \sum_{n=1}^{\infty} c_n \phi_n(s) \right) h(s - t) ds dt \quad (4.21)$$

$$= \int_0^T \int_0^T \int h(\tau - t) h(s - t) dt \left( \sum_{n=1}^{\infty} c_n \phi_n(s) \right) \left( \sum_{n=1}^{\infty} c_n \phi_n(\tau) \right) ds d\tau \quad (4.22)$$

$$= \int_0^T \int_0^T R_{hh}(\tau - s) \left( \sum_{n=1}^{\infty} c_n \phi_n(s) \right) \left( \sum_{n=1}^{\infty} c_n \phi_n(\tau) \right) ds d\tau \quad (4.23)$$

$$= \int_0^T \left( \sum_{n=1}^{\infty} c_n \int_0^T R_{hh}(\tau - s) \phi_n(s) ds \right) \left( \sum_{n=1}^{\infty} c_n \phi_n(\tau) \right) d\tau \quad (4.24)$$

$$= \int_0^T \left( \sum_{n=1}^{\infty} \kappa_n c_n \phi_n(\tau) \right) \left( \sum_{n=1}^{\infty} c_n \phi_n(\tau) \right) d\tau \quad (4.25)$$

$$= \sum_{n=1}^{\infty} \kappa_n c_n^2 \int_0^T |\phi_n(\tau)|^2 d\tau \quad (4.26)$$

$$= \sum_{n=1}^{\infty} \kappa_n c_n^2 \quad (4.27)$$

In the receiver side, after matched filter, SNR is

$$\text{SNR}_{\text{chirp}} = \frac{\left[ \int_0^T \left( \sum_{n=0}^{\infty} \kappa_n c_n \phi_n(t) \right) \left( \sum_{n=0}^{\infty} c_n \phi_n(t) \right) dt \right]^2}{\frac{N_0}{2} \int_0^T \left( \sum_{n=0}^{\infty} c_n \phi_n(t) \right)^2 dt} \quad (4.28)$$

$$= \frac{\left( \sum_{n=0}^{\infty} (\kappa_n c_n^2) \right)^2}{\frac{N_0}{2} \sum_{n=0}^{\infty} c_n^2} \quad (4.29)$$

$$= \frac{2E_t^2}{N_0 \sum_{n=0}^{\infty} c_n^2} \quad (4.30)$$

So, the maximum SNR gap between time reversal modal modulation system and time reversal chirp system is

$$g_{\text{SNR}} = \frac{\kappa_{\text{max}} E_t \sum_{n=0}^{\infty} c_n^2}{E_t^2} \quad (4.31)$$

$$= \frac{\kappa_{\text{max}} \sum_{n=0}^{\infty} c_n^2}{\sum_{n=1}^{\infty} \kappa_n c_n^2} \quad (4.32)$$

If  $T$  goes to infinity,  $c_n$  can be treated equally and Eq. 4.32 is reduced to

$$g_{\text{SNR}} = \frac{(\max \{|H(f)|\})^2}{\frac{1}{W} \int_{f_0}^{f_1} |H(f)|^2 df} \quad (4.33)$$

which can be treated as the peak to average ratio from perspective of frequency domain.

When  $T$  is equal to 1ns, 10ns, 100ns and goes to infinity, the maximum SNR gap will become 2.5dB, 4.5dB, 8.4dB and 12.7dB, respectively. The result is based on the measurement data shown in Fig. 4.2.

#### From Data Rate Point of View

If L-level pulse amplitude modulation (PAM) is considered and there are L equally likely amplitude values placed at level  $\pm d, \pm 3d, \dots, \pm(L-1)d$ . In time reversal system, the waveform filter in the transmitter side is  $G_T(t)$  and the corresponding frequency response is  $G_T(f)$ ; the time reversal filter is  $h(-t)$  and the corresponding frequency response is  $H^*(f)$ . So, the average transmitted power is

$$P_t = \frac{d^2}{T_s} \frac{L^2 - 1}{3} \int_{-\infty}^{\infty} |G_T(f)|^2 |H(f)|^2 df \quad (4.34)$$

In the receiver side, after matched filter, the minimum distance of the signal is

$$d_{\text{min}}^2 = d^2 \left[ \int_{-\infty}^{\infty} |G_T(f)|^2 |H(f)|^2 df \right]^2 \quad (4.35)$$

and the noise power is

$$\sigma^2 = \frac{N_0}{2} \int_{-\infty}^{\infty} |G_T(f)|^2 df \quad (4.36)$$

where  $N_0/2$  is the double sided PSD of the white Gaussian noise. Thus, the PAM probability of symbol error is

$$P_e = 2 \left(1 - \frac{1}{L}\right) Q \left( \frac{d_{\text{min}}}{\sigma} \right) \quad (4.37)$$

$$= 2 \left(1 - \frac{1}{L}\right) Q \left( \sqrt{\frac{3}{L^2 - 1} \frac{2T_s P_t \int_{-\infty}^{\infty} |G_T(f)|^2 |H(f)|^2 df}{N_0 \int_{-\infty}^{\infty} |G_T(f)|^2 df}} \right) \quad (4.38)$$

where  $Q(x)$  is defined as  $Q(x) = \frac{1}{\sqrt{2\pi}} \int_x^\infty e^{-t^2/2} dt$  and the corresponding bit error rate (BER)  $P_b$  can be determined as follows if  $L$  is given,

$$P_b = \frac{P_e}{\log_2 L} \quad (4.39)$$

Meanwhile we assume that the time duration of  $G_T(t)$  is  $T$  and  $T_S = T + 2T_h$ . So, the number of bits that can be transmitted in each  $T'_S$  is

$$b = \log_2 L \quad (4.40)$$

and  $L$  can be equal to  $2, 2^2, 2^3, \dots$

In the time reversal chirp system,  $G_T(t)$  is  $c_h(t)$  defined in Eq. 4.18. If  $T, P_b$  and  $L_c$  are given, we can get  $2T_s P_t / N_0$  from Eq. 4.37 and Eq. 4.39 and the data rate of the time reversal chirp system is

$$R_c = \frac{\log_2 L_c}{T_S} \quad (4.41)$$

In the time reversal modal modulation system, there are many parallel orthogonal channels and each channel corresponds to the orthonormal eigenfunction  $\phi_n(t)$  and eigenvalue  $\kappa_n$  from Eq. 4.14. We assume  $\kappa_1 \geq \kappa_2 \geq \kappa_3 \geq \dots$ . Meanwhile, the bits transmitted in these different channels are assumed to be totally independent.

For the  $n$ th channel, the PAM level is  $L_n$ ;  $G_{Tn}(t)$  is  $x_n \phi_n(t)$  and  $x_n$  is the value to be determined later; the transmitted power is  $P_{tn}$ ; BER is  $P_{bn}$ ; the PAM probability of symbol error is  $P_{en}$ ; the number of bits transmitted in each  $T'_S$  is  $b_n$ . So, from Eq. 4.34, it follows that,

$$P_{tn} = \frac{d^2}{T_S} \frac{L_n^2 - 1}{3} \int_{-\infty}^{\infty} |G_{Tn}(f)|^2 |H(f)|^2 df \quad (4.42)$$

$$= \frac{d^2}{T_S} \frac{L_n^2 - 1}{3} \int_{-\infty}^{\infty} |x_n \phi_n(f)|^2 |H(f)|^2 df \quad (4.43)$$

$$= \frac{d^2}{T_S} \frac{L_n^2 - 1}{3} x_n^2 \int_{-\infty}^{\infty} |\phi_n(f)| |\phi_n(f)| |H(f)|^2 df \quad (4.44)$$

$$= \frac{d^2}{T_S} \frac{L_n^2 - 1}{3} \kappa_n x_n^2 \int_{-\infty}^{\infty} |\phi_n(f)|^2 df \quad (4.45)$$

$$= \frac{d^2}{T_S} \frac{(L_n^2 - 1) \kappa_n x_n^2}{3} \quad (4.46)$$

and from Eq. 4.38, it follows that,

$$P_{en} = 2 \left(1 - \frac{1}{L_n}\right) Q \left( \sqrt{\frac{3}{L_n^2 - 1} \frac{2T_s P_{tn}}{N_0} \frac{\int_{-\infty}^{\infty} |G_{Tn}(f)|^2 |H(f)|^2 df}{\int_{-\infty}^{\infty} |G_{Tn}(f)|^2 df}} \right) \quad (4.47)$$

$$= 2 \left(1 - \frac{1}{L_n}\right) Q \left( \sqrt{\frac{3}{L_n^2 - 1} \frac{2T'_s P_{tn}}{N_0} \frac{\int_{-\infty}^{\infty} |x_n \phi_n(f)|^2 |H(f)|^2 df}{\int_{-\infty}^{\infty} |x_n \phi_n(f)|^2 df}} \right) \quad (4.48)$$

$$= 2 \left(1 - \frac{1}{L_n}\right) Q \left( \sqrt{\frac{3}{L_n^2 - 1} \frac{2T'_s P_{tn}}{N_0} \frac{\int_{-\infty}^{\infty} |\phi_n(f)|^2 |H(f)|^2 df}{\int_{-\infty}^{\infty} |\phi_n(f)|^2 df}} \right) \quad (4.49)$$

$$= 2 \left(1 - \frac{1}{L_n}\right) Q \left( \sqrt{\frac{3}{L_n^2 - 1} \frac{2T_s P_{tn} \kappa_n}{N_0}} \right) \quad (4.50)$$

and

$$P_{bn} = \frac{P_{cn}}{\log_2 L_n} \quad (4.51)$$

and

$$b_n = \log_2 L_n \quad (4.52)$$

Thus, the total power  $P_t$  used for time reversal modal modulation is

$$P_t = \sum_{n=1}^{\infty} P_{tn} \quad (4.53)$$

$$= \frac{d^2}{T_S} \sum_{n=1}^{\infty} \frac{(L_n^2 - 1) \kappa_n x_n^2}{3} \quad (4.54)$$

and the total bits transmitted in each  $T_S$  is

$$b = \sum_{n=1}^{\infty} b_n \quad (4.55)$$

$$= \sum_{n=1}^{\infty} \log_2 L_n \quad (4.56)$$

So, the data rate of time reversal modal modulation system is

$$R_m = \frac{b}{T_S} \quad (4.57)$$

From the data rate point of view, we have the optimization problem shown as below,

$$\begin{aligned} \max b &= \sum_{n=1}^{\infty} b_n \\ \text{s.t. } P_t &= \sum_{n=1}^{\infty} P_{tn} \\ P_{bn} &= \text{constant} \end{aligned} \quad (4.58)$$

The data rate of time reversal modal modulation system is  $b/T_S$ .

The iterative loading algorithm shown in Appendix C is used here to solve the above the optimization problem. So, the data rate gap is defined as,

$$g_{\text{rate}} = \frac{R_m}{R_c} \quad (4.59)$$

$$= \frac{\sum_{n=1}^{\infty} \log_2 L_n}{\log_2 L_c} \quad (4.60)$$

When BER  $P_b$  is set to  $10^{-4}$  and the same pulse amplitude modulation (PAM) constellation is considered, the data rate gap between time reversal modal modulation system and time reversal chirp system is calculated as follows:

When  $L_c = 2$ ,  $g_{rate} = 0, 3.0, 7.0$  (dB) for  $T = 1, 10, 100$  (ns); when  $L_c = 4$ ,  $g_{rate} = 5.4, 7.4, 10.2$  (dB) for  $T = 1, 10, 100$  (ns); when  $L_c = 8$ ,  $g_{rate} = 7.5, 11.1, 13.9$  (dB) for  $T = 1, 10, 100$  (ns).

From the comparison, we know the performances of time reversal modal modulation system are better than those of time reversal chirp system when  $T_S \geq T + 2T_h$ . If we want to fully employ the advantage of chirp signal, the requirement of  $T_S$  should be relaxed. In this case, the introduction of ISI is inevitable. In Section 4.3.5, we will consider the system performance from BER point of view when  $T_S$  is less than  $T$ .

### 4.3.5 BER Performance for Time Reversal Chirp System

In this section we consider the time reversal chirp system with the existence of ISI. In this case, duration of symbol  $T_S$  is far less than  $T$ . Supposing PAM signals are used in a single-user system, the transmitted signal can be expressed as

$$s(t) = \sum_{n=0}^{\infty} I_n p(t - nT_S) \quad (4.61)$$

where

$$p(t) = c_h(t) * h(-t) \quad (4.62)$$

$I_n$  represents the  $n$ th discrete information symbol with duration  $T_S$ ,  $c_h(t)$  is the chirp signal with the bandwidth  $W$  and the time duration  $T$ , and  $h(-t)$  is the time reversed channel impulse response  $h(t)$ . The received signal is

$$r(t) = \sum_{n=0}^{\infty} I_n y(t - nT_S) + n(t) \quad (4.63)$$

where

$$y(t) = p(t) * h(t) \quad (4.64)$$

$n(t)$  is AWGN.

The received signal  $r(t)$  passes the matched filter followed by a sampler with a sampling rate of  $1/T_S$ . The impulse response of the matched filter is  $c_h(-t)$ . So the output of the matched filter is expressed as

$$q(t) = \sum_{n=0}^{\infty} I_n R_{pp}(t - nT_S) + v(t) \quad (4.65)$$

where  $R_{pp}(t)$  is the autocorrelation of  $p(t)$  and  $v(t)$  is the response of the matched filter for AWGN noise  $n(t)$ . Denote

$$R_{k-n} = R_{pp}(t - nT_S)|_{t=kT_S} \quad (4.66)$$

$$v_k = v(t)|_{t=kT_S} \quad (4.67)$$

we get

$$q_k = \sum_{n=0}^{\infty} I_n R_{k-n} + v_k \quad (4.68)$$

$$= R_0 I_k + \sum_{n=0, n \neq k}^{\infty} I_n R_{k-n} + v_k \quad (4.69)$$

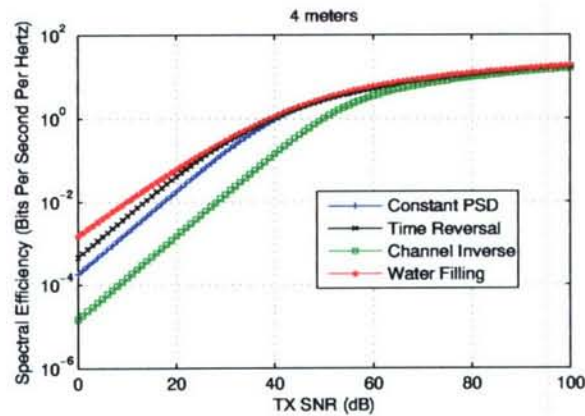


Figure 4.11: Spectral efficiency in a rectangular metal cavity.

where  $I_k$  term represents the expected information symbol of the  $k$ th sampling period, the  $2^{nd}$  term is ISI and  $v_k$  is the additive Gaussian variable at the  $k$ th sampling point.

Here we performed the time reversal chirp simulation using the channel depicted in Fig. 4.3. The time reversal chirp system has 2-level PAM and 500Mbps data symbol rate. The frequency range of the chirp signal is from 3GHz to 10GHz and the duration is 100ns. Perfect synchronization was assumed. The simulation result is depicted in Fig. 4.10. From the BER curve we can see that the  $E_b/N_0$  penalty for  $10^{-3}$  is approximately 17dB. As  $E_b/N_0$  reaches 25dB, the trend of the slope becomes flat and  $E_b/N_0$  approaches between  $10^{-4}$  and  $10^{-5}$ . For a large class of UWB applications, it's sufficient for BER at  $10^{-3}$  with data rate up to 500MHz in harsh environment with 1us delay spread.

#### 4.4 Capacity in Rectangular Metal Cavity

The channel transfer function is  $H(f)$  with bandwidth  $W = f_1 - f_0$  where  $f_0$  is the starting frequency and  $f_1$  the end frequency. Here,  $H(f)$  contains path loss and multipath. The functional relation between path loss and multipath is complicated to parameterize. Instead, we use the measured  $H(f)$  for calculation. No fading is observed for a fixed transceiver pair.

In the transmitter side, different precoding schemes are employed to shape the spectrum of the signal. Here, water filling, time reversal, channel inverse, and constant power spectrum density (PSD) of signal are considered. See Appendix A for details. Their relative spectral efficiencies are compared in Fig. 4.11. By simulation it is easy to find that the curve of constant PSD can represents that of ideal chirp signal, while spectral efficiency of time reversal is almost the same as that of ideal time reversal chirp signal. The channel inverse scheme is good for detection, but performs poorly in terms of capacity.

The capacity is limited by the PSD of the transmission signal. In the US, the FCC requires that the maximum PSD be  $-41.3\text{dBm/MHz}$ . If the PSD of the AWGN noise is  $-114\text{dBm/MHz}$ , then the ratio of the transmitted signal power and the received noise power, called TX SNR (defined in Appendix A) in Fig. 4.11, is around 70dB.

## Appendix A Spectral Efficiency

The PSD of the signal in the transmitter side and noise the receiver side are, respectively, denoted as  $S(f)$  and  $\frac{N_0}{2}$ . The power of the signal is defined as

$$P = \int_{f_0}^{f_1} S(f) df \quad (4.70)$$

The power of noise in the receiver side is expressed as

$$N = \frac{N_0}{2}(f_1 - f_0) = \frac{N_0}{2}W \quad (4.71)$$

with ratio of the transmitted signal power to received noise power (TX SNR)

$$\rho = \frac{P}{N} \quad (4.72)$$

The capacity is

$$C = \int_{f_0}^{f_1} \log_2 \left( 1 + \frac{S(f)|H(f)|^2}{\frac{N_0}{2}} \right) df \quad (4.73)$$

and the spectral efficiency is

$$\frac{C}{W} = \frac{\int_{f_0}^{f_1} \log_2 \left( 1 + \frac{S(f)|H(f)|^2}{\frac{N_0}{2}} \right) df}{f_1 - f_0} \quad (4.74)$$

If water filling is used, then

$$S(f) = \left( \mu - \frac{N_0}{2|H(f)|^2} \right)^+ \quad (4.75)$$

where  $(x)^+ = \max[0, x]$ , the constant  $\mu$  is the water level chosen to satisfy the power constraint with equality

$$\int_{f_0}^{f_1} S(f) df = P \quad (4.76)$$

and the spectral efficiency in this case is

$$\frac{C}{W} = \frac{\int_{f_0}^{f_1} \left( \log_2 \left( \frac{\mu|H(f)|^2}{\frac{N_0}{2}} \right) \right)^+ df}{f_1 - f_0} \quad (4.77)$$

When time reversal is used, it follows that

$$S(f) = \alpha |H(f)|^2 \quad (4.78)$$

the constant  $\alpha$  is the factor chosen to satisfy the power constraint with equality

$$P = \int_{f_0}^{f_1} S(f) df \quad (4.79)$$

$$= \int_{f_0}^{f_1} \alpha |H(f)|^2 df \quad (4.80)$$

$$= \alpha \int_{f_0}^{f_1} |H(f)|^2 df \quad (4.81)$$

and

$$\alpha = \frac{P}{\int_{f_0}^{f_1} |H(f)|^2 df} \quad (4.82)$$

so

$$S(f) = \frac{P|H(f)|^2}{\int_{f_0}^{f_1} |H(f)|^2 df} \quad (4.83)$$

The spectral efficiency in this case is

$$\frac{C}{W} = \frac{\int_{f_0}^{f_1} \log_2 \left( 1 + \frac{P|H(f)|^4}{\frac{N_0}{2} \int_{f_0}^{f_1} |H(f)|^2 df} \right) df}{f_1 - f_0} \quad (4.84)$$

$$= \frac{\int_{f_0}^{f_1} \log_2 \left( 1 + \frac{\rho W |H(f)|^4}{\int_{f_0}^{f_1} |H(f)|^2 df} \right) df}{f_1 - f_0} \quad (4.85)$$

For channel inverse transmission scheme, it follows that

$$S(f) = \frac{\alpha}{|H(f)|^2} \quad (4.86)$$

where the constant  $\alpha$  is the factor chosen to satisfy the power constraint with equality

$$P = \int_{f_0}^{f_1} S(f) df \quad (4.87)$$

$$= \int_{f_0}^{f_1} \frac{\alpha}{|H(f)|^2} df \quad (4.88)$$

$$= \alpha \int_{f_0}^{f_1} \frac{1}{|H(f)|^2} df \quad (4.89)$$

with

$$\alpha = \frac{P}{\int_{f_0}^{f_1} \frac{1}{|H(f)|^2} df} \quad (4.90)$$

Thus,

$$S(f) = \frac{P}{\int_{f_0}^{f_1} \frac{1}{|H(f)|^2} df |H(f)|^2} \quad (4.91)$$

and the spectral efficiency in this case is

$$\frac{C}{W} = \frac{\int_{f_0}^{f_1} \log_2 \left( 1 + \frac{P}{\frac{N_0}{2} \int_{f_0}^{f_1} \frac{1}{|H(f)|^2} df} \right) df}{f_1 - f_0} \quad (4.92)$$

$$= \frac{\int_{f_0}^{f_1} \log_2 \left( 1 + \frac{\rho W}{\int_{f_0}^{f_1} \frac{1}{|H(f)|^2} df} \right) df}{f_1 - f_0} \quad (4.93)$$

$$= \log_2 \left( 1 + \frac{\rho W}{\int_{f_0}^{f_1} \frac{1}{|H(f)|^2} df} \right) \quad (4.94)$$

If the transmitted signal is of the constant PSD from  $f_0$  to  $f_1$ ,

$$S(f) = \frac{P}{W} \quad (4.95)$$

so the spectral efficiency is

$$\frac{C}{W} = \frac{\int_{f_0}^{f_1} \log_2 \left( 1 + \frac{P|H(f)|^2}{\frac{N_0}{2}W} \right) df}{f_1 - f_0} \quad (4.96)$$

$$= \frac{\int_{f_0}^{f_1} \log_2 (1 + \rho |H(f)|^2) df}{f_1 - f_0} \quad (4.97)$$

#### Appendix B Maximum SNR after Matched Filter for Time Reversal Modal Modulation

From Eq. 4.14, we assume the maximum  $\kappa_n$  is  $\kappa_{\max}$  and the corresponding orthonormal eigenfunction is  $\phi(t)$ ,  $0 \leq t \leq T$ .

If the transmitted signal is  $x\phi(t) * h(-t)$ , then the energy of the transmitted signal is

$$E_t = \int [x\phi(t) * h(-t)]^2 dt \quad (4.98)$$

$$= x^2 \int \int_0^T \phi(\tau) h(\tau - t) d\tau \int_0^T \phi(s) h(s - t) ds dt \quad (4.99)$$

$$= x^2 \int_0^T \int_0^T \int h(\tau - t) h(s - t) dt \phi(s) \phi(\tau) ds d\tau \quad (4.100)$$

$$= x^2 \int_0^T \int_0^T R_{hh}(\tau - s) \phi(s) \phi(\tau) ds d\tau \quad (4.101)$$

$$= x^2 \int_0^T \kappa_{\max} \phi(\tau) \phi(\tau) d\tau \quad (4.102)$$

$$= \kappa_{\max} x^2 \int_0^T |\phi(\tau)|^2 d\tau \quad (4.103)$$

$$= \kappa_{\max} x^2 \quad (4.104)$$

In the receiver side, after matched filter, the maximum SNR is

$$\text{SNR}_{\max} = \frac{\left[ \int_0^T \kappa_{\max} x \phi(t) (x \phi(t)) dt \right]^2}{\frac{N_0}{2} \int_0^T |x \phi(t)|^2 dt} \quad (4.105)$$

$$= \frac{2(\kappa_{\max} x)^2}{N_0} \quad (4.106)$$

$$= \frac{2\kappa_{\max} \kappa_{\max} x^2}{N_0} \quad (4.107)$$

$$= \frac{2\kappa_{\max} E_t}{N_0} \quad (4.108)$$

## Appendix C Iterative Loading Algorithm

The iterative loading algorithm is employed here to solve the optimization problem. The algorithm can be expressed as:

1 Initialization:  $b_n = 0, n = 1, 2, \dots; L_n = 1, n = 1, 2, \dots; P_{tn} = 0, n = 1, 2, \dots; P_{bn} = \text{constant}, n = 1, 2, \dots$

2 For each channel  $n$ , if one more bit is loaded, the incremental power is calculated as follows,

$$\Delta P_{tn} = P_{tn}(b_n + 1) - P_{tn}(b_n) \quad (4.109)$$

where  $P_{tn}(b_n)$  satisfies

$$P_{bn}(\log_2 L_n) = 2 \left(1 - \frac{1}{L_n}\right) Q \left( \sqrt{\frac{3}{L_n^2 - 1} \frac{2T_s P_{tn}(b_n) \kappa_n}{N_0}} \right) \quad (4.110)$$

and  $P_{tn}(b_n + 1)$  satisfies

$$P_{bn}(1 + \log_2 L_n) = 2 \left(1 - \frac{1}{2L_n}\right) Q \left( \sqrt{\frac{3}{4L_n^2 - 1} \frac{2T_s P_{tn}(b_n + 1) \kappa_n}{N_0}} \right) \quad (4.111)$$

3 We get the channel index  $j$  according to

$$j = \arg \min_n \Delta P_{tn} \quad (4.112)$$

If  $\sum_{n=1}^{\infty} P_{tn} + \Delta P_{tj} \leq P_t, b_j + 1 \rightarrow b_j, 2L_j \rightarrow L_j, P_{tj} + \Delta P_{tj} \rightarrow P_{tj}$  and go to step 2; otherwise, go to step 4.

4 The number of total bits transmitted is  $b = \sum_{n=1}^{\infty} b_n$ .

## Bibliography

- [1] E. Heyman, G. Friedlander and L. B. Felsen, "Ray-Mode Analysis of Complex Resonances of an Open Cavity," *Proc. IEEE*, Vol. 77, No. 5, pp. 780-787, May 1989.
- [2] M. Z. Win and R. A. Scholtz, "Ultra-wide Bandwidth Time-hopping Spread-spectrum Impulse Radio for Wireless Multiple-access Communications," *IEEE Trans. Commun.*, vol.48, no. 4, pp.679-691, April 2000.
- [3] R. C. Qiu, H. Liu, and X. Shen, "Ultra-Wideband for Multiple Access," *IEEE Commun. Mag.*, Vol. 43, No. 2, pp. 80-87, Feb. 2005.
- [4] R. C. Qiu, R. Scholtz and X. Shen, "Ultra-Wideband Wireless Communications— A New Horizon," Editorial on Special Session on UWB, *IEEE Trans. Veh. Technol.*, Vol. 54, No. 5, Sept. 2005.
- [5] X. Shen, M. Guizani, H. H. Chen, R. Qiu and A. F. Molisch, "Ultra-wideband Wireless Communications," Editorial on Special Issue on UWB, *IEEE J. Select. Areas Commun.*, Vol. 24, 2nd Quarter 2006.
- [6] M. R. Bell and R. A. Grubbs, "JEM Modeling and Measurement for Radar Target Identification," *IEEE Tran. Aerospace Electronic Systems*, Vol. 29, No. 1, pp. 73-87, Jan. 1993.
- [7] IEEE 802.15.4a, available <http://www.ieee802.org/15/pub/TG4a.html>.
- [8] R. C. Qiu, "A Theory of Time-Reversed Impulse Multiple-Input Multiple-Output (MIMO) for Ultra-Wideband (UWB) Communications (*invited paper*)," *2006 Int'l Conf. UWB*, Waltham, MA, Oct. 2006.
- [9] R. C. Qiu, C. Zhou, J. Q. Zhang and N. Guo, "Channel Reciprocity and Time-Reversed Propagation for Ultra-Wideband Communications," *IEEE AP-S International Symposium on Antennas and Propagation*, Honolulu, Hawaii, USA, June 2007.
- [10] R.C. Qiu, C. Zhou, N. Guo and J.Q. Zhang, "Time Reversal with MISO for Ultra-Wideband Communications: Experimental Results," *IEEE Antenna and Wireless Propagation Letters*, pp. 269-273, Vol. 5, 2006.
- [11] J. R. Barry, E. A. Lee and D. G. Messerschmitt, "Capacity Penalty Due to Ideal Zero-Forcing Decision-Feedback Equalization," *IEEE Trans. Inform. Theory*, Vol. 42, No. 4, July 1996.
- [12] R. G. Gallager, *Information Theory and Reliable Communication*, New York: John Wiley, 1966.
- [13] J. L. Holsinger, "Digital Communication over Fixed Time-Continuous Channels with Memory—With Special Applications to Telephone Channels," *Tech. Report No. 430*, Research Lab of Electronics, MIT, Oct. 1964.
- [14] J. Cioffi, *Digital Communications*, Course Reader, Chapter 4, 2007, available <http://www.stanford.edu/group/cioffi/>.

- [15] E. J. Baghdady, *Lectures on Communication System Theory*, Ch. 14, 1961, New York: McGraw-Hill.
- [16] R. W. Lucky, J. Salz and E. J. Weldon *Principles of Data Communication*, 1968, New York: McGraw-Hill.
- [17] R. W. Lucky, J. Salz and E. J. Weldon *Principles of Data Communication*, 1968, New York: McGraw-Hill.
- [18] I. Gradshteyn and I. Ryzhik, *Tables of Integral, Series, and Products*, New York: Academic Press, 1994.
- [19] A. J. Berni and W. D. Gregg, "On the Utility of Chirp Modulation for Digital Signaling," *IEEE Trans. Commun.*, Vol. 21, No. 6, pp. 748-751, June 1973.

## Chapter 5

# Chirp UWB Systems

Chirp UWB—accepted into IEEE 802.15.4a in December 2006—is a promising technology. Our interest mainly lies in solving the problems faced with impulse radio—narrowband interference and synchronization. Range extension is our goal.

### 5.1 Chirp UWB

#### 5.1.1 Challenges for IR-UWB

Though IR-UWB has the advantages of low complexity, low power, etc., it is facing two challenges, limited range and Narrow Band Interference (NBI).

The range for IR-UWB communications is limited by the transmit power. At present, typical range is less than 30m. In order to extend the range, an IR-UWB system has to increase its transmit power. However, UWB system is a power-limited system. Since IR-UWB pulse has ultra-short period while ultra-low duty cycle, increasing the transmit power will increase the pulse's Peak-to-Average Power Ratio (PAPR) largely. Such high PAPR makes it difficult to implement in hardware.

The second challenge for UWB is narrow band interference (NBI). Since UWB covers a large bandwidth, it is easy to suffer NBI with a Signal to Interference power Ratio (SIR) less than -20dB. NBI suppression algorithms have to be used but the complexity of such a system will be very high.

Timing and synchronization is the classical problem in an impulse radio, even if non-coherent transmitted reference and energy detection is used.

#### 5.1.2 Range Extension

In this report we would like to propose another UWB system that has the potential to overcome the above challenges. It's Chirp UWB, a chirp spread spectrum (CSS) based UWB system. CSS is originated from the RADAR system's

pulse compression theory. Pulse compression is developed to solve the RADAR system's paradox: maximizing the detection range while minimizing the resolution of the detected object. Pulse compression requires signals that can be simultaneously spread in time and frequency. Spreading in time keeps the transmit power low while accumulates high SNR after pulse compression at the receiver. Spreading in frequency ensures high resolution for the detected object. Chirp signal inherently has this dual spreading nature. A typical chirp signal has the form of Equation 5.1.

$$c_h(t) = \cos\left(2\pi\left(f_0 t \pm \mu \frac{t^2}{2}\right)\right), \quad -\frac{T_c}{2} \leq t \leq \frac{T_c}{2} \quad (5.1)$$

$f_0, T_c, \mu$  are center frequency, signal duration and sweep rate, respectively. From Figure 5.1, we can see that chirp signal is a linear frequency modulation (LFM) signal. Figure 5.2 is its amplitude spectrum. Its frequency 'sweeps' continuously and its duration can be changed independently. Signal with '+ $\mu$ ' is an up chirp while '- $\mu$ ' is a down chirp. They are matched to each other. Equation 5.2 and Equation 5.3 are the match filter's impulse response and matched output for Equation 5.1, respectively.

$$h(t) = \sqrt{4\mu} \cos\left(2\pi\left(f_0 t \mp \mu \frac{t^2}{2}\right)\right), \quad -\frac{T_c}{2} \leq t \leq \frac{T_c}{2} \quad (5.2)$$

$$g(t) = \sqrt{4\mu} \cos(2\pi f_0 t) \frac{\sin(\pi\mu t (T_c - |t|))}{2\pi\mu t}, \quad -T_c \leq t \leq T_c \quad (5.3)$$

Figure 5.3 illustrates the compressed pulse. After match filtering, a compressed pulse is generated, which has a short duration of  $2/B$  and a peak of  $\sqrt{TB}$ . As a result, a flat envelope pulse with duration  $T_c$  is compressed after matched filtering. Note that the  $TB$  product is the processing gain, which increases the SNR after match filtering.

This feature can solve the challenge of limited range for UWB, because higher SNR in turn compensates the path loss costs by distance. SNR gain equals to  $TB$  product of a chirp, which can be expressed in Equation 5.4.

$$SNR = \frac{E_s}{N_0} - TB, \text{ in dB} \quad (5.4)$$

As a result, the receiver sensitivity can be as low as  $(E_s/N_0 - TB)$  in dB. Since the entire chirp signal is spread in time and frequency, an increased signal power can be achieved by increasing  $T_c$  or bandwidth, while maintaining the same transmit power and PAPR. This is fundamentally different from IR-UWB. Take a CSS system for example. A Chirp UWB pulse has  $T = 1\mu\text{s}$  and  $B = 1\text{ GHz}$ , and the processing gain is  $TB = 30$  in dB. BPSK modulation is used. Under the FCC power spectrum limit and -114dBm noise level, the transmit power is -41.3dBm and the transmit SNR is 72.7dB. The path loss model of LOS channel [1] is depicted in Figure 5.4. With 30dB processing gain, the receiver sensitivity is about -20dB, which means that the communication range can be 1000m with BER of  $10^{-3}$ . In this case, when BPSK modulation is used, the data rate is 1Mbps.

### 5.1.3 NBI Suppression

Chirp based system also has a simple solution for NBI suppression. Chirp signal's spectrum can be controlled in the time domain. If NBI appears at a certain frequency, that frequency can be filtered out by 'gating' in the time domain.

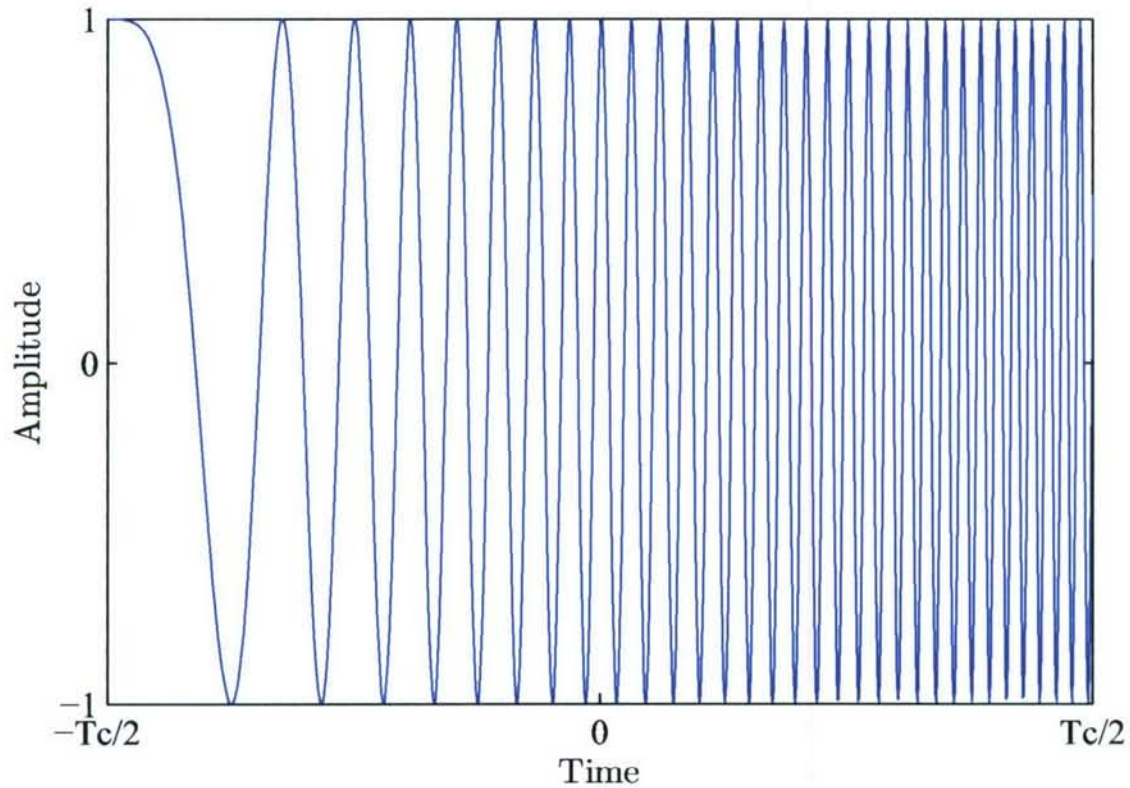


Figure 5.1: Waveform of an up chirp

The block diagram is depicted in Figure 5.5. Figure 5.6 is a 'gated' chirp. Figure 5.7 is its amplitude spectrum. Equation 5.5 and Figure 5.5 illustrate the 'gating' process.

$$\begin{aligned}
 h_g(t) &= m_i \sum_{i=1}^N \cos\left(2\pi f_0 t - \frac{\mu t^2}{2}\right) \\
 t &= t_0 + \sum_{i=1}^k i \left(\frac{T_c}{N}\right), \text{ with } m_i = 0, 1
 \end{aligned}
 \tag{5.5}$$

It can be noticed that a "gated" chirp is summed up with  $N$  continuous chirp signals. Each  $m_i$  represents a frequency component. A certain frequency can be "filtered" by setting corresponding  $m_i$  to 0. If  $m_i = 1$  for all  $i$ , the summed signal becomes a normal chirp.

From the amplitude response we can conclude that such 'gated' chirp acts like a notch filter. However, this notch filter is easy to implement. It has been reported that this gating process can be done by the surface acoustic wave (SAW) device, which is analog [2]. Figure 5.8 and Figure 5.9 shows the NBI suppression result. It can be seen that when SIR is -20dB, compared with the normal match filter, the NBI is suppressed successfully after the 'gated'

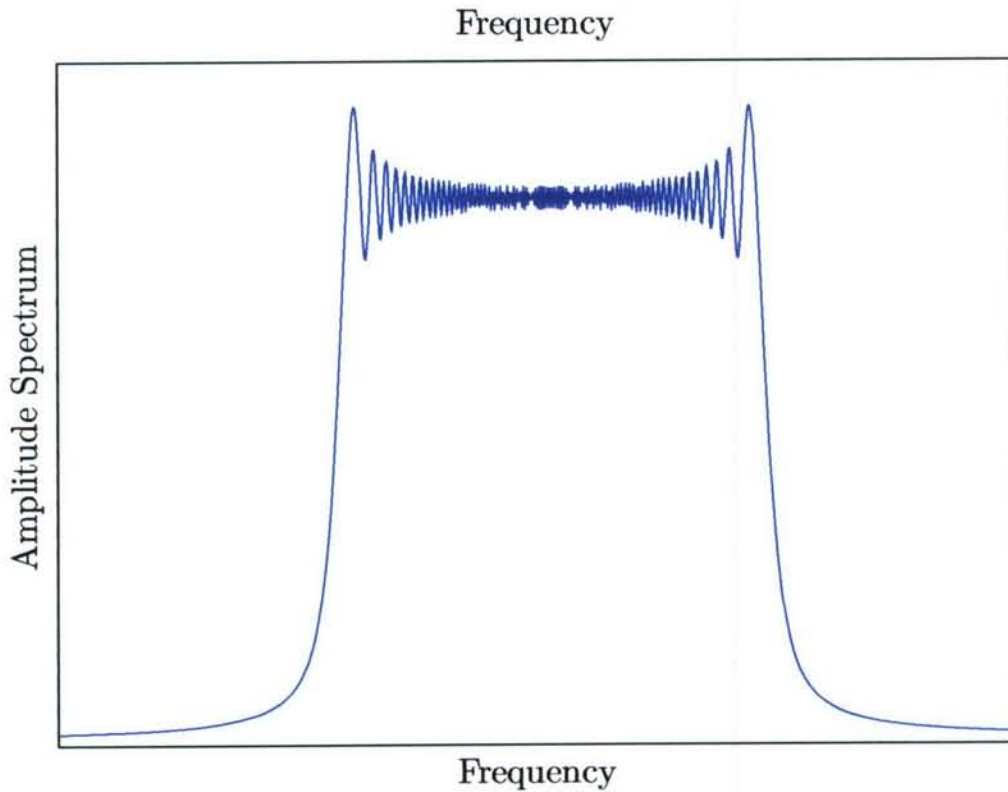


Figure 5.2: Amplitude spectrum of chirp

SAW. It should be noted that this gating process is implemented by a fast adaptive switching network, which is digital. Such analog-digital hybrid system makes it easy to control the spectrum.

#### 5.1.4 Other Advantages

In addition to the range extension and NBI suppression ability, Chirp UWB has the advantage of fast synchronization because of its analog match filter and high processing gain. Match filter can be implemented by the SAW device in the analog domain. SAW is a passive device. A compressed pulse with processing gain will automatically appear after match filtering. Timing acquisition becomes a task of peak searching, which is not difficult to implement. Also, chirp signal is 'immune' to frequency offset. A frequency offset  $\Delta f$  will result a timeshift  $\delta t$  in the match filter output. Suppose a chirp signal with frequency offset  $\Delta f$  has the form of Equation 5.6.

$$s(t) = \cos \left( 2\pi \left( (f_0 + \Delta f) t + \frac{\mu t^2}{2} \right) \right), \frac{T_c}{2} \leq t \leq \frac{T_c}{2} \quad (5.6)$$

Equation 5.7 is the output of the match filter.

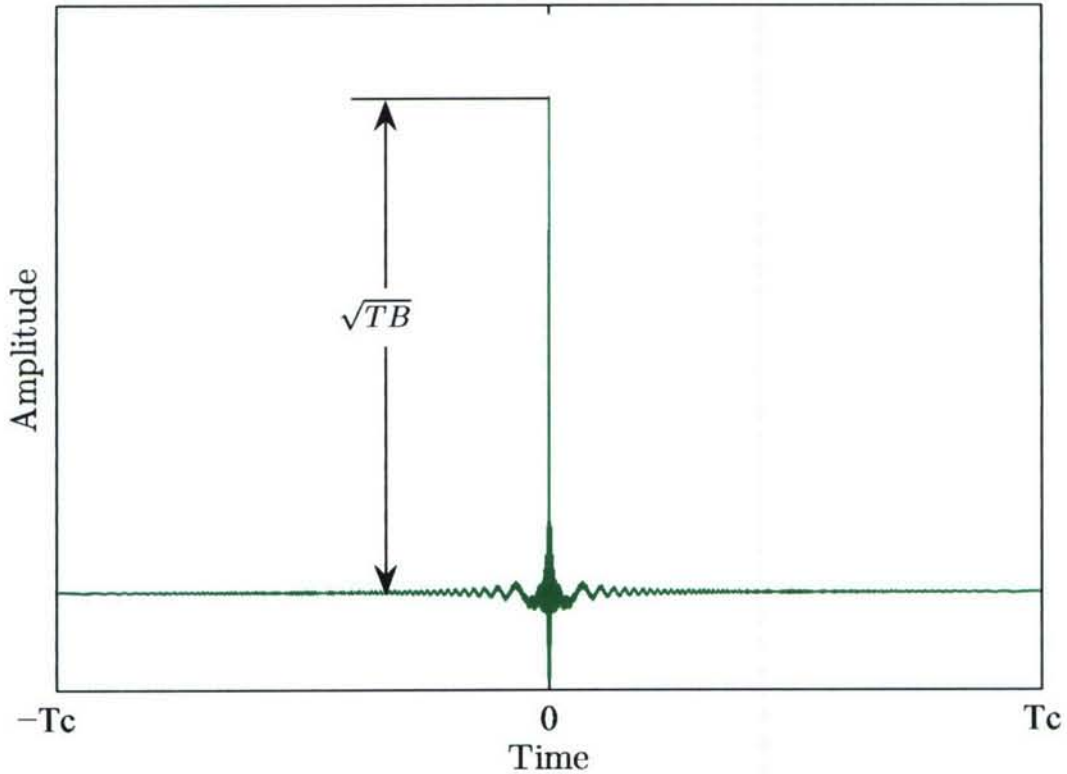


Figure 5.3: Waveform of a compressed pulse

$$\begin{aligned}
 r(t) &= \int_{-\infty}^{\infty} s(\tau) h(t-\tau) d\tau \\
 &= \sqrt{4\mu} \cos(2\pi(f_0 + \Delta f)t) \frac{\sin(\pi(\Delta f + \mu t)(T_c - |t|))}{2\pi(\Delta f + \mu t)}, \quad -T_c \leq t \leq T_c
 \end{aligned} \tag{5.7}$$

Equation 5.7 shows that the output is still a compressed pulse. However, comparing it with Equation 5.3, there is a timeshift determined by  $\Delta f$ . The relationship between  $\Delta f$  and  $\delta t$  can be shown in Equation 5.8.

$$\delta t = \frac{\Delta f}{\mu} \tag{5.8}$$

Compared with the sweep rate  $\mu$ , frequency offset is very small, and the influence can be ignored. For example, if we add  $\Delta f = 1$  MHz to a chirp with  $\mu = 500$  MHz/ $\mu$ s, the timeshift is only 2 ns. In all, the tasks of timing and frequency synchronization can be accomplished together by simple peak searching.

Since Chirp UWB satisfies the definition of UWB, it has all the merits of traditional UWB. It has the same multipath resolution as IR-UWB. Ranging is not a problem for Chirp UWB, since pulse compression with CSS has already

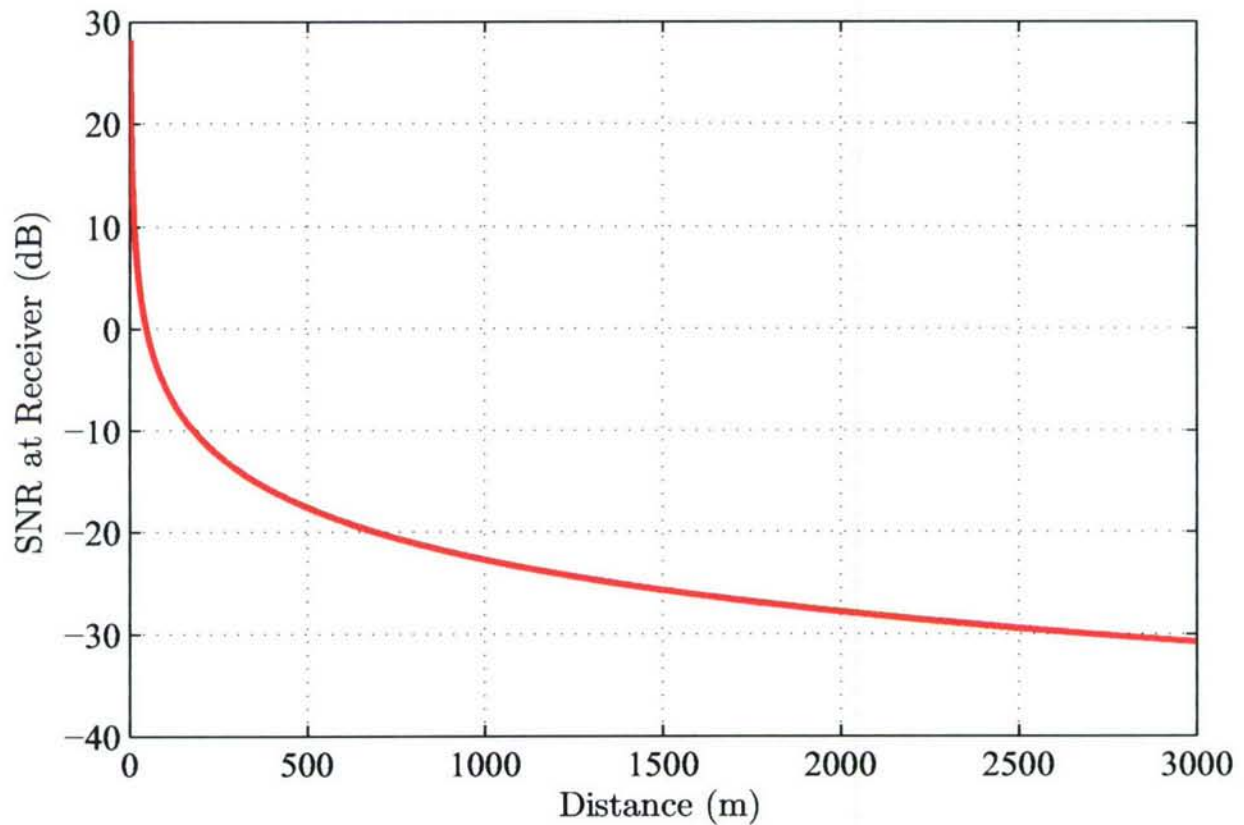


Figure 5.4: Path loss model for indoor LOS channel

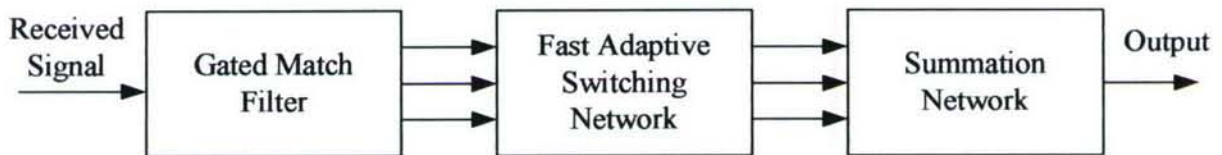


Figure 5.5: Block diagram for gating process

been popular in RADAR applications. Besides, Chirp UWB can be implemented by the analog SAW device, its power consumption will be low and it will have long battery life. As a result, Chirp UWB provides the ability to enhance current UWB performance.

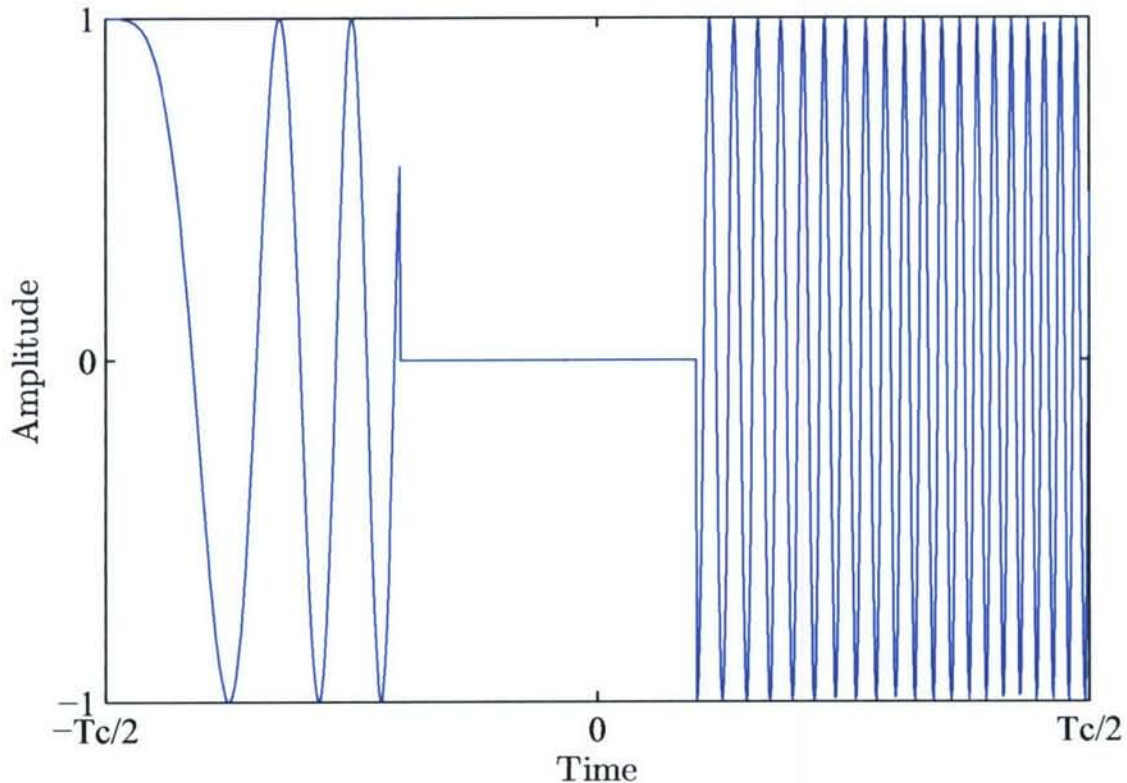


Figure 5.6: Waveform of a 'gated' chirp

## 5.2 Advantages of CSS over DSSS

CSS is similar to Direct Sequence Spread Spectrum (DSSS). Instead of spreading the spectrum using PN code like DSSS, CSS uses chirp signals. However, CSS is featured with Doppler immunity, fast synchronization and controllable spectrum, which are impossible for DSSS. In RADAR applications, DSSS is also a choice for pulse compression. But it is well known that BAKER code is very sensitive to Doppler. DSSS with large bandwidth and high processing gain requires very high speed Digital-to-Analog Converter (DAC) and Digital Signal Processor (DSP). Both DAC and DSP's performances are limited by the state-of-art and they consume a lot of dissipation. For synchronization, DSSS needs to do the digital domain correlation to generate a compressed pulse and detect its autocorrelation peak. This process cost a lot of hardware resource and increases the system complexity. It is also impossible for DSSS to filter out NBI as easily as CSS, because the pulse for DSSS is fixed.

## 5.3 Implementation

The key device in the Chirp UWB system is SAW. SAW is widely used as bandpass filter, delay line and pulse compression Dispersive Delay Line (DDL). It is estimated that the current world-wide production of SAW is well in excess of 1000 million devices per year [3]. For CSS purpose, DDL SAW is exclusively used. A DDL based solution

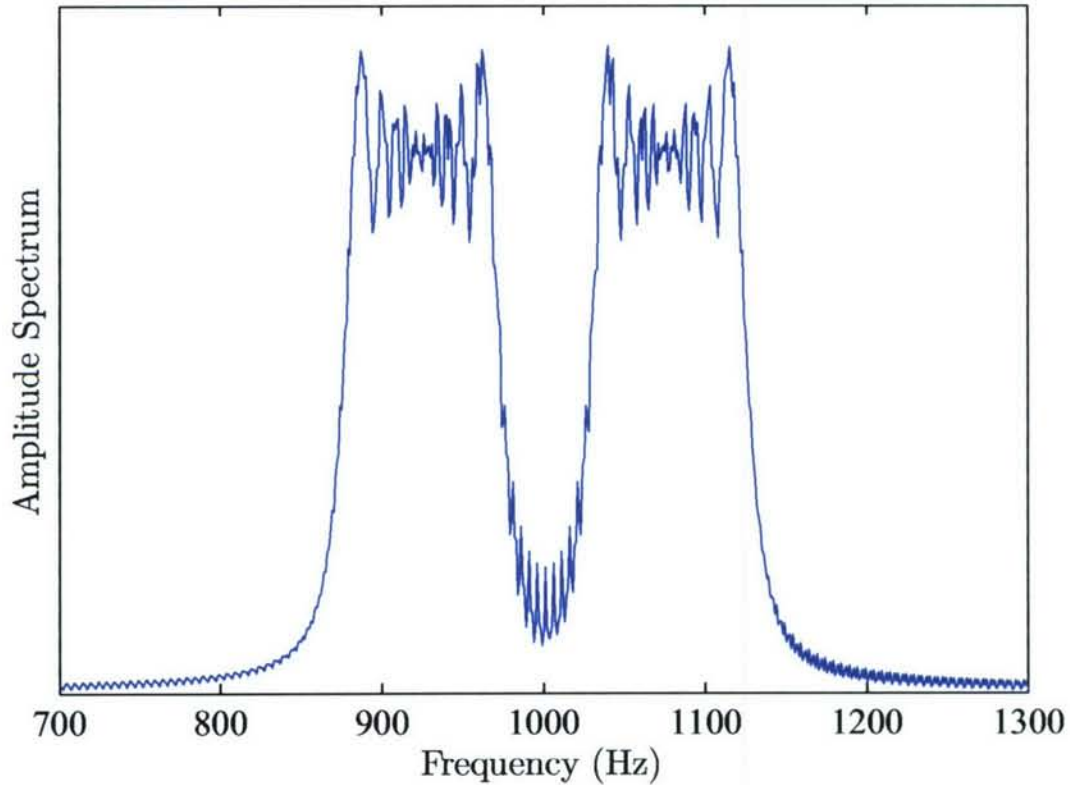


Figure 5.7: Amplitude spectrum of the 'gated' chirp

was approved by IEEE 802.15.4a WPAN task group in March, 2007. In the system, a pair of SAW devices are used as chirp generator and match filter. Each SAW generates an up/down chirp with 80MHz bandwidth and  $1\mu\text{s}$  duration [4]. It is reported that under  $10^{-3}$  Bit Error Rate (BER), such communication link can support transmission distance up to 9800m with 1W transmit power [5]. However, the acceptance of IEEE standart only justifies CSS's performance for wideband. CSS's UWB application, Chirp UWB, should be of interest. The state-of-art performances of SAW devices can generate a chirp signal with bandwidth over 500MHz [6, 7, 8] or fraction bandwidth over 25% [9], satisfying both UWB definitions. In addition, small size, low cost and mass production are the features of SAW [6], which will be perfect for sensor network applications. Combining CSS with UWB, Chirp UWB system will inherit the advantages of both CSS and UWB.

## 5.4 The History of CSS

The idea of pulse compression was proposed by different researchers in different countries after World War II [10, 11, 12, 13]. In the late fifties, several major labs published their research results on chirp RADAR [14, 15, 16]. The first paper applying chirp for communications other than RADAR was published in 1962 by M. Winkler [17], where he suggested using up and down chirps to represent binary '0' and '1', respectively. This is the basics of a Binary Orthogonal Keyed (BOK) system, utilizing the quasi-orthogonal property of up and down chirps. In

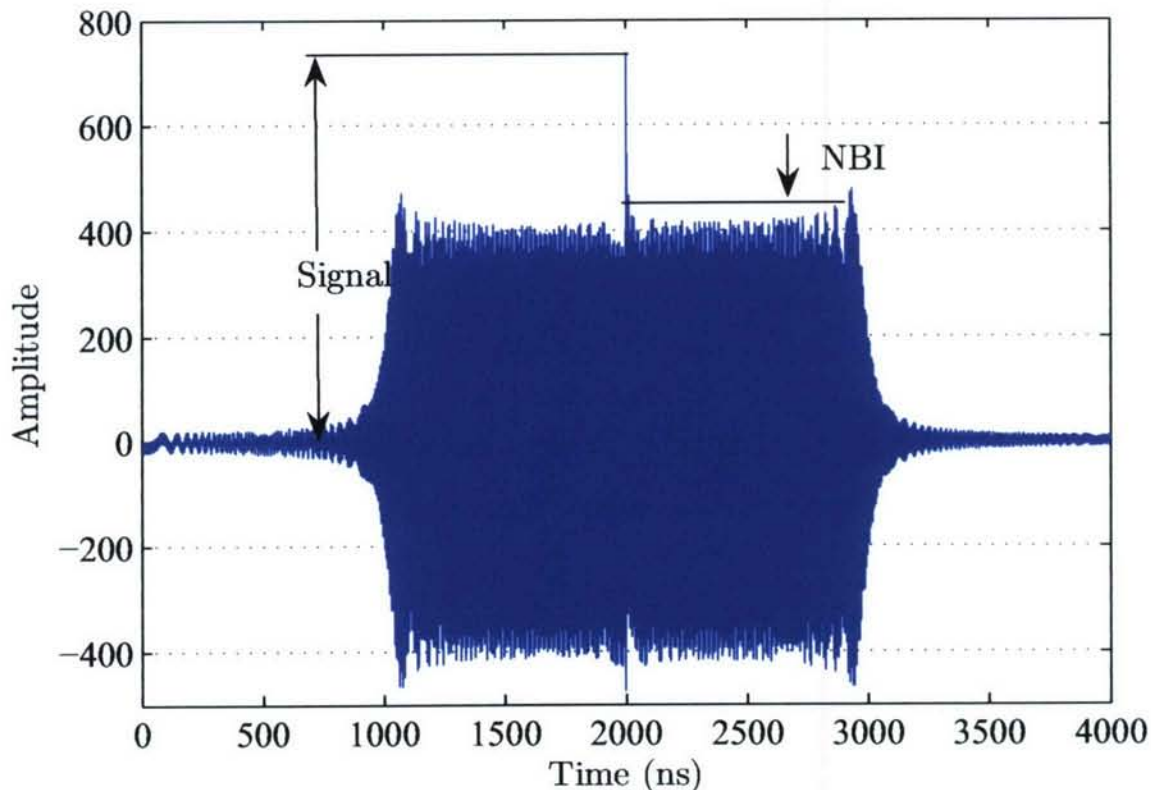


Figure 5.8: Normal match filter output with NBI, SIR = -20dB

1966, Hata [18] and Gott [19] independently proposed a BOK system for the High Frequency (HF) band. In their proposals, chirp signal's Doppler Effect immunity was utilized. After Gott's work, Forgan [20] and Edge [21] had finished their research on chirp signals and they all reference some Royal Aircraft Establishment and Ministry of Defense reports. It seems that their research was supported by the British military and they had shown great interests in CSS. The paper of Zaytsev [22] also showed some interests from the Russian military. In the early seventies, Gott and his group published several papers on Low Earth Orbit (LEO) satellites and ground-to-air communications in the HF band [23, 24, 25, 26, 27]. However, the idea of using SAW device as a chirp generator was first proposed by Bush [28] in 1973. Before that, the only practical chirp signal generator was lumped element filters. Interest in CSS became less since late seventies. At that time DSSS and Frequency Hopping Spread Spectrum (FHSS) was the more popular choice because of the development of Digital Signal Process (DSP) algorithms. Only a few papers mentioned CSS by applying it to DSSS against the Doppler Effect [29, 30, 31]. At that time, SAW device was mainly developed for RADAR pulse compression [32, 33, 34], satellite signal processing [35, 36, 37] and channel sounders [38, 39]. Interest in CSS fell can be explained by the target frequencies and the SAW implementation techniques of that time. The excess delay for HF band is in the order of milliseconds, which means that the chirp signal's duration must be no less than that level. Since the velocities in SAW are thousands of meters per second, the corresponding physical size of SAW would be over 1 meter, which is impractical.

However, when the frequencies are not limited in HF band, SAW devices found its applications. For indoor applications, the excess delay is in the order of microseconds, which is practical for physical size of SAW. SAW devices

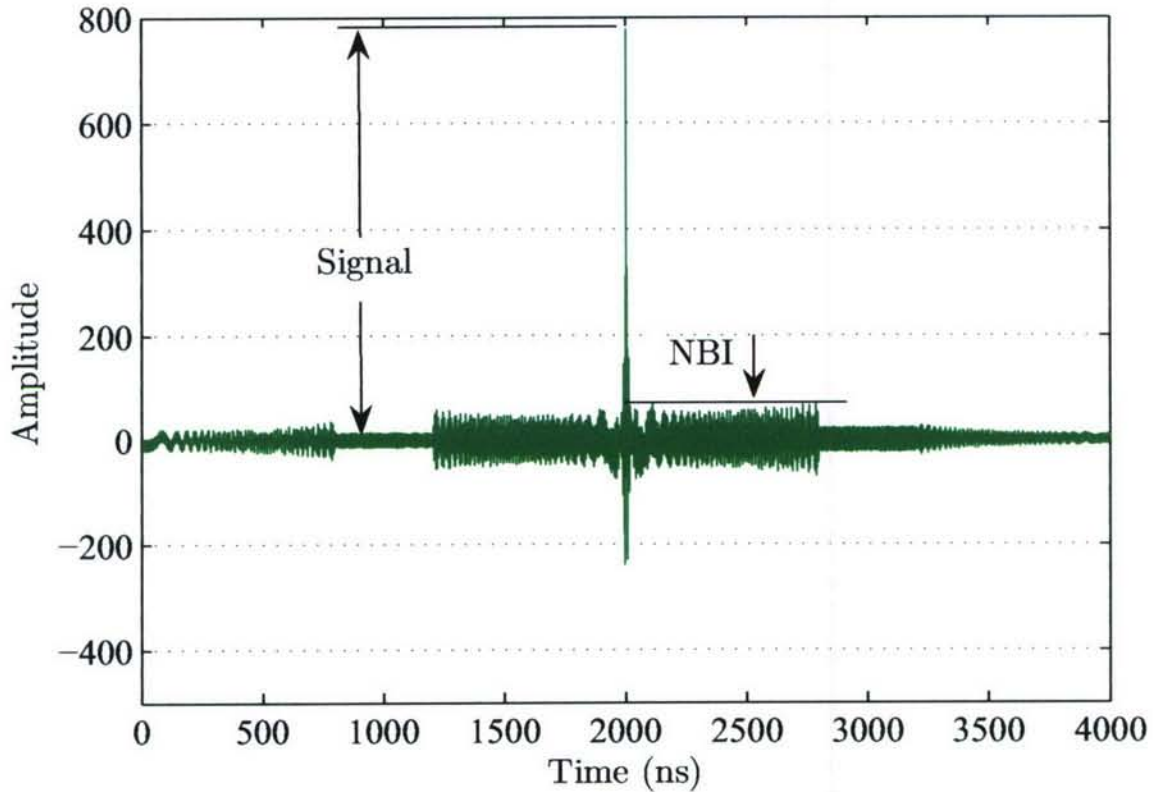


Figure 5.9: 'Gated' match filter output with NBI, SIR = -20dB

were first applied in the indoor channels by Tsai and Chang in 1994, using BOK scheme [40]. After that, several groups took interests in CSS. Huemer [41] in 1998 published another BOK based system. Gugler's group [42] and Pinkney [43] focused their CSS research on Direct Modulation (DM), another CSS modulation scheme which is more efficient than BOK. In their study, the data rate could be as high as 70Mbps with 80MHz bandwidth. In March, 2007, IEEE approved Nanotron's CSS physical layer (PHY) in its new wireless standard 802.15.4a. A pair of SAWs are used in its BOK scheme. The target applications for such system are Real Time Location Systems (RTLS), industrial control, sensor networking and medical devices in the ISM band, taking the advantages of CSS: long range, high robustness and low power consumption.

## 5.5 A Time Reversed Chirp UWB—Forward Looking

Chirp UWB radio can be regarded as a compromise between the optimum waveform and ease of implementation— analog or digital, by selecting chirp waveform for signal modulation. The research proposed here has a significance of practical value, and the chirp system is used as a benchmark to be compared against the optimum modal modulation.

A RF harsh environment shown in Fig. 2.1(a) has been investigated. One simulation example is included here. A



Figure 5.10: The photo of a pair of SAW filters. The size is about 1 x 2 inches.

data rate of 500Mbps can be supported using time reversal chirp waveform with a bandwidth 7GHz and waveform duration  $T = 100$  ns—the time-bandwidth product is  $TB = 700$ . BPSK modulation is used. For a bit error rate (BER) of  $10^{-4}$ , the ratio of bit energy to the noise,  $E_b/N_0$ , is required to be larger than 23 dB.

One PhD student (Peng Zhang)—who did his MS thesis on chirp UWB for three years—joined the PI's team in 2006. He is currently working on the testbed for chirp UWB, using a SAW chirp device. On this topic, Mr. Zhang is working with one R&D engineer Dr. N. Guo and another MS student Amanpreet Singh Saini. A pair of SAW filters shown in Fig. 5.10 are available at the PI's lab. The vendor is Sawcom Tech, Inc. (<http://www.sawcomtech.com/>).

This is the first phase of the chirp UWB radio. The goal is to prove the concept as quickly as possible. The second phase of this project is to cope with the cognitive radio concept, which is the proposed topic for this proposal. The SAW filters can be electronically-controlled. Narrowband interference suppression is an important research task, due to the co-existence of UWB and narrowband systems such as Wi-Fi and Wi-MAX.

A chirp UWB system combines the concepts of CSS and UWB with the following features:

1. Long range transmission
2. NBI suppression
3. Fast synchronization
4. Low transmit power, low probability of intercept
5. Low power consumption
6. Low system complexity, low cost

In summary, chirp UWB is practical and useful. Its combination with time reversal is a promising transmission scheme. Time reversal deals with the extremely quasi-continuous multipath—unique to UWB—while a pair of chirp pulses is used for signaling. Time-bandwidth-product ( $TB$ ) solely determines the system performance. The range and data rate can be trade-offed, by conveniently controlling the time-bandwidth-product.



## Bibliography

- [1] S. S. Ghassemzadeh, V. Tarokh, "The Ultra-wideband Indoor Path Loss Model," IEEE P802.15 Working Group for Wireless Personal Area Networks (WPANs), July, 8, 2002.
- [2] A. Phol, M. Brandl, R. Steindl, L. Reindl, F. Seifert, "Gated chirps for signal processing and communication engineering," in *Proc. of 1998 IEEE Ultrasonics Symposium*, vol. 1, pp. 359-362, October, 1998.
- [3] C. K. Campbell. (2007). *Understanding Surface Acoustic Wave (SAW) Devices for Mobile and Wireless Applications and Design Techniques*. CA. [Online]. Available: <http://www3.sympatico.ca/colin.kydd.campbell/>
- [4] Nanotron Technologies, "nanoNET Chirp-based wireless network," Nanotron Technologies GmbH, Version 1.04, 2007.
- [5] J. Lampe, Z. Ianneli, "Introduction to Chirp Spread Spectrum (CSS) Technology," Nanotron Technologies, November 11, 2003.
- [6] M. Chomiki, "SAW-based solutions for UWB Communications," *European Microwave Conference*, vol. 3, October, 2005.
- [7] PHONON website: <http://www.phonon.com/>
- [8] R. Brocato, E. Heller, J. Wendt, J. Blaich, G. Wouters, E. Gurule, G. Omdahl, D. Palmer, "UWB Communication using SAW Correlators," *IEEE Radio and Wireless Conference*, vol. 19-22, pp. 267-270, September, 2004.
- [9] THALES MESL website: <http://www.racal-mesl.com/products/sawpcsum.htm>
- [10] W. Cauer, German Patent No. 892 772, December 19, 1950.
- [11] R. H. Dicke, "Object detection system," US Patent No. 2 624 876, January 6, 1953.
- [12] D. Sproule and J. Hughes, "Improvements in and relating to systems operating by means of wave trains," British Patent No. 604 429, July 5, 1948.
- [13] S. Darlington, "Pulse transmission," US Patent No. 2 678 997, May 18, 1954.
- [14] C. Cook, "Pulse compression - the key to more efficient radar transmission," in *Proc. of IRE*, vol. 48, pp. 310-316, March 1960.
- [15] C. Cook, "General matched filter analysis of linear fm pulse compression," in *Proc. of IRE*, vol. 49, pp. 831, April 1961.

- [16] J. Klauder, A. Price, and S. Darlington, "The theory and design of chirp radars," *Bell Systems Technical Journal*, vol. 39, pp. 745-808, 1960.
- [17] M. Winkler, "Chirp signals for communications," *Wescon Convention Record*, vol. Pt. 7, 1962.
- [18] M. Hata, "Application of a swept fm carrier pulse to a new digital data transmission system," *Japan. Inst. Electron. Comm. Engineers*, vol. 49, no. 11, pp. 2256-63, Nov. 1966.
- [19] G. Gott, *An Investigation into the Application of Chirp Signals in HF Digital Communications Systems*, PhD thesis, University of Nottingham, 1966.
- [20] H. Forgan, *A Study of Digital Radio Links Using Chirp Signals*, PhD thesis, University of Nottingham, 1971.
- [21] D. Edge, *A Mathematical Introduction to the Chirp Signal and its Application to Communications*, PhD thesis, University of Nottingham, 1974.
- [22] D. Zaytsev and V. Zhuravlev, "Noise immunity of a digital transmission system using linearly frequency modulated pulses," *Telecommun. Radio Sys.*, vol. 22, no. 4, pp. 13-17, 1968.
- [23] G. Gott and J. Newsome, "H.F. data transmission using chirp signals," in *Proc. of the IEE*, vol. 118, no. 9, pp. 1162-1166, September 1971.
- [24] G. Gott and A. Karia, "Differential phase-shift keying applied to chirp data signals," in *Proc. of the IEE*, vol. 121, no. 9, pp. 923-928, September 1974.
- [25] D. Forgan and J. Newsome, "Application of dispersive networks in data-transmission receivers," in *Proc. of the IEE*, vol. 121, no. 4, pp. 237-244, April 1974.
- [26] G.L. Grisdale, "Proposals for using pulse compression modulation to combat multipath propagation," *IEE Conf. Pub. Signal Processing Methods for Telephony*, no. 64, pp. 18-22, May 1970.
- [27] A. Berni and W. Gregg, "On the utility of chirp modulation for digital signaling," *IEEE Trans. on Communications*, vol. COMM-21, no. 6, pp. 748-751, 1973.
- [28] Bush H, A. Martin, R. Cobb, and E. Young, "Application of chirp SWD for spread spectrum communications," in *Proc. of the 1973 IEEE Ultrasonics Symposium*, pp. 494-497, 1973, Monterey, Ca.
- [29] M. Kowatsch and J. Lafferri, "A spread spectrum concept combining chirp modulation and pseudonoise coding," *IEEE Transactions*, vol. COM-30, no. 10, pp. 1122-1142, October 1983.
- [30] J. Kim and T. Pratt, "Coded multiple chirp spread spectrum system," *IEEE Miami Technicon: An International Conference Record*, pp. 141-144, 1987, Miami, FL.
- [31] T. Wysocki, "Generalized chirp modulation technique," *Signal Processing Magazine*, vol. 6, no. 6, pp. 679-683, November 1995.
- [32] C. Newton, "Nonlinear chirp radar signal waveforms for surface acoustic wave pulse compression filters," *Wave Electronics*, vol. 1, no. 5-6, pp 387-401, June 1976.
- [33] W. Shreve, "Signal processing using surface acoustic waves," *IEEE Communications Magazine*, vol. 23, no. 4, pp. 6-11, April 1985.
- [34] M. Tan and C. Flory, "Minimization of diffraction effects in SAW devices using a wide aperture," in *Proc. 1986 IEEE Ultrasonics Symposium*, pp. 13-17, 1986.

- [35] V. Ringset, E. Olsen, A. Ronnekleiv, PM. Bakken, and G. Bjornstrom, "SAW technology for multicarrier demodulation in advanced payloads," *Journal of the British Interplanetary Society*, vol. 43, no. 3, pp. 112-118, March 1990.
- [36] L. Borgarelli, R. Cortesini, and C. Dionisio, "Digital chirp generator suits space applications," *Microwaves and RF*, vol. 32, no. 6, pp. 83,86,88-90, June 1993.
- [37] W. Pietsch, "A convolver based spread spectrum data communication system," *IEEE 43rd Vehicular Technology Conference*, pp. 831-834, May 18-20 1993, Secaucus, NJ.
- [38] A. Poole, "Advanced sounding I, the FMCW alternative," *Radio Science*, vol. 1, no. 20, pp. 209-212, December 1985.
- [39] G. Levnes, S. Paulsen, and R. Raekken, "A millimeter-wave channel sounder based on the chirp correlation technique," *IEE Colloquium on High Bit rate UHF/SHF Channel Sounders - Technology and Measurement*, no. 1993/233, pp. 52 8/1-7, 1993.
- [40] Y. Tsai and J. Chang, "The feasibility of combating multipath interference by chirp spread spectrum techniques over Rayleigh and Rician fading channels," *IEEE Conference on Spread Spectrum*, pp. 282-285, 1994.
- [41] M. Huemer, A. Pohl, W. Gugler, A. Springer, R. Weigel, and F. Seifert, "Design and verification of a SAW-based chirp spread spectrum system," in *Proc. of the IEEE MTT-S International Microwave Symposium*, vol. 1, pp. 189-192, June 7-12 1998, Baltimore.
- [42] W. Gugler, A. Springer, H.P. Kupfer, and R. Weigel, "Simulation of a SAW-based WLAN using chirp  $\frac{\pi}{4}$  DQPSK modulation," in *Proc. the IEEE Ultrasonics Symposium*, vol. 1, pp. 381-384, 1998, Sendai, Japan.
- [43] J. Pinkney, A. B. Sesay, S. Nichols, and R. Behin, "A high-speed DQPSK chirp spread spectrum system for wireless applications," *Electronics Letters*, vol. 34, no. 20, pp. 1910-1911, October 1998.



## Chapter 6

# UWB Channel Sounding

In this chapter, UWB channel sounding is discussed. In general, our Lab has the capabilities of sounding the channel in both time domain and frequency domain, with and without multiple antennas. The goal of these measurements is to evaluate the non-fading wireless communications enabled by time reversal transmission. Both space and time are investigated as a function of signal bandwidth. A critical question is: What is the optimum signal bandwidth? This question depends on the specific transmission scheme—we are interested in two schemes: time reversal modal modulation, and time reversal chirp UWB.

### 6.1 Measurement Setup

The knowledge about the UWB radio channel can be gained by using either time or frequency domain measurement technique. We will discuss both techniques in detail in this section.

#### 6.1.1 Time Domain Measurement Technique

We will discuss the time domain measurement technique based on impulse transmission. In this technique a narrow pulse is sent through the propagation channel and the channel impulse response is recorded by using a Tektronix Digital sampling oscilloscope (DSO). The pulse sent through the channel is modulated by a special waveform like sine, square or ramp which enables us to analyze the effects of different paths on the received signal[1]. The data stored in DSO can be processed by using a computer. The bandwidth of received signal depends on the shape and width of transmitted pulse. The time domain measurement setup consists of a pulse generator, transmitter antenna and receiver antenna, a triggering signal generator, Low noise amplifier (LNA) and the DSO. The setup for time domain measurement is shown in Fig. 6.1

The whole setup consist of two section, i.e transmit and receive part. The signal generator and pulse generator constitute the transmitter part and DSO along with LNA constitutes the receiver part. The signal generator is used to trigger the pulse generator and pulse generator generates the pulse that is transmitted through the channel. On the receiver side the signal is passed through LNA and amplified. The final results are displayed on the DSO. A triggering signal from signal generator is used to synchronize the DSO to record the measurements. By using

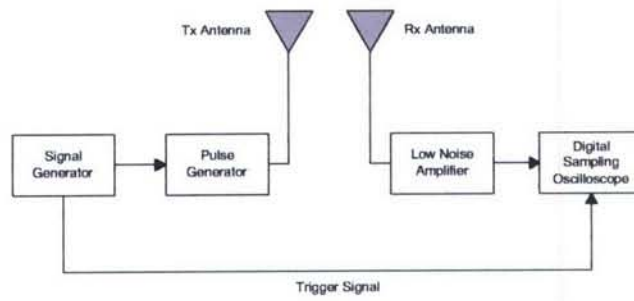


Figure 6.1: Time domain measurement setup block diagram

averaging the signal to noise ratio (SNR) is improved.

The main advantages of this technique are less complexity, lower cost and channel responses is readily available in time domain. With multiple antennas, our system can sound the UWB MIMO channel in the time domain, by using two sample modules from Tektronix.

### 6.1.2 Frequency Domain Measurement Technique

In the frequency domain measurement technique, the channel sounding is carried out by sweeping a set of narrow-band sinusoid signals (tones) through a wide frequency band. Each tone has the same power (typically 3dBm is used in our experiments). The channel frequency response is recorded by using a vector network analyzer (VNA). The VNA is operated in transfer function mode where one of its port serves as transmitting port and the other as receiving port. S-parameters are used to measure the complex frequency domain transfer function. The setup for frequency domain measurements is shown in Fig. 6.2

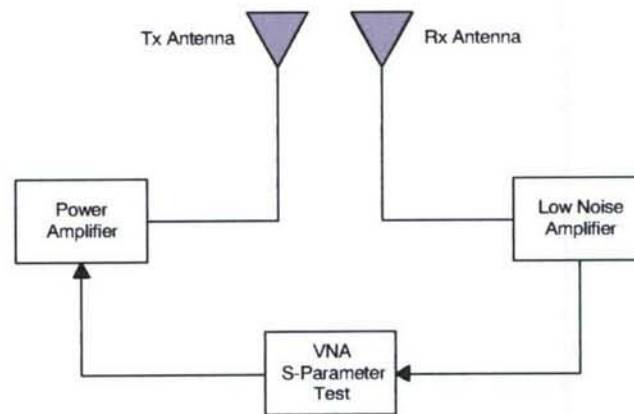


Figure 6.2: Frequency domain measurement setup block diagram

Generally  $S_{21}$  parameter is used where port 1 and 2 are acting as transmitting and receiving port respectively. VNA sends a frequency tone  $f$  through the channel and the frequency response of the channel is represented as  $S_{21}(f)$  corresponding to frequency tone  $f$ . By sweeping a frequency range from  $f_0$  to  $f_1$  we can get the frequency response of that particular band. If  $N$  is the number of frequency points per sweep with frequency step  $k$  MHz, their

relationship with bandwidth B MHz can be represented as

$$k = \frac{B}{N - 1} \quad (6.1)$$

where B is

$$B = f_1 - f_0 \quad (6.2)$$

The maximum detectable delay of the channel can be calculated as [2]

$$\tau_{max} = \frac{N - 1}{B} \quad (6.3)$$

The main advantage of the frequency domain measurement technique is that the cables and connectors can be calibrated before measurement to compensate for different kind of errors and frequency dependent losses that can occur during the measurement. There are three different kind of measurement errors [3]

- Systematic errors
- Random errors
- Drift errors

*Systematic errors* are caused by imperfections in the test equipment and test setup. These errors can be removed by calibration. Systematic errors are related to signal leakage, signal reflections, and frequency response.

*Random errors* are random in nature and are unpredictable. As a result they cannot be removed by calibrations. Random errors are present mainly due to instrument noise. So they can be removed by increasing the source power or by narrowing the IF bandwidth.

*Drift errors* occurs when the system performance changes after the completion of calibration process. Drift errors occurs mainly due to change in temperature of measurement environment and can be removed by additional calibrations.

A mechanical calibration kit consists of a set of physical devices called standards [4]. Each standard has a precisely known magnitude and phase response as a function of frequency. These standards are

- Open,short/offset short,load/sliding load
- Adapters
- Precision offsets waveguide or coaxial

There are various calibration method.The four most widely used are

- short, open, load, and through (SOLT)
- LRM

- LRRM
- TRL

Out of the above mentioned methods the most dominant one is SOLT. With SOLT, the four known references are: short, open, load, and through. Once the calibration is done, the calibration state can be saved and recall while performing the experiment. By using frequency domain measurement technique we can get larger dynamic range which improves the measurement precision. The channel impulse response (CIR) which yields the required information to characterize the UWB channel, is obtained by taking the inverse fast Fourier transform (IFFT) of the recorded signal. So this technique requires extra signal processing.

One of the main limitation of frequency domain measurement technique is that it need static environment through out the measurement. But Time domain measurement technique can support non-stationary channels. Another problem is the high attenuation of the cables so frequency-domain measurement is good for short range.

## 6.2 Measurement Examples

In this section, we will discuss some of the experiments to gain more insight about the channel sounding.

### 6.2.1 Measurement for SISO Case

The measurement is performed is for SISO case in three different environments i.e rectangular metal cavity, hallway and office to analyze the characteristics of the UWB channel in these environments. The VNA used is Agilent N5230A (300kHz-13.5GHz). The calibration method used is SOLT. Table 6.1 list the main parameters for the measurement This set of parameters is used for measurement in all the three cases. The measurement is done for

Table 6.1: Measurement Parameters setup

Parameter	value
Frequency Band	3GHz-10GHz
Bandwidth	7GHz
Number of points	7001
Transmission power	10dBm
Frequency step	1MHz
Antenna Polarization	vertical
Averaging number	128

Line of sight (LOS) situation. The distance between transmitter antenna and receiver antenna varies from 0.5m to 4m in steps of 0.5m and both the antennas are placed at 1.35 meters above the ground for all the three measurement environments.

**Measurement in Rectangular Metal Cavity**

The rectangular metal cavity used in this measurement measures 16 feet by 8 feet by 8 feet. The material of inside walls of the cavity is aluminum. The setup for measurement in rectangular metal cavity is shown in Fig. 6.3

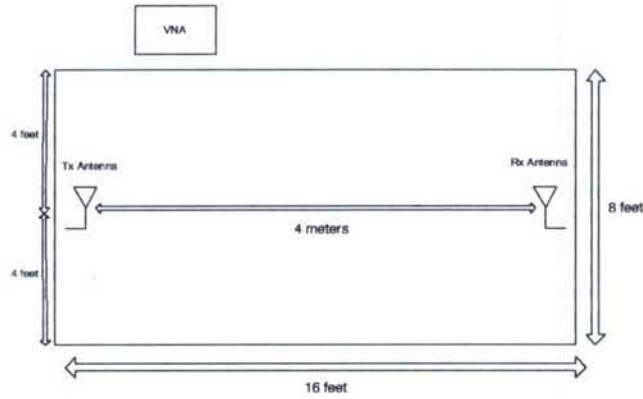


Figure 6.3: Setup for measurement in rectangular metal cavity

The transmitter antenna is fixed, and the receiver antenna is moved from distance 0.5m to 4m in steps of 0.5m w.r.t transmitter antenna along the middle line of the rectangular metal cavity. The frequency domain response at distance 1m, 2m, 3m and 4m between transmitter antenna and receiver antenna is shown in Fig. 6.4

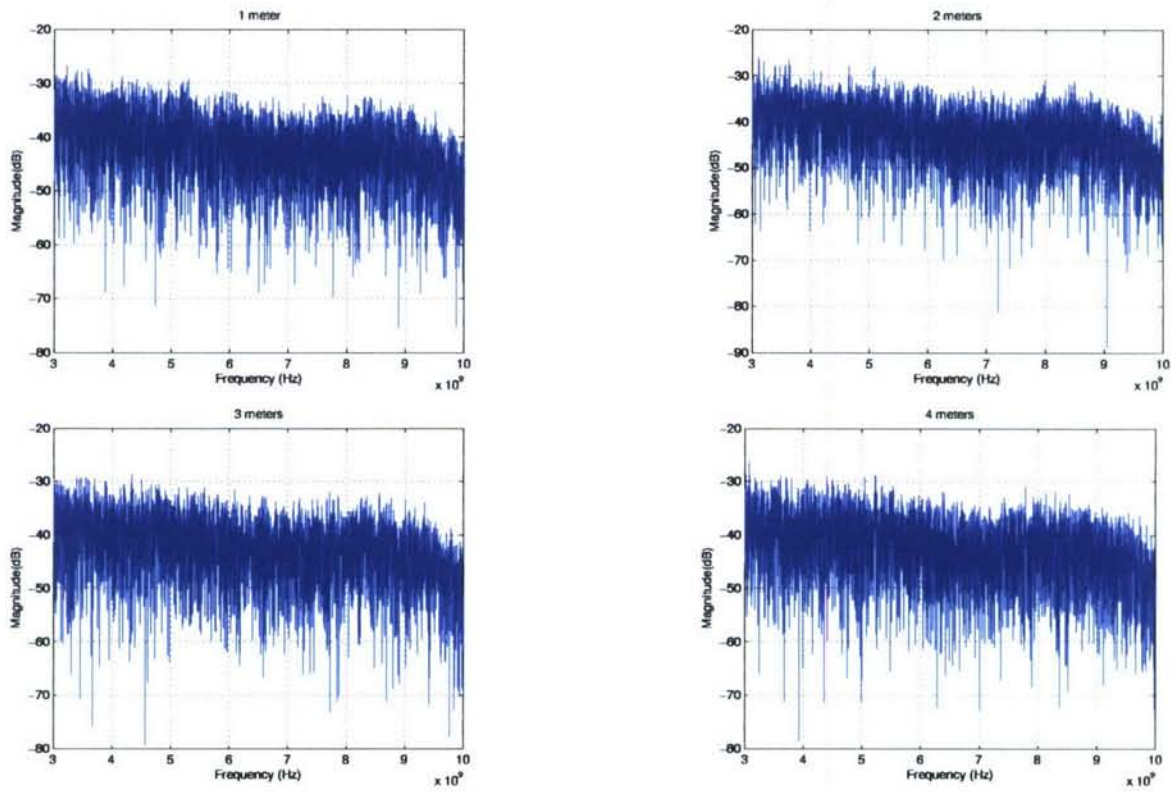


Figure 6.4: Frequency domain response  $H(f)$  at distance 1m,2m,3m and 4m between transmitter antenna and receiver antenna in rectangular metal cavity

After the channel response is measured, zero padding is done between 0Hz and 3 GHz, conjugate reflection between -10 GHz and 0Hz and inverse fast Fourier transform (IFFT) is used to get channel impulse response in time domain. The time domain response at distance 1m, 2m, 3m and 4m between transmitter antenna and receiver antenna is shown in Fig. 6.5

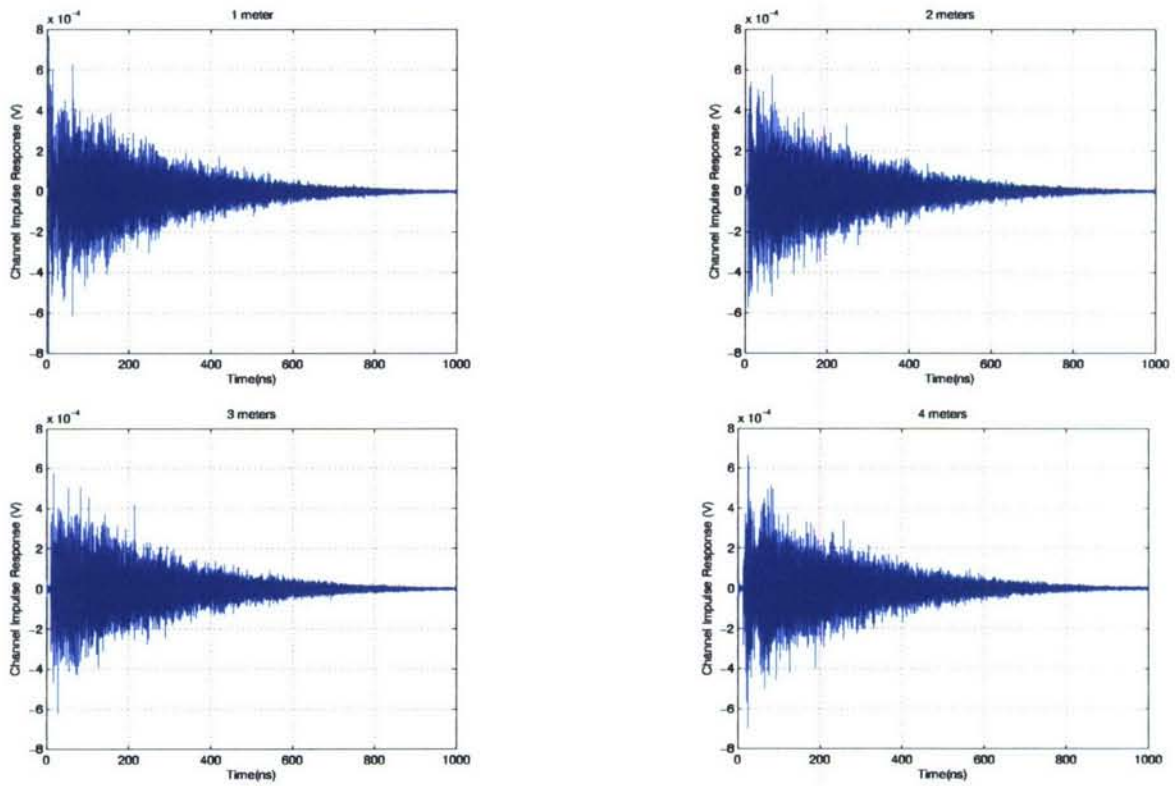


Figure 6.5: Channel impulse response  $h(t)$  at distance 1m, 2m, 3m and 4m between transmitter antenna and receiver antenna in rectangular metal cavity

The channel impulse response forms a channel autocorrelation function according to

$$R_{hh} = h(t) * h^*(-t) \tag{6.4}$$

where  $h^*(-t)$  is the time reversed conjugated version of  $h(t)$ . The autocorrelation of channel pulse response at distance 1m, 2m, 3m and 4m between transmitter antenna and receiver antenna is shown in Fig. 6.6

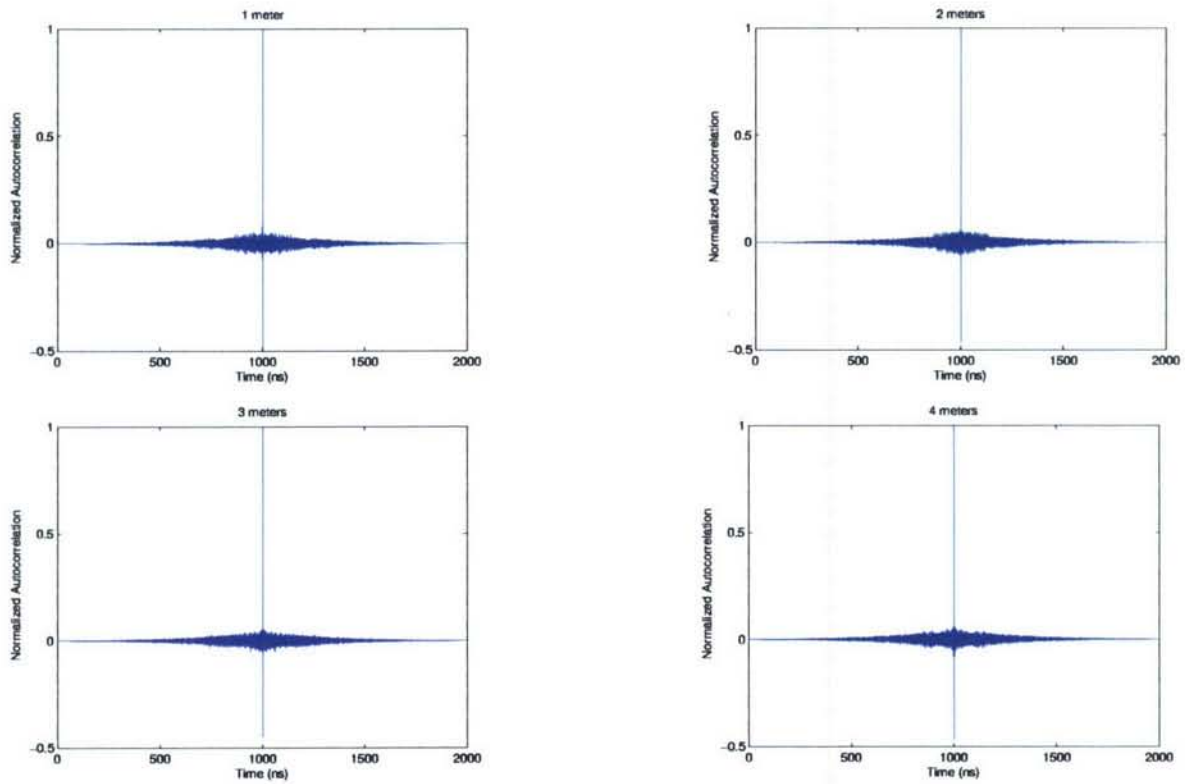


Figure 6.6: Autocorrelation function  $R_{hh}(t)$  at distance 1m, 2m, 3m and 4m between transmitter antenna and receiver antenna in rectangular metal cavity

**Measurement in Office Environment**

The same procedure of measurement is repeated in office environment. The same set of parameters as shown in table 6.1 is used. The frequency domain response at distance 1m, 2m, 3m and 4m between transmitter antenna and receiver antenna is shown in Fig. 6.7

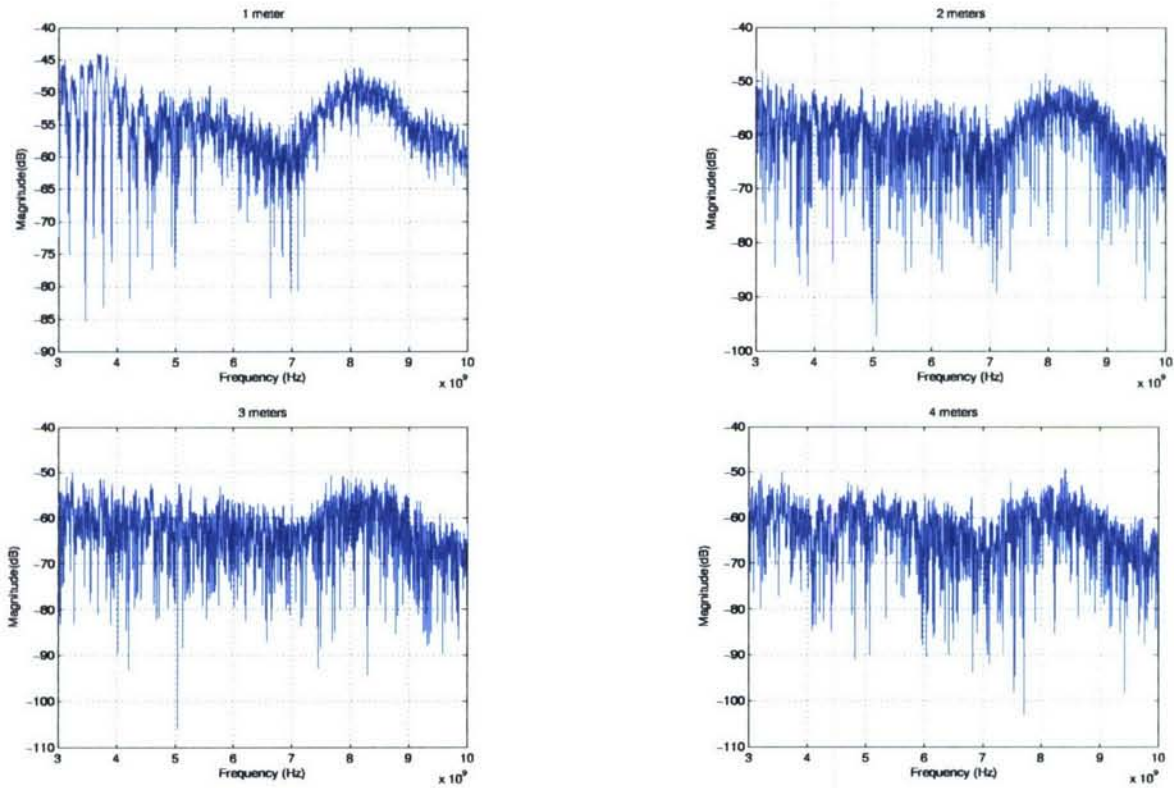


Figure 6.7: Frequency domain response  $H(f)$  at distance 1m,2m,3m and 4m between transmitter antenna and receiver antenna in office

The time domain response at distance 1m, 2m, 3m and 4m between transmitter antenna and receiver antenna is shown in Fig. 6.8

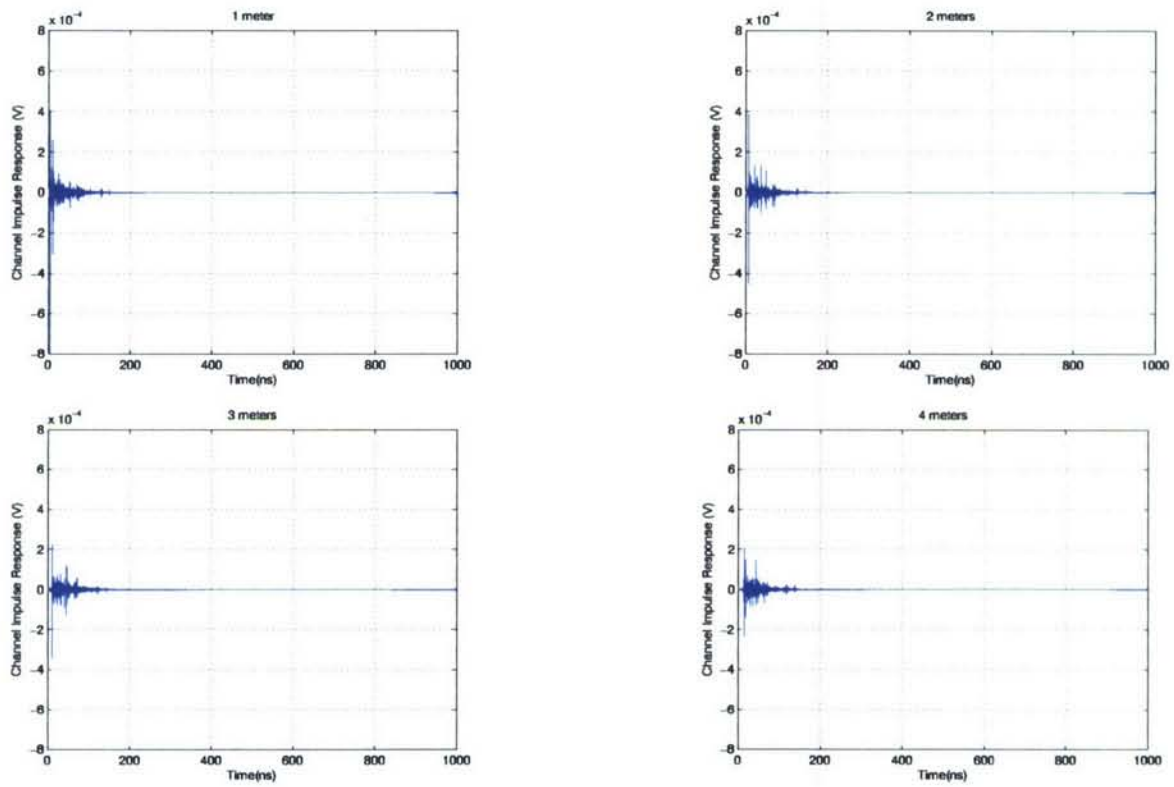


Figure 6.8: Channel impulse response  $h(t)$  at distance 1m,2m,3m and 4m between transmitter antenna and receiver antenna in office

The autocorrelation of channel pulse response at distance 1m, 2m, 3m and 4m between transmitter antenna and receiver antenna is shown in Fig. 6.9.

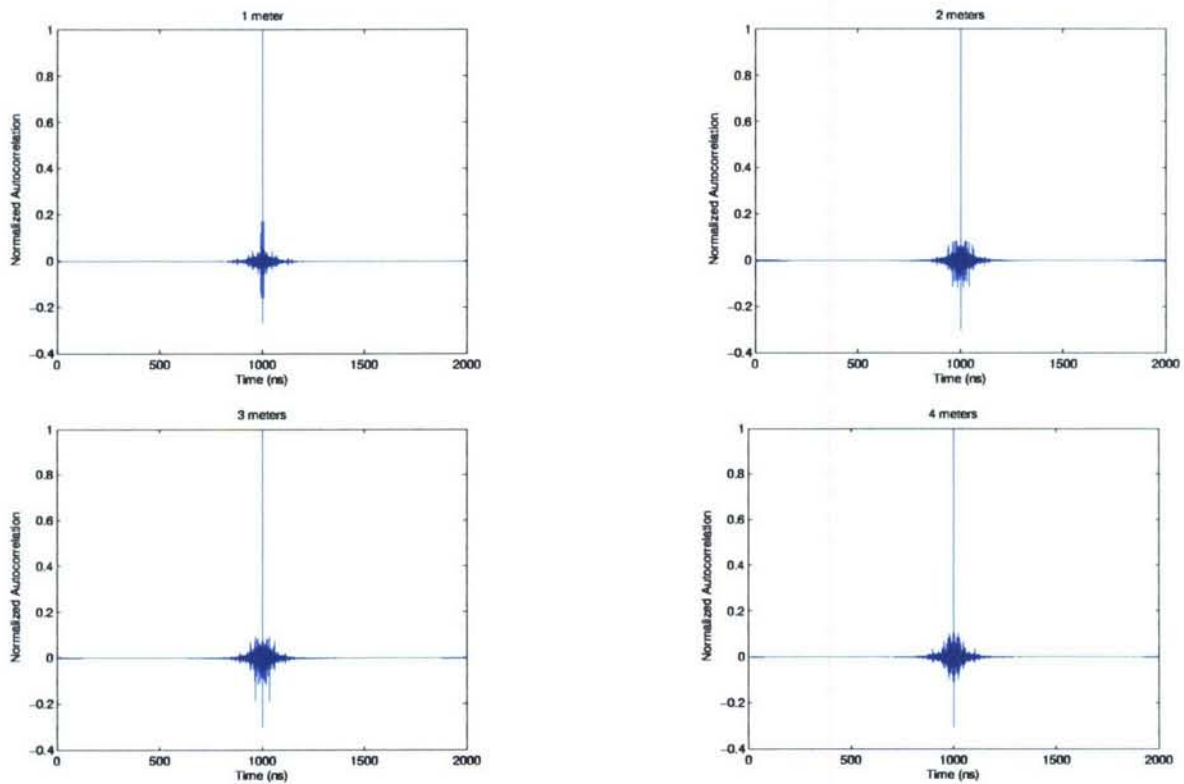


Figure 6.9: Autocorrelation function  $R_{hh}(t)$  at distance 1m, 2m, 3m and 4m between transmitter antenna and receiver antenna in office

**Measurement in Hallway Environment**

The same procedure of measurement is repeated in hallway environment. The same set of parameters as shown in table 6.1 is used. The frequency domain response at distance 1m, 2m, 3m and 4m between transmitter antenna and receiver antenna is shown in Fig. 6.10

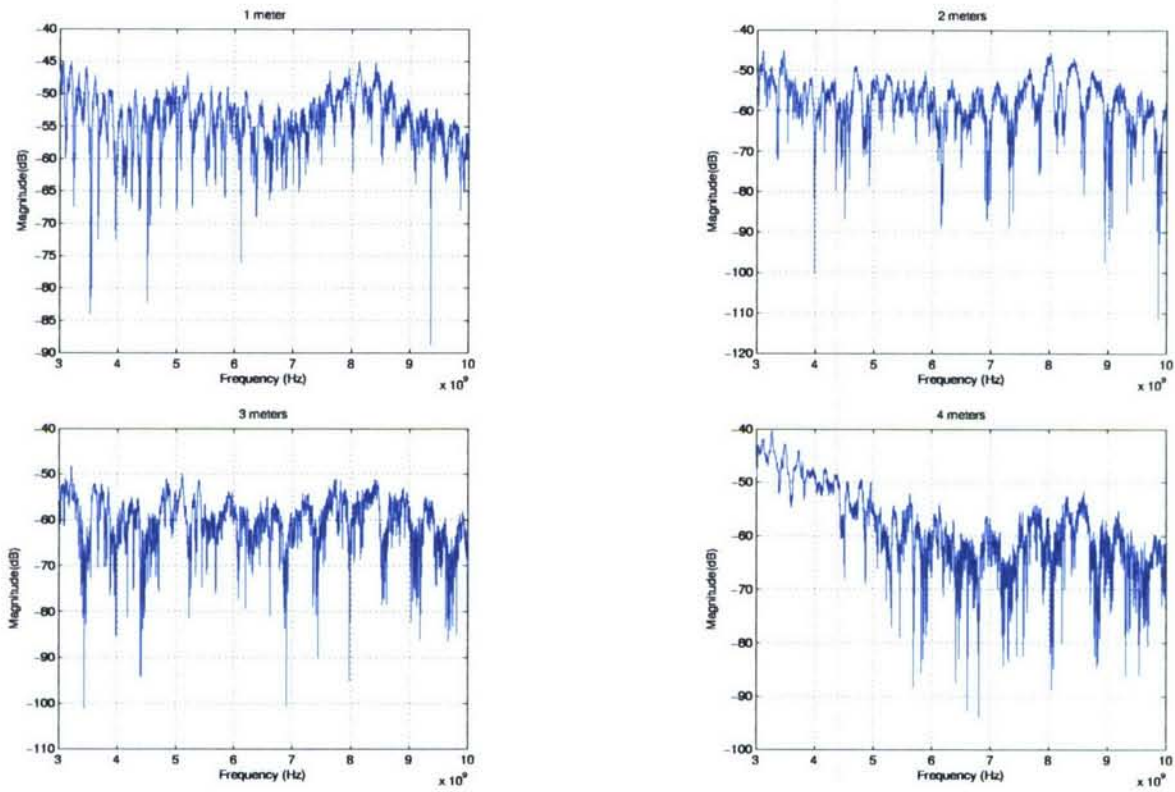


Figure 6.10: Frequency domain response  $H(f)$  at distance 1m,2m,3m and 4m between transmitter antenna and receiver antenna in hallway

The time domain response at distance 1m, 2m, 3m and 4m between transmitter antenna and receiver antenna is shown in Fig. 6.11

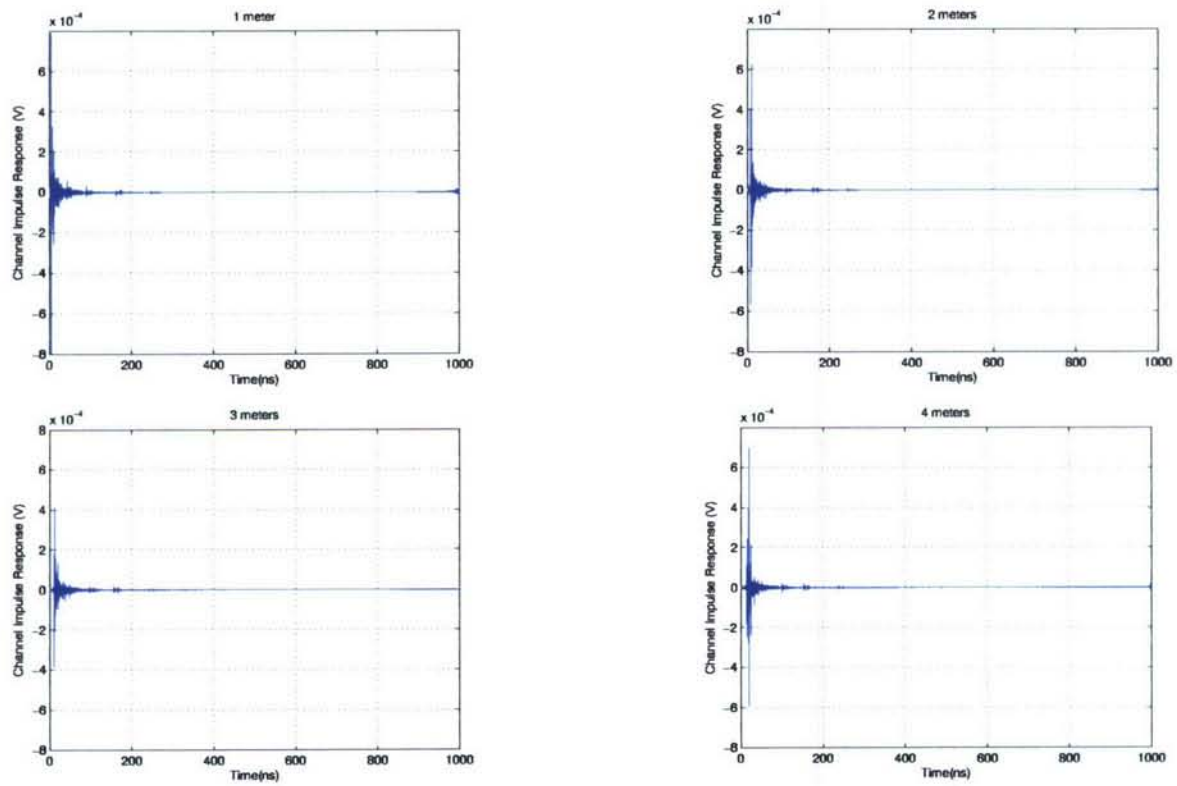


Figure 6.11: Channel impulse response  $h(t)$  at distance 1m,2m,3m and 4m between transmitter antenna and receiver antenna in hallway

The autocorrelation of channel pulse response at distance 1m, 2m, 3m and 4m between transmitter antenna and receiver antenna is shown in Fig. 6.12

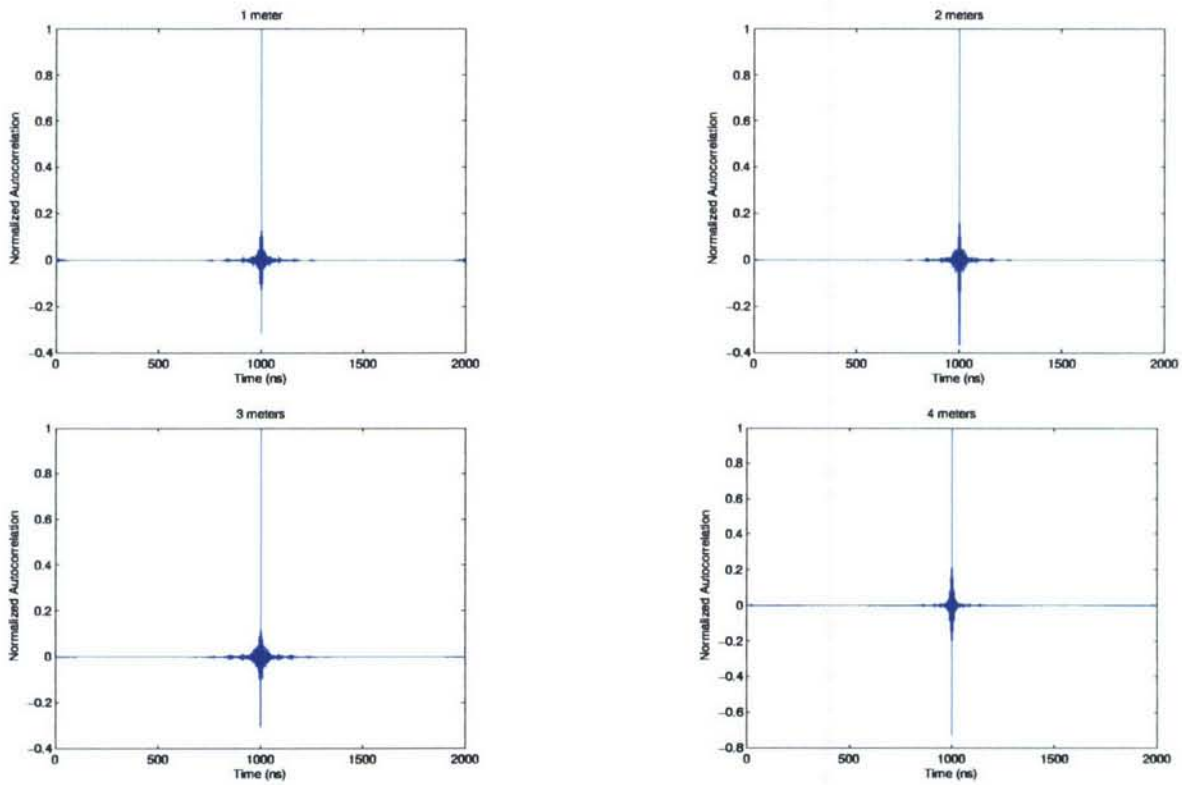


Figure 6.12: Autocorrelation function  $R_{hh}(t)$  at distance 1m,2m,3m and 4m between transmitter antenna and receiver antenna in hallway

**Comparison of Energy for Rectangular Metal Cavity, Office and Hallway Environments**

The energy of channel impulse response for the three cases can be calculated by using

$$E_h = \int_0^{T_h} h^2(t) dt \tag{6.5}$$

where  $T_h$  is the time duration of the channel. The energy for the three cases is shown in Fig. 6.13

From the Fig. 6.13, it can be seen clearly that the total energy of the channel impulse response in a confined metal cavity decays very slowly, as compared to those in office and hallway.

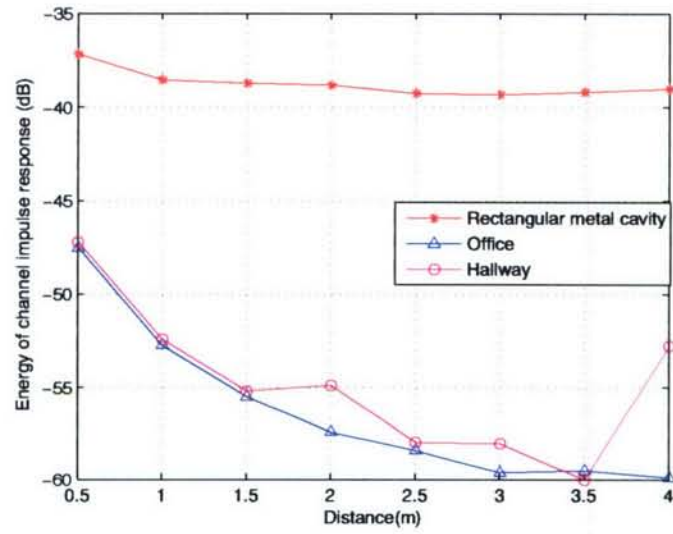


Figure 6.13: Energy of channel impulse response for rectangular metal cavity,office and hallway environments

### 6.2.2 Measurement for MIMO Case

The measurement is performed for a 3x3 MIMO case using virtual array inside the rectangular metal cavity. The measurement parameters used are the same as described in table 6.1. The distance between the antennas in transmitter array and receiver array is 2 feet. The setup for the measurement is shown in Fig. 6.14

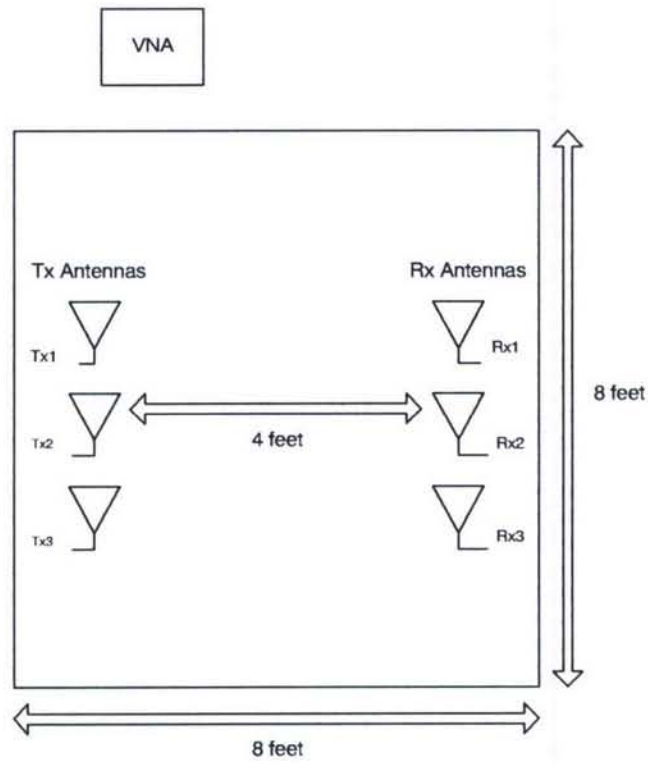


Figure 6.14: Setup for 3x3 virtual MIMO case in rectangular metal cavity

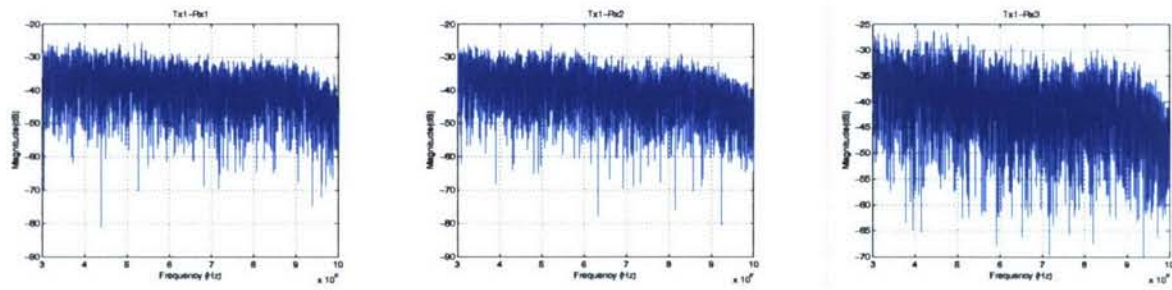


Figure 6.15: Frequency domain response  $H(f)$  from transmitter antenna 1 to different receiver antennas

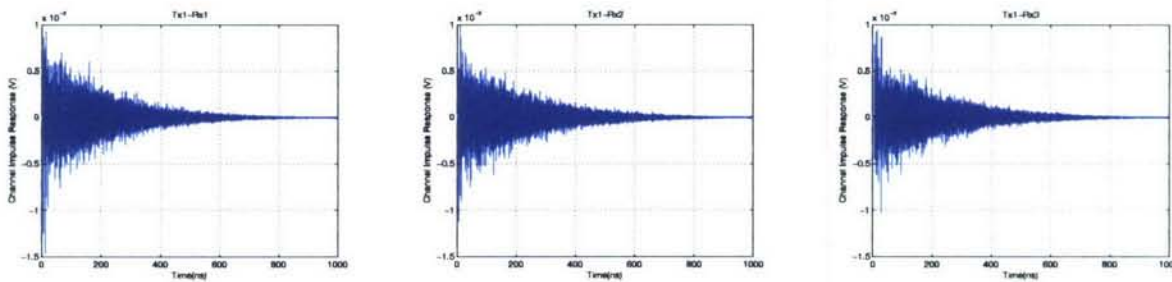


Figure 6.16: Channel impulse response  $h(t)$  from transmitter antenna 1 to different receiver antennas

The frequency domain response and time domain response from transmitter antenna 1 to different receiver antennas is shown in Fig. 6.15 and Fig. 6.16

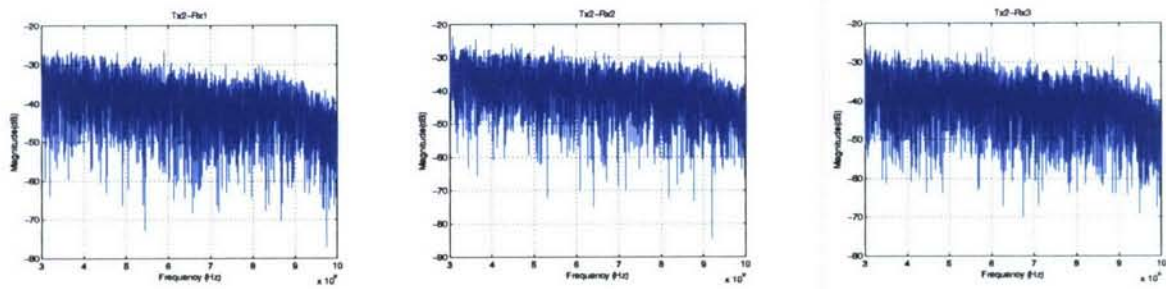


Figure 6.17: Frequency domain response  $H(f)$  from transmitter antenna 2 to different receiver antennas

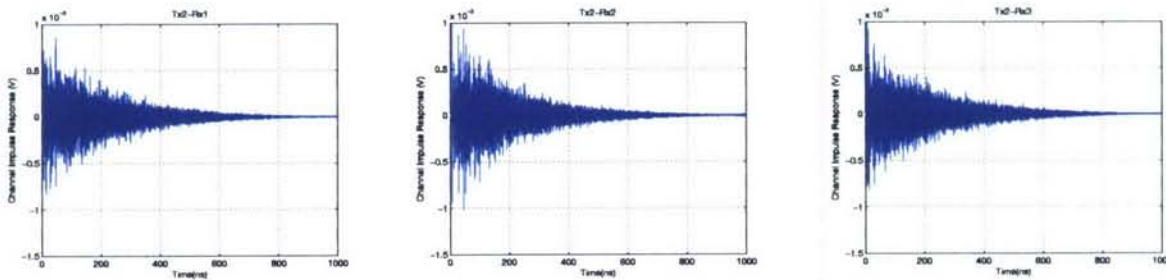


Figure 6.18: Channel impulse response  $h(t)$  from transmitter antenna 2 to different receiver antennas

The frequency domain response and time domain response from transmitter antenna 2 to different receiver antennas is shown in Fig. 6.17 and Fig. 6.18

The frequency domain response and time domain response from transmitter antenna 3 to different receiver antennas is shown in Fig. 6.19 and Fig. 6.20

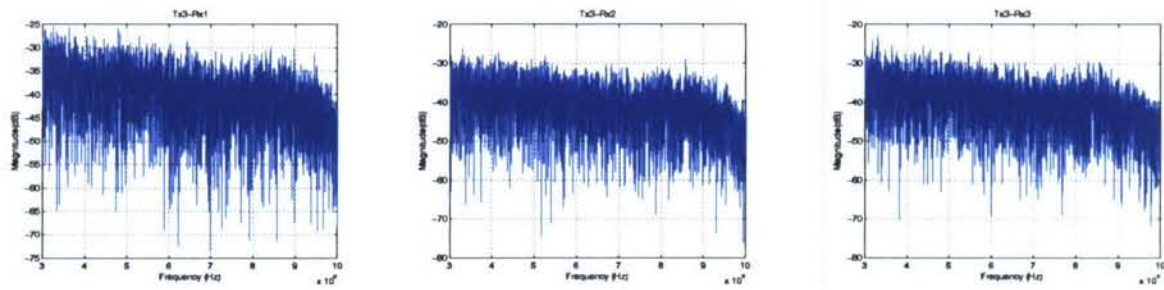


Figure 6.19: Frequency domain response  $H(f)$  from transmitter antenna 3 to different receiver antennas

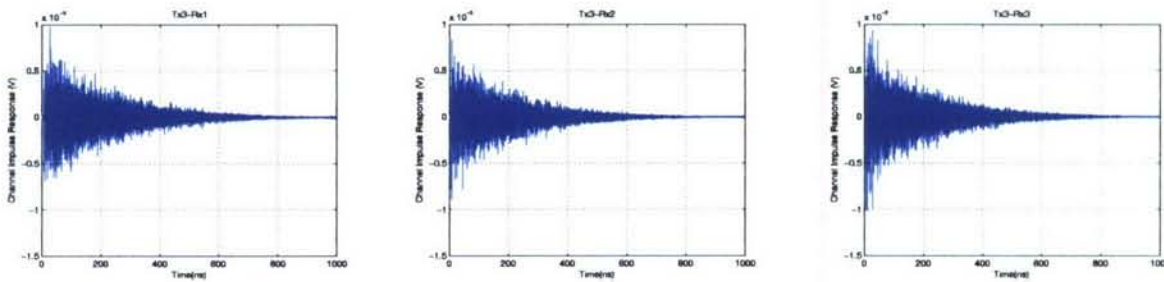


Figure 6.20: Channel impulse response  $h(t)$  from transmitter antenna 3 to different receiver antennas

### 6.3 Conclusion

In this chapter, channel sounding for UWB channel is discussed. Time domain measurement technique and frequency domain measurement technique are discussed in detail. Then two measurement examples are considered. Firstly we compare the characteristics of UWB SISO channel in rectangular metal cavity, in office and in hallway, and then the measurement case for a 3x3 UWB MIMO channel in rectangular metal cavity is also considered.



## Bibliography

- [1] W. Ciccognani, A. Durantini and D. Cassioli, "Time domain Propagation Measurements of the UWB Indoor Channel Using PN-Sequence in the FCC-Compliant Bnad 3.6-6 GHz," *IEEE Transactions on Antenna and Propagation*, Vol. 53, No. 4, April 2005.
- [2] A. Taparugssanagorn, L. Hentila, and S. Karhu, "Time-Varying Autoregressive Process for Ultra-Wideband Indoor Channel Model," <http://www.eurasip.org/content/Eusipco/IST05/papers/214.pdf>.
- [3] Agilent AN 1287-3, "Applying Error Correction to Network Analyzer Measurements," *Application Note*.
- [4] Agilent, "Electronic vs. Mechanical Calibration Kits: Calibration Methods and Accuracy," *White Paper*.



**Part II**

**Experimental Testbed**

## Chapter 7

# Overview of Testbed

This report documents some of our recent development work with focus on design and implementation aspect.

The ultimate goal is to achieve range extension by optimizing system design. Specifically, the overall goal is to implement a UWB radio test-bed with waveform optimization. The work of design is to provide a feasible solution under some theoretical and practical criteria. We proposed a system architecture relying on continuous-time (or waveform level) time reversal technique, though there are a few other types of optimization rules. One of the key components in the UWB time reversal system is the programmable waveform generator based on advanced FPGA and D/A conversion technologies. A Xilinx Virtex 5 chip, one of the fastest FPGA chips to date, is chosen to perform major digital back-end functions at the transmitter. The ultra-wide bandwidth and ultra-high sampling rate pose many design and implementation challenges. Major difficulties are associated with the interfaces between the FPGA and mixed-signal devices, timing closure issues in FPGA routing, fixed-point implementation with limited hardware resources, etc.

Management wise, in addition to frequently documenting and periodically reporting, we have come up with a manageable mechanism including detailed plans and goals for different periods of times, weekly project meetings, monthly project reviews, and work assignments on daily basis.

Currently the system architecture has been stabilized and we are working toward the next milestone (see milestone list in Table I).

The rest part of this report is organized as follows.

TABLE I. Milestones

Stable Architecture	8/2007
Time Reversal System with Cable	1/2008
Time Reversal System over the Air (Some Field Test)	6/2008
Fully Functional UWB System with Time reversal	1/2009
System Field Test	6/2009
Potential Technology Transfer to US Navy	12/2009



## Chapter 8

# System Design and Architecture

With the overall goal and constraints from both theoretical and practical perspectives, a completed top-down solution has been given. A very broad range of issues need to be considered. Here just name a few: frequency and band, data rate, modulation, synchronization, coexistence, commercial availability of devices, etc. Simply speaking, a feasible and advanced design must be made.

### 8.1 Bandpass Time Reversal

From implementation point of view, it is too difficult to build a system working from DC to 500 MHz or higher. Instead, a pass-band system is more feasible and flexible. To reduce the requirement for sampling rate, a typical technique used with digital signal processing is up- and down- conversion. The carrier phase difference between the received signal and the output of local oscillator is usually unknown. We will show that quadrature conversion can take care of this unknown phase difference.

For convenient description in the following, complex representation is accepted to represent bandpass signals. Assume a bandpass sounding signal  $p(t)e^{j(\omega t + \theta_0)}$  is transmitted over the channel, where  $\omega$  is the carrier frequency and  $\theta_0$  is an unknown initial phase. All filtering effect introduced over the radio link is taken into account by  $p(t)$ . Consider a channel with its channel impulse response (CIR)  $h(t)$  modeled as tap delay line (implying no consideration of frequency selective pulse distortion)

$$h(t) = \sum_i \alpha_i \delta(t - \tau_i). \quad (8.1)$$

Up on receiving the noisy sounding signal

$$r(t) = \sum_i \alpha_i p(t - \tau_i) e^{j[\omega(t - \tau_i) + \theta_0]} + n(t), \quad (8.2)$$

the receiver's down-conversion stage outputs a baseband signal

$$y(t) = \sum_i \alpha_i p(t - \tau_i) e^{j(\omega \tau_i - \theta_0 + \theta_1)} + n'(t), \quad (8.3)$$

where  $\theta_1$  is an unknown phase introduced in down-converting. There are a variety of estimation techniques to reduce the impact of noise  $n'(t)$  and multiple sounding pulse may be necessary. To describe the central idea more conveniently, we assume perfect estimation here. Based on this baseband signal  $y(t)$ , there can be a few waveform for performing time reversal at the transmitter. Consider the following two optional waveforms:

option 1

$$h(t) = \sum_i \alpha_i \delta(t - \tau_i).$$

option 2

$$\tilde{p}(t) = \sum_i \alpha_i p(t - \tau_i) e^{j(\omega\tau_i - \theta_0 + \theta_1)}. \quad (8.4)$$

The option 1 needs a great deal of effort in the estimation stage, while the option 2 is extremely simple since it does not require any parametric estimation. In particular, the option 2 can work directly with “arbitrary” waveform generator with need for pulse shaping.

Let us consider a simple case of one pulse per symbol and use

$$\tilde{p}(T_0 - t) e^{j(\omega t + \theta_2)} = \sum_i \alpha_i p(T_0 - t - \tau_i) e^{j([\omega(t + \tau_i) - \theta_0 + \theta_1 + \theta_2]} \quad (8.5)$$

as the symbol waveform, where  $T_0$  is a constant to guarantee the transmitted signal being causal. The received symbol waveform can be expressed as

$$\begin{aligned} & \sum_i \sum_k \alpha_i \alpha_k p(T_0 - t - \tau_i + \tau_k) e^{j([\omega(t + \tau_i - \tau_k) - \theta_0 + \theta_1 + \theta_2]} \\ &= \sum_i \alpha_i^2 p(T_0 - t) e^{j([\omega t - \theta_0 + \theta_1 + \theta_2]} + \sum_{i \neq k} \alpha_i \alpha_k p(T_0 - t - \tau_i + \tau_k) e^{j([\omega(t + \tau_i - \tau_k) - \theta_0 + \theta_1 + \theta_2]}, \end{aligned} \quad (8.6)$$

which leads to a baseband version after down-conversion:

$$\sum_i \alpha_i^2 p(T_0 - t) e^{j\theta} + \sum_{i \neq k} \alpha_i \alpha_k p(T_0 - t - \tau_i + \tau_k) e^{j[\omega(\tau_i - \tau_k) + \theta]}, \quad (8.7)$$

where

$$\theta = -\theta_0 + \theta_1 + \theta_2 + \theta_3 \quad (8.8)$$

has been applied. In (8.6) and (8.7) the summations  $\sum_i$  and  $\sum_{i \neq k}$  correspond to main lobe and side lobes, respectively. For coherent demodulation, there has to be some mechanism to estimate the unknown phase  $\theta$ , but this is not necessary for non-coherent demodulation. Also, down-conversion is not required for energy detector based scheme.

## 8.2 System Architecture

The transmitter and receiver architectures are shown in Fig. 1 and 2, where either one can be divided into four major functional parts: RF front-end, mixed-signal, digital back-end and control/interface via PC.

## 8.3 Link Budget

The link budget estimation shown below is based on OOK modulation and free space propagation.

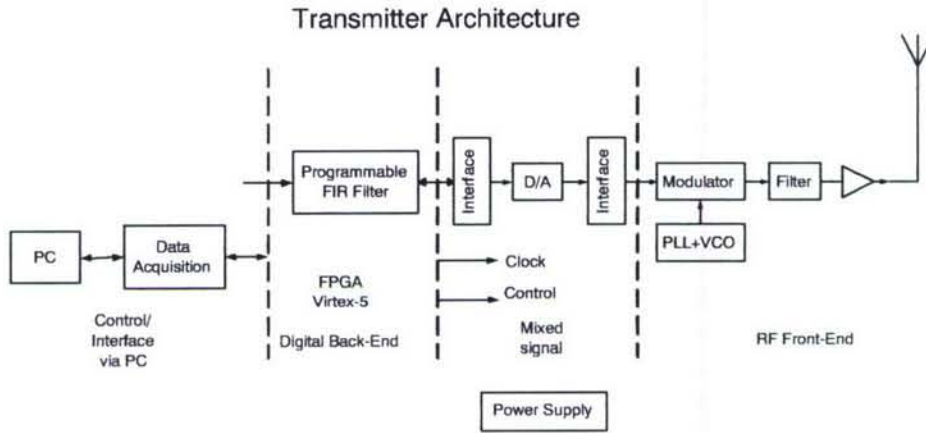


Figure 8.1: Transmitter Architecture.

TABLE II. A Link Budget Example.

Bit rate	5 Mb/s
Minimum required SNR per bit	$E_b/N_{0,min} = 16$
Center frequency	4 GHz
Transmitter antenna gain	2 dBi
Receiver antenna gain 2	dBi
Distance between the two antennas	40 meters
Receiver noise figure	7 dB
Implementation loss	6 dB
Transmitted power to antenna	0.51 dBm (1.13 mW)
Bandwidth (approximately)	500 MHz
1 m EIRP spectral density over the whole bandwidth	-68.96 dBm/MHz
Path loss	76.52 dB
Received power the antenna	-72.01 dBm
Link margin	6.00 dB
Proposed minimal receiver sensitivity	-78.01 dBm

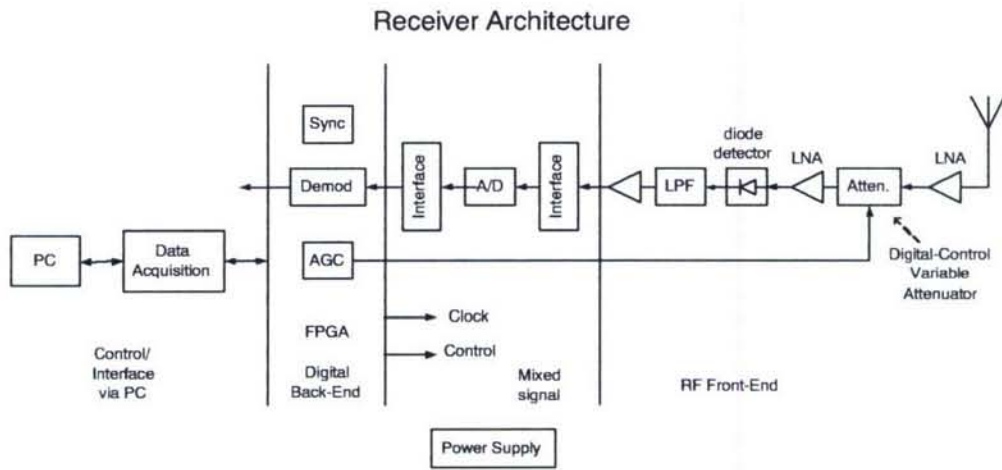


Figure 8.2: Architecture of a reference receiver design.

## Chapter 9

# RF Front-Ends and Mixed-Signal Stage

We mainly rely on off-the-shelf products in our test-bed development. Reported in this section include selection of components/modules and some test results. Major components and modules listed in Table III.

TABLE III. A list of Selected Components/Modules.

Local oscillator	center frequency 3.5 GHz or 4 GHz
Modulator (up-converter)	bandwidth 500 MHz
Dual-channel D/A	sampling rate 1GS/s or higher, with LVDS ports
A/D	sampling rate up to 1.5 GS/s

### 9.1 Local Oscillator

PSA3550C produced by Z-Communication, Inc. is used as the local oscillator (LO) whose frequency range is from 3545MHz to 3555MHz. Fig. 9.1 shows the picture of evaluation board of PSA3550C.

PSA3550C includes ADF4106 made by Analog Device, which is used as the frequency synthesizer. ADF4106 is programmable through P5 port on the evaluation board. When we do the test, the power supply is set to 6Vdc. The amplified RF output P2 is connected to Spectrum Analyzer. P3 is connected to the termination. No attenuations are used. The onboard 12MHz reference oscillator is used, so P1 is not connected to the external reference oscillator temporarily. The REF IN frequency is set to 12MHz. The desired pfd reference frequency is set to 1000KHz. If the desired VCO output frequency is set to 3550MHz, the spectrum of the output is shown in Fig. 9.2.

### 9.2 Modulator

TRF3703-15 produced by Texas Instruments is used as the quadrature modulator. Fig. 9.3 shows the picture of evaluation board of TRF3703-15.

The TRF 3703 is a very low-noise direct quadrature modulator, capable of converting complex modulated signals from baseband directly up to RF. The TRF3703 is ideal for high performance direct RF modulation from 400MHz



Figure 9.1: The picture of evaluation board of PSA3550C used as the local oscillator.

up to 4GHz. The RF output block consists of a differential to single-end converter and an RF amplifier capable of driving a single-end  $50\Omega$  load without any need of external components [1].

When we do the test, we connect the 5Vdc supply to headers W1 and W2; we use PSA3550C to supply the LO signal at 3555MHz to J1 and terminate J2 with  $50\Omega$  to ground; we use a waveform generator to provide the pulse waveform whose width is 20ns as the I input signal and set the common mode voltage on the input signals; we connect a Spectrum Analyzer to the SMA connector marked RFOUT (J7) and monitor the output. The spectrum of the output is shown in Fig. 9.4.

### 9.3 Digital to Analog Converter

MB86064 produced by Fujitsu is used as the Digital to analog converter (DAC). Fig. 9.5 is the picture of evaluation board of MB86064. Fig. 9.6 shows the GUI of control software for MB86064.

The Fujitsu MB86064 is a dual 14-bit  $1\text{Gsa/s}$  DAC, delivering exceptional dynamic performance. Each high performance DAC core is capable of generating multi-stand, multi-carrier communication transmitted signals. DAC data is input via two high-speed LVDS ports. These operate in a pseudo double data rate (DDR) mode, with data latched on both rising and falling edges of the clock. To simplify system integration the DAC operates from a clock running at half the DAC conversion rate [2]. A function block diagram is shown in Fig. 9.7. The reasons why we choose MB86064 as DAC in our test-bed can be summarized below.

From clock point of view, MB86064 requires a RF input clock at half the DAC conversion rate, with sufficient spectral purity to not impact the target analog output performance. Because the DAC cores are clocked on both rising and falling edges of the input clock, the requirement of the external clock source is reduced. The sampling rate of DAC cores is  $1\text{Gsa/s}$  and the frequency of the RF input clock is 500MHz which is easier to be generated by the current FPGA devices. At first, we use AD9734 as DAC in our test-bed. Though the sampling rate of AD9734 is  $1.2\text{Gsa/s}$ , the DAC clock with frequency of 1.2GHz is needed.

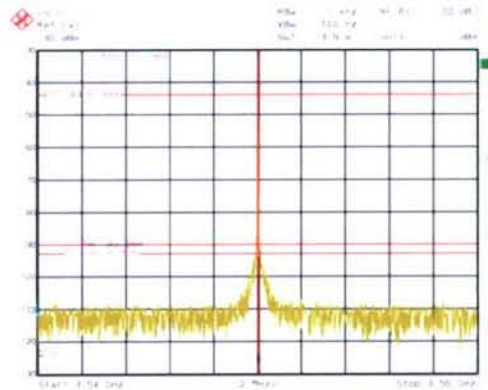


Figure 9.2: The spectrum of the PSA3550C output when the desired VCO output frequency is set 3550MHz.

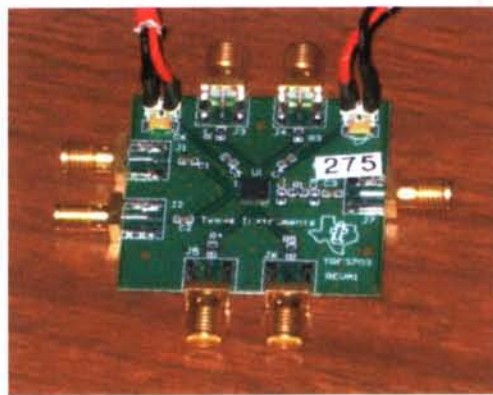


Figure 9.3: The picture of evaluation board of TRF3703-15 used as the quadrature modulator.

From the number of DAC cores point of view, MB86064 has two DAC cores which can generate two signals for I/Q simultaneously. So, we do not need to buy and integrate two DACs with only one core in the test-bed, which will greatly reduce the difficulty of the system integration.

From the interface point of view, The evaluation board of MB86064 is designed to accommodate up to six SMA connectors-two for the differential clock input and four for the two differential analog outputs. Boards are supplied with transformers on-board to perform single ended-to-differential and differential-to-single ended conversions [3]. So using MB86064, we can easily make one simple adapter to connect the evaluation board of MB86064 and the evaluation board of TRF3703-15.

From the waveform memory module point of view, MB86064 incorporates a waveform memory module featuring two 16k point on-chip waveform memories [4]. These allow the DAC cores to be driven with user programmed waveforms without the need for external high speed, pattern generators which can increase the flexibility of system design.

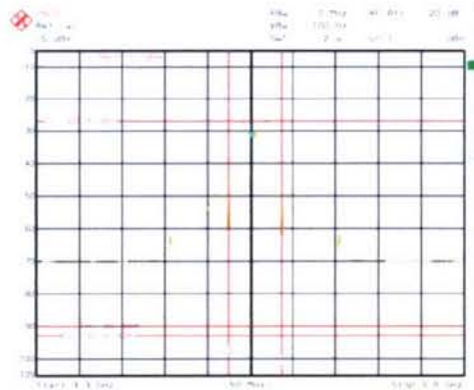


Figure 9.4: The spectrum of TRF3703-15 output.

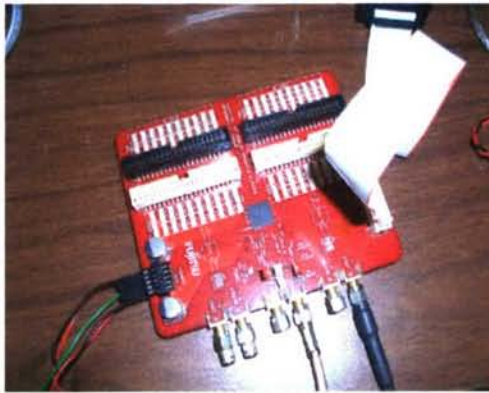


Figure 9.5: The picture of evaluation board of mb86064 used as DAC.

Now, we just test the function of the waveform memory module. According to the user manual, we follow the steps to power up and start to use the evaluation board of MB86064. A single-ended clock source is connected to SMA connector CLK; the single-ended analog outputs on SMAs IOUTA and IOUTB are connected to the test equipment; the jumper links LK1 and LK2 are set as required; the PC USB programming cable is connected to the CONTROL I/F header; the power supply cable is connected to the POWER header with correct orientation; the power supplies are turned on; the PC control software are installed and operated.

## 9.4 MAX108 A/D

An 8-bit monolithic bipolar A/D converter with sampling rate up to 1.5Gbps is employed to convert the baseband signal (analog signal) into digital domain. A baseband amplifier between the low pass filter following the square law



Figure 9.6: The GUI of control software for MB86064.

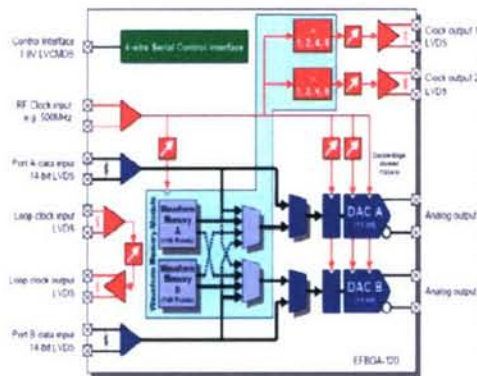


Figure 9.7: The function block diagram of MB86064.

detector and ADC is necessary for signal conditioning. To facilitate digital interface, the A/D converter features an on-chip, selectable 8:16 output demultiplexing that slows the 1.5Gsp/s data rate to 750 mega-words/second ported to two parallel, differential 8-bit, low-voltage (PECL) outputs. A programmable high-frequency clock synthesizer is used to generate the sampling clock for the A/D converter. The output frequency of the clock synthesizer is controlled by FPGA, so variable ADC sampling rate is achieved. The number of bits of the A/D converter is dynamically adapted to the conditions of the environment. It can downscale the digital baseband complexity and total power assumption. A double-data-rate (DDR) interface with FIFO is implemented in FPGA to connect the A/D converter to FPGA. For the design of the high-speed interface between ADC and FPGA, signal integrity has become a critical issue. Many signal integrity problems are electromagnetic phenomena in nature and hence related to the EMI/EMC. There are two concerns for signal integrity - the timing and the quality of the signal. Signal timing mainly depends on the delay caused by the physical length that the signal must propagate. Signal waveform distortions can be caused by reflection, cross talk and power/ground noise. An interface board has been carefully designed to solve the signal integrity issue.

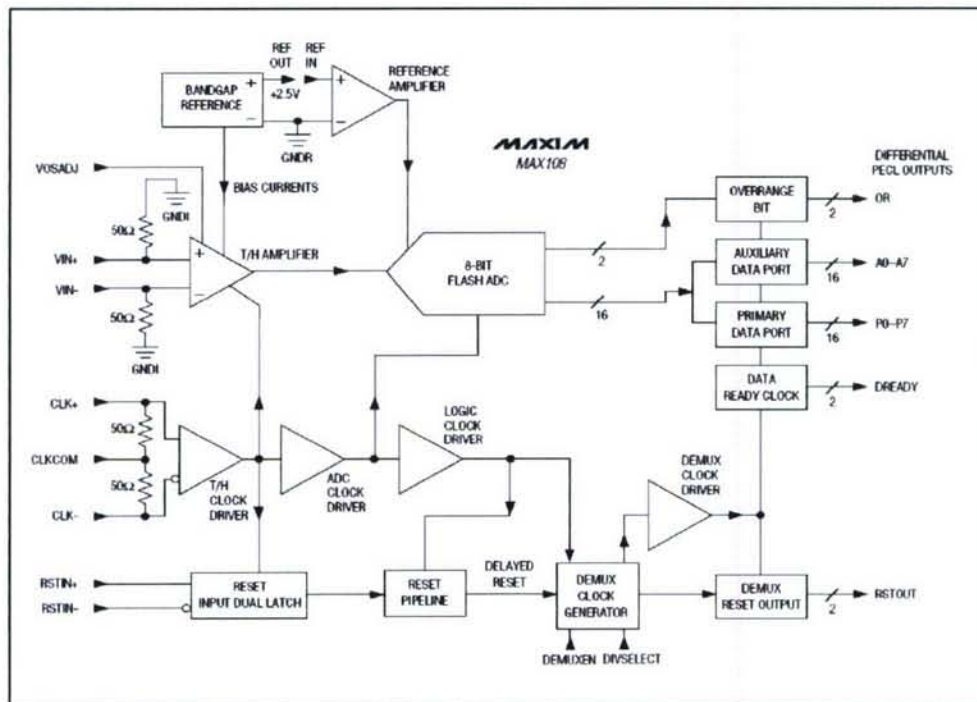


Figure 9.8: MAX108 function diagram.

## 9.5 SPI Control

In this system, There are many devices need to configure and control, such as LO, AGC, DAC. Each one has its own way of initialization and configuration. In order to reduce the system's complexity. SPI Bus is chosen to configure all these devices, Also it could be implemented in FPGA, which is easy and efficient.

SPI standards for Serial Peripheral Interface, It is a simple interface that allows one chip to communicate with one or more other chips. It can easily achieve a few Mbps (mega-bits-per-second). Basically: (1) It is synchronous. (2) It is serial. (3) It is full-duplex. (4) It is not plug-and-play. (5) There is one (and only one) master, and one (or more) slaves. In more details: (1) A clock is generated by the master, and one bit of data is transferred each time the clock toggles. Because SPI is synchronous and full-duplex, every time the clock toggles, two bits are actually transmitted (one in each direction). (2) Data is serialized before being transmitted, so that it fits on a single wire. There are two wires for data, one for each direction. (3) The master and slave know beforehand the details of the communication (bit order, length of data words exchanged, etc.) (4) The master is always the one who initiates communication. Only one slave is active at a time.

A SPI master can communicate with single slave as well as multiples slaves by connecting most signals in parallel and adding SSEL lines. SPI requires 4 wires to be used in between the two chips. As you can see, the wires are called SCK, MOSI, MISO and SSEL, and one of the chip is called the SPI master, while the other the SPI slave. Fig. 9.10 shows A SPI master communicate with one slave and three slaves.

(1) MOSI - Master device data out, Slave device data in (2) MISO - Master device data in, Slave device data out (3)

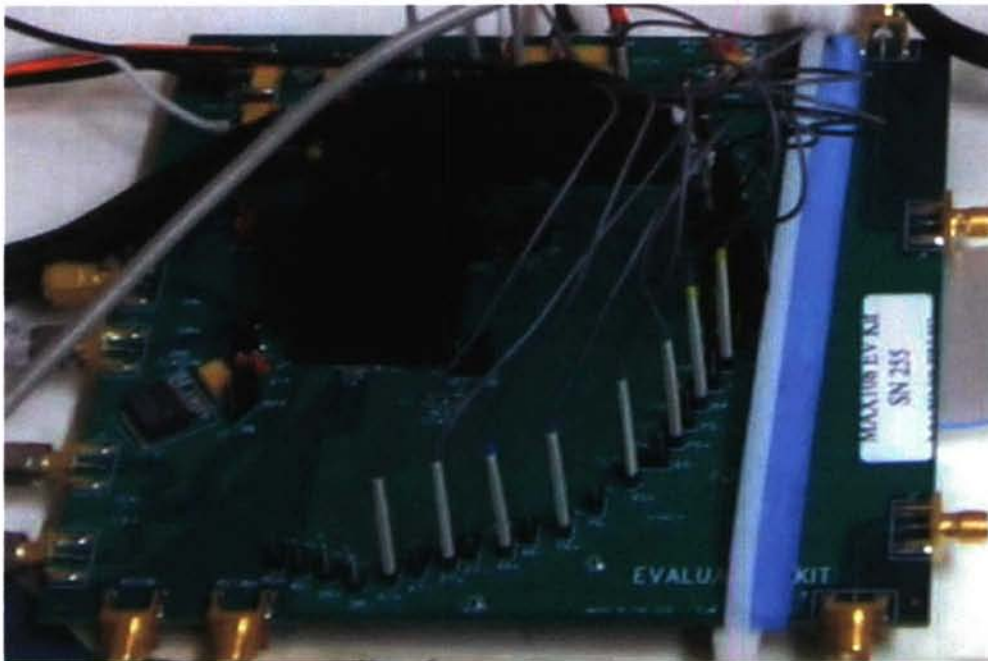


Figure 9.9: MAX 108 development board.

SCLK - Clock, Generated by Master Device (4) SSEL -Slave device enable, controlled by Master device

When there are three slaves. The master must have three SSEL lines, and activate only one SSEL line at a time. Since all three slaves are connected to the MISO line, slaves that are not activated must not drive the MISO line.

Let's assume that the master and slave expect 8-bits data transfers, with MSB transmitted first. Fig. 9.11 shows how would look a single 8-bits data transfer and its the internal interface.

(1) The master pulls SSEL down to indicate to the slave that communication is starting (SSEL is active low). (2) The master toggles the clock eight times and sends eight data bits on its MOSI line. At the same time it receives eight data bits from the slave on the MISO line. (3) The master pulls SSEL up to indicate that the transfer is over.

If the master had more than one 8-bits data to send/receive, it could keep sending or receiving and re-assert SSEL only when it is done.

In our system, SPI bus is used to implement system control.

For LO, The evaluation board is supposed to come with a cable for connecting to the printer port of a PC. The silk screen and cable diagram for the evaluation board are shown below as Fig. 9.12. We intend to replace the PC by FPGA, Using SPI protocol to write ADF4106 registers through the DB-9 interface. The ADF4106 has a simple SPI-compatible serial interface for writing to the device. CLK, DATA, and LE control the data transfer.

For DAC, Its configuration and control are expected to through Fujitsu's PC USB Programming cable and accompanying PC software, as well as download test vectors to the waveform memory module. The programming cable interfaces between a host PC's USB port and the 4-wire serial interface implemented on the device, The connection

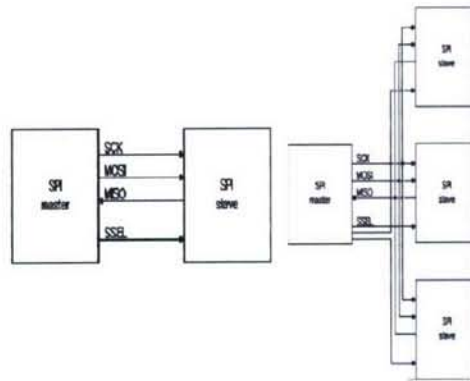


Figure 9.10: The block diagram of SPI Bus.

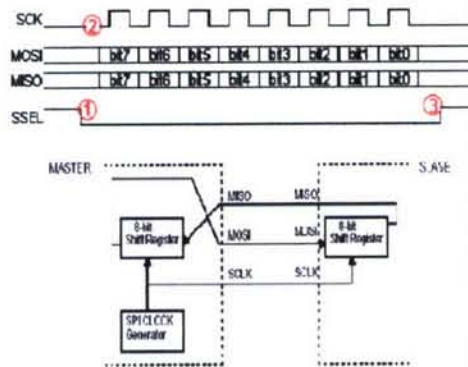


Figure 9.11: The block diagram of SPI Transfer.

is shown in Fig. 9.13.

Similarly we also intend to configure the device by SPI protocol. To facilitate this, An appropriate connector should be fitted to the target board, providing connections to the signals as: (1) SERIAL IN. (2) SERIAL OUT. (3) SERIAL CLK. (4) SERIAL EN. Fig. 9.14 shows this connection.

Other devices could be configured with SPI protocol similarly.

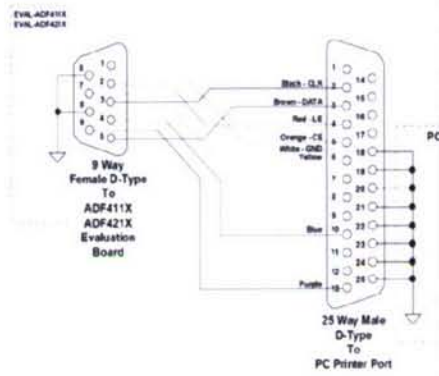


Figure 9.12: The diagram of LO interface.



Figure 9.13: The diagram of DAC Kit.

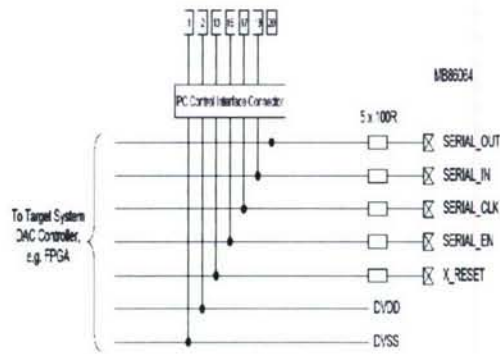


Figure 9.14: The diagram of DAC interface.

## Bibliography

- [1] "TRF3703 0.4-GHz to 4-GHz Quadrature Modulator," Texas Instruments, 2007.
- [2] "MB86064 Dual 14-bit 1GSa/s DAC Datasheet," Fujitsu, 2004.
- [3] "DK86064-2 Dual 14-bit 1GSa/s DAC Development Kit," Fujitsu, 2004.
- [4] "MB86064 Dual 14-bit 1GSa/s DAC Product Flyer," Fujitsu, 2004.



## Chapter 10

# Digital Back-Ends

Major function played by the digital back-ends include system control/management, parameter setting, AGC, synchronization, interfacing with PC, as well as modulation and demodulation.

### 10.1 System Control Flow

### 10.2 Filter Design

In order to realize time reversal in the test-bed, we need to build the time reversal waveform generator in the transmitter side. According to the design of the test-bed, the FIR filter built in FPGA will be used to generate the waveform of time reversal signaling. Meanwhile, FIR filter will be used in the receiver side to accomplish the functions of matched filter, correlation and so on in the digital domain.

#### 10.2.1 The Typical Methods for Filter Design

The typical methods for the FIR filter design in FPGA are intellectual property (IP) core based method and user-defined coding based method. IP core based method means we use IP core in FPGA to realize the function of digital filter. There are two kinds of IP cores in FPGA can be employed for this purpose. One kind is filter based IP core and the other kind is memory based IP core. The user-defined coding based method means we directly write Verilog code to build the FIR filter according to the design specification.

Multiply accumulate (MAC) FIR filter IP core and distributed arithmetic (DA) FIR filter IP core are the frequently used filter based IP cores. The MAC FIR IP core implements a highly configurable, high-performance, and area efficient FIR filter. All internal data-paths provide full-precision arithmetic to avoid the possibility of overflow. The full-precision sum-of-products is presented on the data output port. A set of three handshake control signals provides an easy-to-use user interface. The MAC FIR filter IP core uses one or more time-shared multiply accumulate functional units to service the  $N$  sum-of-product calculations in the filter [1]. The DA FIR filter IP core is also a highly parameterizable, area-efficient high-performance FIR filter. The main difference between the MAC FIR filter

and the DA FIR filter is the latter employs no explicit multipliers in the design, only look-up tables (LUTs), shift registers, and a scaling accumulator.

In its most obvious and direct form, DA-based computations are bit-serial in nature serial distributed arithmetic (SDA) FIR. The advantage of a distributed arithmetic approach is its efficiency of mechanization. The basic operations required are a sequence of table look-ups, additions, subtractions and shifts of the input data sequence [1]. All of these functions efficiently map to FPGAs. Input samples are presented to the input parallel-to-serial shift register (PSC) at the input signal sample rate. As the new sample is serialized, the bit-wide output is presented to a bit-serial shift register or time-skew buffer (TSB). The TSB stores the input sample history in a bit-serial format and is used in forming the required inner-product computation. The nodes in the cascade connection of TSBs are used as address inputs to a look-up table. This LUT stores all possible partial products over the filter coefficient space.

In a conventional MAC FIR filter realization, the sample throughput is coupled to the filter length. As the filter length is increased, the system sample rate is proportionately decreased. With a DA architecture, the system sample rate is related to the bit precision of the input data samples. The trade off introduced here is one of silicon area (FPGA logic resources) for time. As the filter length is increased in a DA FIR filter, more logic resources are consumed, but throughput is maintained [1]. Meanwhile, one approach to increase the speed of FIR filter using DA architecture is to partition the input words into  $M$  subwords and process these subwords in parallel [1]. This method requires  $M$ -times as many memory look-up tables and so comes at a cost of increased storage requirements. Maximum speed is achieved by factoring the input variables into single-bit subwords. The resulting structure is a fully parallel DA (PDA) FIR filter. With this factoring a new output sample is computed on each clock cycle. Another advantage of the DA FIR filter IP core is the on-line coefficient reload which provides additional flexibility to the system design. While the new coefficient values are being loaded, and some internal data structures are subsequently initialized, the filter ceases to process input samples. The coefficient reload time is a function of the filter length and type [1]. When we use the DA FIR filter IP core to build the single rate FIR filter, the reload delay is 210 clock cycles if the number of taps is 10, the coefficient width is 10 and the input width is 1. Fig. 10.3 shows the simulation result of the coefficient timing using DA FIR filter IP core in FPGA.

If we want to use memory based IP core to realize the FIR filter, FIFO Generator IP core and Block Memory Generator IP core can be employed. The basic thought of this method is that the data of the candidate waveform are put into the memory firstly and then the data are read from the memory according to some control signals later. IP core in FPGA has powerful functions. Even though IP core can work efficiently, it will occupy more resources than we expect. So if our design is not complex, we can directly write Verilog code to build FIR filter. For example, we can build the shift register and adder by coding to generate the waveform of time reversal signaling.

### 10.2.2 Quantization Consideration

Quantization issue is very important for the FIR filter design in FPGA, because any number in FPGA should be finite word length. Quantization will introduce error in the filter implementation. There are three sources of quantization error - coefficient quantization, input quantization and the internal rounding that is the quantization of the results of arithmetic operations within the filter [2]. According to [2], if each coefficient is quantized to  $m + 1$  bits and the input is also quantized to  $n + 1$  bits where  $n < m$ , the output quantization noise power is nearly optimal for internal rounding precision set to less than  $m + 1$  and greater than  $n + 1$  bits if there is no restriction on the output quantization. However, in our test-bed, the output quantization is fixed and set to 14 bits, because the input resolution of DAC is 14 bits. Meanwhile if we use shift register to build time reversal waveform generator, we will only have coefficient quantization and internal rounding problems. If the time reversal waveform has no overlapping in the

transmitter side, the coefficient quantization should be 14 bits which is the same as the output quantization. Based on Dr. Guo's research results, nearly half of the ideal energy of the channel impulse response can be attained in the receiver side using 1 bit coefficient if inter-symbol interference (ISI) is not present. Because mono-bit resolution will cause the big side lobe in the received signal. So, if waveform overlapping is required in the transmitter side and ISI is present in the receiver side, the resolution of the coefficient and the internal rounding should be increased in order to suppress the side lobe and increase the energy of the main lobe in the received signal. Because the channel state varies in different scenarios, we should make the tradeoffs between the system performance and system complexity to determine the resolution of the coefficient and the internal rounding when the output resolution is fixed and given. This research issue will be further studied.

In sum, no matter what method we use, we should follow some steps to design the FIR filter in FPGA. (1) Use Matlab to design a floating-point FIR filter. (2) Convert the floating-point FIR filter into fixed-point FIR filter using Matlab. (3) Build a hardware description in FPGA and verify that the fixed-point design functions correctly. (4) Evaluate the fixed-point FIR filter in terms of its performance and hardware efficiency [3]. (5) Program FPGA and verify the FIR filter's performance experimentally on the workbench.

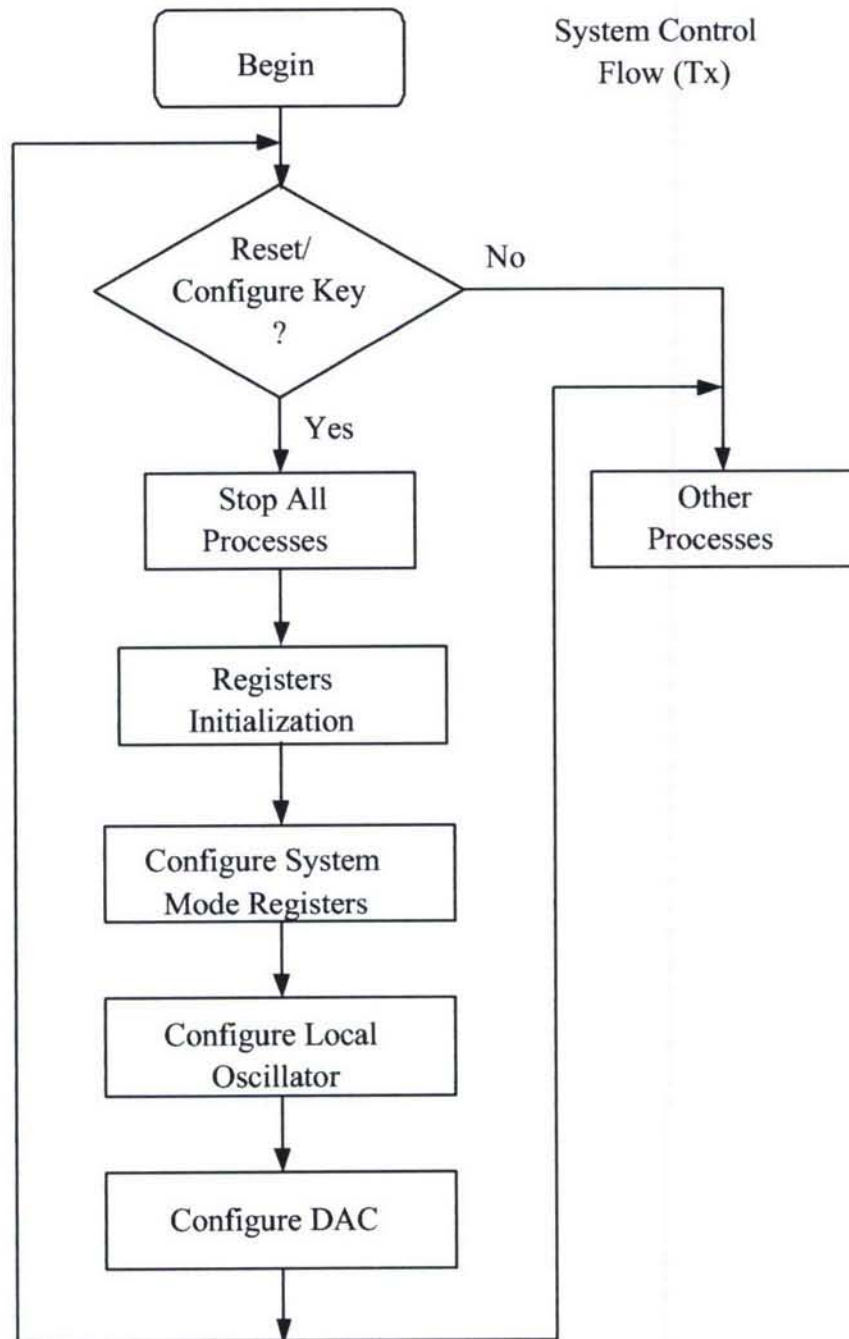


Figure 10.1: System control flow for transmitter.

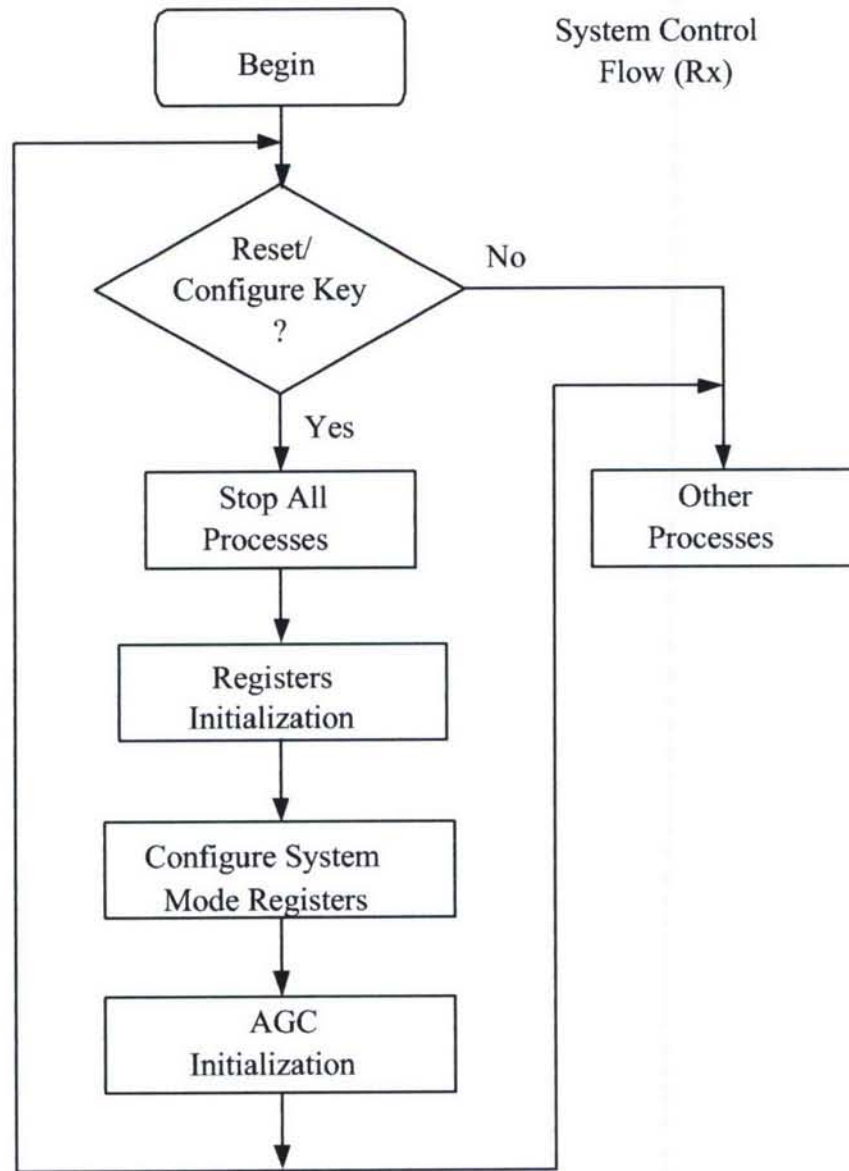


Figure 10.2: System control flow for receiver.

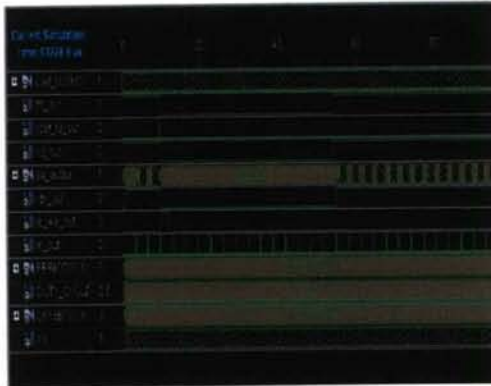


Figure 10.3: The simulation result of coefficient reload timing using DA FIR filter IP core in FPGA.

## Bibliography

- [1] "Distributed Arithmetic FIR Filter Product Specification," Xilinx, 2005.
- [2] M. Magar and L.S. DeBrunner, "Balancing the Tradeoffs Between Coefficient Quantization and Internal Quantization in FIR Digital Filters," in Conference Record of the Thirty-Eighth Asilomar Conference on Signals, Systems and Computers, vol. 1, November 2004.
- [3] K.A. Kotteri, A.E. Bell and J.E. Carletta, "Quantized FIR Filter Design: A Collaborative Project for Digital Signal Processing and Digital Design Courses," in Proceedings of the 2004 American Society for Engineering Education Annual Conference Exposition, 2004.



## Chapter 11

# Graphic User Interface (GUI) between FPGA and PC

In this section we'll introduce the PC interface in our test-bed system. The PC interface is responsible for input/output communications between host PC and FPGA.

### 11.1 Architecture

Fig. 11.1 shows the architecture of the PC/FPGA connection with PC interface. Here we use laptop as the host PC, since it's powerful enough and easy to carry. The data acquisition (DAQ) board acts as the PC interface. For digital data output, DAQ gets data from PC then send it to FPGA. For digital data input, DAQ samples data from FPGA then sends it to PC. We use USB cable for the interface between PC and DAQ while flying lead wire for DAQ/FPGA connection (Fig. 11.2).

### 11.2 Communications between FPGA and host PC

FPGA is extensively used in our test-bed system. However, if we want to change the parameters in FPGA for testing, there will be some difficulties. We can let the FPGA change the parameters by itself, but this will take up the valuable FPGA resource. Also, FPGA does not have graphical user interface (GUI). We must change the codes and download them to FPGA each time, which is time consuming and not intuitive. With a PC interface between host PC and FPGA, we can bypass these difficulties. We can set up the parameters in GUI then transmit them to FPGA via PC

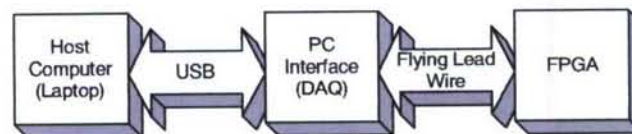


Figure 11.1: The architecture of the PC/FPGA connection with PC interface

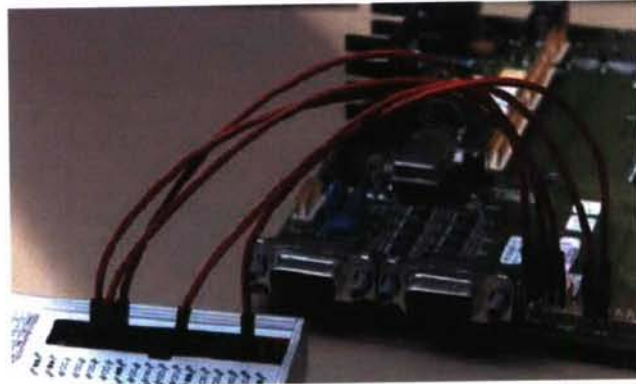


Figure 11.2: The flying lead wire interface.



Figure 11.3: Byte Paradigm, GP22050 DAQ board

interface without making any changes in FPGA. This is much more efficient and intuitive.

We can also use PC interface to read data from FPGA. Though this function can be done by logic analyzer, it can only display static signals, not real time signals. Also, it does not support real time signal processing. With PC interface bridged between FPGA and PC, real time data can be sampled and stored to PC. After capturing, the data can be processed and viewed in the monitor in real time.

### 11.3 Implementation

We choose Byte Paradigm's GP22050 as our DAQ (Fig. 11.3). It is a powerful DAQ supporting up to 16 bidirectional data and 6 bidirectional control signals. The maximum processing rate is 50MHz. Therefore, the maximum burst throughput can be up to 100MByte/s. GP22050 is also provided with C language interface. The C functions can be called to control DAQ by Visual C (VC), Labview and other programs [1, 2]. Thus, a user-friendly GUI can be made to control the PC interface between DAQ and FPGA.

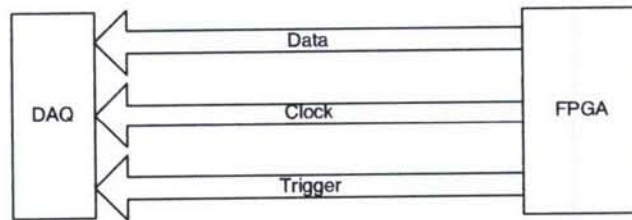


Figure 11.4: Data stream structure for PC/DAQ connection.

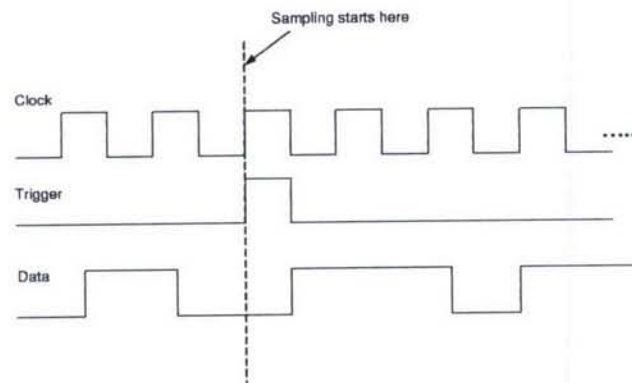


Figure 11.5: The relationship of the clock, trigger and data signals.

## 11.4 Application: BER Measurement

Now we are developing the bit error rate (BER) measurement application. To get the BER, we need to compare the received data with transmitted data. To simplify the process, the transmitted data periodic and known at the receiver. Also, at the beginning of each period, there is a trigger signal to inform the program when to start comparing. In our PC interface based system, the received data, trigger signal and clock signal are the output of FPGA. DAQ uses three data streams to get those signals. The data stream structure is illustrated in Fig. 11.4. DAQ will not start sampling until it receives the trigger signal. After 5 clock cycles of the trigger signal [3], DAQ samples data from FPGA at each clock rising edge. The relationship of the clock, trigger and data signals is illustrated in Fig. 11.5. DAQ samples at rising edge of a clock and it only starts sampling after trigger signal is detected [3]. The maximum sampling rate is the same as DAQ's maximum sampling rate, which is 50MHz [4]. Since DAQ can sample 16 data lines in parallel, the maximum throughput can be 100Mbyte/s [4].

Fig. 11.6 is the BER measurement software GUI. Before BER measurement, we need to initialize the measurement environment in the "Settings" dialog first (Fig. 11.7). If "Stop Manually" is chosen, the software will keep running until the "Stop" button in Fig. 11.6 is clicked. Otherwise, it stops when it reaches "Number of bits" or "Errors" set by user. BER values will be updated every 100ms in the "BER" edit box. A new BER value will be plotted onto the "Real time display" box every 1 second. BER VS Distance (or SNR) curves will be displayed on "Statistic display" box for each environment. They can be saved and loaded any time.

This software is still under construction. It is expected to be finished in one week.

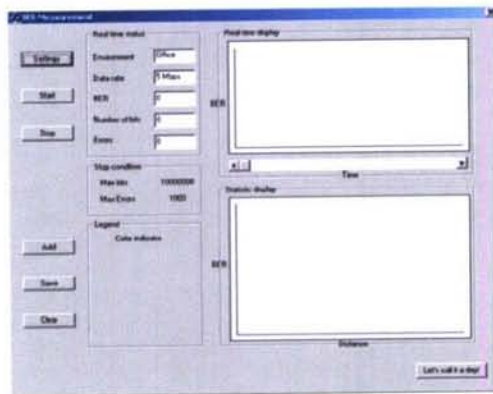


Figure 11.6: The BER software GUI.

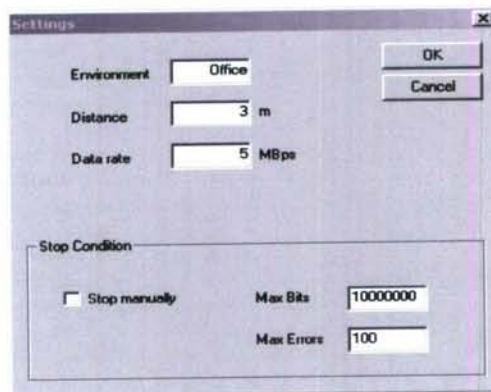


Figure 11.7: The Settings dialog. This dialog is used to initialize the measurement environment.

## 11.5 Application: FPGA Test

We are going to develop an FPGA test software. In order to test FPGA codes, we need to change the parameters frequently, such as FIR filter's coefficients, system data rate, transmitted data, etc.. Since FPGA does not have GUI, we can either change the code each time or let FPGA change the parameters by itself. Both of these methods are time consuming and not intuitive. With DAQ, however, FPGA will be able to read parameters from PC's GUI without changing the codes. This is a much more intuitive way and saves time.

GP22050's "arbitrary digital waveform generator" (ADWG) function [4] can be applied to our FPGA test application. The ADWG function is able to generate arbitrary 16 bit-depth output at a rate of 50MHz. As a result, GP22050 supports setting 16 coefficients simultaneously in FPGA at a high speed. With the ADWG Library [2] provided by the device, we can customize the GUI design and make the test much more intuitive.

## 11.6 Limitations

Although PC interface provides a way for communications between FPGA and PC, the processing speed is limited. Since PC utilizes a lot of resources to support the operation system and other necessary softwares, the signal processing speed is far lower than the speed of the DAQ. According to result of a test with a Pentium 4 3 GHz PC, the maximum continuous throughput is only 11MByte/s, which is far less than the burst throughput of 100MByte/s.



# Bibliography

- [1] *C/C++ library for Analyser application*, Byte Paradigm, Belgium, 2006.
- [2] *C/C++ library for ADWG application*, Byte Paradigm, Belgium, 2006.
- [3] *8PI Control Panel Users Guide for GP-22050*, Byte Paradigm, Belgium, 2006.
- [4] *GP-22050 complete data sheet*, Byte Paradigm, Belgium, 2006.